

Designing Feedback Mechanisms in Chemically Fueled Emulsions

Patrick Schwarz

Vollständiger Abdruck der von der Fakultät für Chemie der Technischen Universität München zur Erlangung des akademischen Grades eines

Doktors der Naturwissenschaften (Dr. rer. nat.)

genehmigten Dissertation.

Vorsitzende: Prof. Dr. Cathleen Zeymer

Prüfer der Dissertation: 1. Prof. Dr. Job Boekhoven

2. Prof. Dr. Angela Casini

Die Dissertation wurde am 17.01.2022 bei der Technischen Universität München eingereicht und durch die Fakultät für Chemie am 15.02.2022 angenommen.

I. Abstract

The complexity of life and how it could have originated from inanimate matter has excited humankind ever since. However, up to now, both understanding the origin of life and its synthesis remain unsuccessful. The synthesis of life from inanimate matter might give us new insights into life's origin and the development of sophisticated materials with life-like properties, *e.g.*, materials endowed with temporal and spatial control, adaptability, and self-healing ability. The thesis will start with an introduction to the origin of life research and different approaches for the synthesis of life. Moreover, I will discuss essential properties of living systems in Chapter 1 that a synthetic system must have to be considered alive, *e.g.*, energy transduction, compartmentalization, information processing, growth and division, and adaptability. In Chapter 2, I will talk about the different types of compartments in biological systems and show that phase-separated droplets are ideal candidates for compartments in synthetic living systems. I will show that biology uses chemical reactions to control where and when phase separation occurs. This means that any synthetic system, in which the phase separation of droplets is regulated by chemical reactions, already combines two essential properties of living systems: energy transduction and compartmentalization. Moreover, I will demonstrate in Chapter 2 that properties of droplets can significantly differ from droplets under thermodynamic control when they are regulated by chemical reactions, *e.g.*, suppression and acceleration of Ostwald ripening, self-division, or reduced concentration oscillations. Despite the impressive progress in chemically fueled self-assembly, these systems are still far from being alive. Other essential properties of living systems could emerge when the assembly also reciprocally regulates the kinetics of the reaction cycle by feedback mechanisms. In Chapter 3, I will discuss the role of feedback regulations in biological systems and present recent examples of feedback mechanisms in synthetic chemically fueled systems. Following a bottom-up approach for the synthesis of life, Chapter 4 will expose how to create life-like behavior in a chemically fueled system composed of simple molecules and precursors which is the overall aim of the thesis.

Inspired by feedback regulation of networks in biological systems, we investigated in Chapter 5 how a negative feedback mechanism of anhydride oil droplets on their deactivation affects the kinetics of the anhydride products when multiple, simultaneously operating reaction cycles compete for fuel. In general, the competition between two reaction cycles for a common nutrient is disadvantageous for both, *i.e.*, both products have lower yields and lifetimes. However, we found that the success of a soluble product can increase when the product of a competitor can phase-separate, *e.g.*, it survives longer or shows reduced concentration oscillations in the presence of periodic fueling. Co-phase separation of the product with

droplets formed by the competitor decelerates its deactivation by hydrolysis and thus increases its success. This behavior is reminiscent of parasitic behavior in biology, where the parasite competes with the host for the shared resources and exploits its protective environment.

Finally, in Chapter 6, we wanted to demonstrate that feedback mechanisms offer new ways to control the properties of transient materials. We designed an opposing feedback mechanism that causes the immediate dissolution of droplets once the system reaches a certain threshold. This opposing feedback mechanism is based on the *in-situ* formation of micelles by the surfactant precursor, which rapidly solubilize the anhydride and thus drastically accelerate the hydrolysis rate. More precursor is released upon hydrolysis of the anhydride, which again accelerates the hydrolysis rate, *i.e.*, the deactivation follows a self-immolative mechanism. The opposing feedback mechanism offers precise control over the material properties, which we showcase in two applications: a self-erasing label and a drug-delivery platform.

In this work, we show that life-like behavior can already be observed in simple chemically fueled reaction cycles. We envision that the co-phase separation mechanism found in Chapter 5 could be crucial to control concentrations of competitors in downstream chemical reactions. Moreover, we believe that self-immolative deactivation reactions described in Chapter 6 could also be designed in other chemically fueled reaction cycles, *e.g.*, reaction cycles that regulate the self-assembly of fibers or coacervates. This could serve as a tool for the development of more sophisticated, life-like materials.

II. Zusammenfassung

Seit jeher beschäftigt die Menschheit die Komplexität des Lebens und wie es aus unbelebter Materie entstanden ist. Sowohl die Aufklärung des Ursprungs des Lebens, als auch die Synthese von Leben aus unbelebter Materie, blieben bisher erfolglos. Die Synthese von Leben im Labor könnte uns neue Einblicke in den Ursprung des Lebens geben, sowie die Entwicklung von anspruchsvollen Materialien mit lebensechten Eigenschaften ermöglichen.

Die Doktorarbeit beginnt mit einer Einführung in die Erforschung des Ursprungs des Lebens sowie verschiedene Ansätze zur Synthese des Lebens im Labor. Darüber hinaus gehe ich in Kapitel 1 auf die wesentlichen Eigenschaften eines lebendigen Systems ein, welche ein synthetisches System haben muss, um als lebendig betrachtet zu werden, wie z.B., Energieumwandlung, Kompartimentierung, Informationsverarbeitung, Wachstum und Teilung oder Anpassungsfähigkeit. In Kapitel 2 werde ich die verschiedenen Arten von Kompartimenten in biologischen Systemen diskutieren und zeigen, dass phasenseparierte Tröpfchen ideale Kandidaten für Kompartimente in synthetischen, lebensähnlichen Systemen sind. Ich werde zeigen, dass biologische Systeme chemische Reaktionen benutzen, um zu kontrollieren, wo und wann Phasenseparierung stattfindet, weshalb synthetische Systeme, in denen die Phasentrennung von Tröpfchen durch chemische Reaktionen reguliert wird, bereits zwei wesentliche Eigenschaften lebender Systeme vereinen: Energieumwandlung und Kompartimentierung. Darüber hinaus werde ich in Kapitel 2 veranschaulichen, dass sich die Eigenschaften von Tröpfchen signifikant von thermodynamisch kontrollierten Tröpfchen unterscheiden können, wenn sie durch chemische Reaktionen reguliert werden, z.B., Unterdrückung und Beschleunigung der Ostwald-Reifung, Selbstteilung oder reduzierte Konzentrationsschwankungen. Jedoch sind synthetische Systeme, trotz der erstaunlichen Fortschritte bei der durch chemische Reaktionen angetriebenen Assemblierung von Molekülen, noch lange nicht lebendig. Andere wesentliche Eigenschaften lebender Systeme könnten sich ergeben, wenn die Assemblierung auch die Kinetik des Reaktionszyklus durch Rückkopplungsmechanismen reziprok reguliert. In Kapitel 3 diskutiere ich die Rolle der Rückkopplungsmechanismen in biologischen Systemen und zeige Beispiele für Mechanismen in synthetischen Systemen, welche durch chemischen Treibstoff angetrieben werden. Das übergeordnete Ziel der Dissertation ist es wie in Kapitel 4 gezeigt, einen Bottom-up-Ansatz für die Synthese von Leben zu verfolgen, um ein chemisch angetriebenes System aus einfachen Molekülen und Vorläufern zu synthetisieren, das ein gewisses lebensähnliches Verhalten zeigt.

Inspiziert von der Rückkopplungsregulation von Netzwerken in biologischen Systemen, untersuchen wir in Kapitel 5 wie ein negativer Rückkopplungsmechanismus von Anhydrid

Öltröpfchen auf ihre Deaktivierung die Kinetik der Anhydrid Produkte beeinflusst, wenn mehrere Reaktionszyklen um Treibstoff konkurrieren. Generell ist die Konkurrenz zweier Zyklen um einen gemeinsamen Nährstoff für beide von Nachteil, z.B., haben beide Produkte geringere Erträge und Lebensdauern. Wir haben jedoch festgestellt, dass der Erfolg eines löslichen Produkts steigen kann, wenn das Produkt eines Konkurrenten in der Lage ist, sich in Phasen zu trennen. Die Co-Phasentrennung des Produktes mit Tröpfchen des Konkurrenten verlangsamt dessen Deaktivierung durch Hydrolyse und steigert somit seinen Erfolg. Dieses Verhalten erinnert an parasitäres Verhalten in der Biologie, bei welchem der Parasit mit dem Wirt um die gemeinsamen Ressourcen konkurriert und die vom Wirt gebotene Schutzumgebung ausnutzt.

In Kapitel 6 wollen wir zeigen, dass Rückkopplungsmechanismen neue Wege ermöglichen um transiente Materialien zu kontrollieren. Wir entwerfen einen gegenläufigen Rückkopplungsmechanismus, welcher die sofortige Auflösung der Tröpfchen verursacht, sobald ein bestimmter Schwellenwert erreicht ist. Der gegenläufige Rückkopplungsmechanismus beruht auf der *in-situ* Bildung von Mizellen durch den oberflächenaktiven Vorläufer, welche die Anhydrid Tröpfchen auflösen und die Hydrolyse drastisch beschleunigen. Bei der Hydrolyse des Anhydrids wird mehr Vorläufer freigesetzt, welcher wiederum die Hydrolyse weiter beschleunigt. In anderen Worten hydrolysiert das Anhydrid mit einem autokatalytischen Zerfallsmechanismus. Der gegenläufige Rückkopplungsmechanismus bietet eine präzise Kontrolle über die Materialeigenschaften, welche es uns ermöglicht, die Emulsion als selbstlöschendes Etikett und als Medikamentenlieferungsplattform anzuwenden.

In dieser Arbeit zeigen wir, dass lebensechtes Verhalten bereits in einfachen chemisch betriebenen Reaktionszyklen beobachtet werden kann. Wir glauben, dass der in Kapitel 5 beschriebene Co-Phasen-Trennmechanismus entscheidend sein könnte, um die Konzentrationen von Konkurrenten in nacheinander geschalteten chemischen Reaktionen zu kontrollieren. Darüber hinaus glauben wir, dass die in Kapitel 6 beschriebenen autokatalytischen Zerfallsmechanismen auch auf andere chemisch angetriebenen Reaktionszyklen übertragbar ist, z. B., Reaktionszyklen, die die Selbst-Assemblierung von Fasern oder Koazervaten regulieren. Dies könnte als Werkzeug für die Entwicklung anspruchsvollerer, lebensechter Materialien dienen.

III. Abbreviations

CMC	critical micelle concentration
e.g.	<i>exempli gratia</i> , for example
i.e.	<i>id est</i> , that is to say
et. al	<i>et alii</i> , and others
HPLC	high-performance liquid chromatography
TCEP	tris-(2-carboxyethyl)phosphin
Fmoc-	fluorenylmethoxycarbonyl-
MLO	membraneless organell
SC	synaptonemal complex
TF	transverse filament
EDC	1-ethyl-3-(3-dimethylaminopropyl)carbodiimide hydrochloride
DIC	<i>N,N'</i> -diisopropylcarbodiimide
ATP	adenosine triphosphate
ADP	adenosine diphosphate
GTP	guanosine triphosphate
GDP	guanosine diphosphate
CAC	critical aggregation concentration
DKS	dynamic kinetic stability
LLPS	liquid-liquid phase separation
NADH	nicotinamide adenine dinucleotide

IV. Table of Contents

I.	Abstract	II
II.	Zusammenfassung	IV
III.	Abbreviations	VI
IV.	Table of Contents	VII
1.	Synthesis of Life	- 1 -
1.1.	History and Approaches	- 2 -
1.2.	When is Something Alive?.....	- 3 -
1.3.	Conclusion and Outlook	- 5 -
2.	Compartmentalization.....	- 6 -
2.1.	Compartments in Biology	- 7 -
2.1.1.	Membrane-Bound Compartments	- 7 -
2.1.2.	Membraneless Compartments	- 7 -
2.2.	Regulation of Phase Separation	- 9 -
2.3.	Active Droplets	- 12 -
2.3.1.	Regulation of Active Droplets	- 13 -
2.3.2.	Noise Reduction by Phase Separation of Active Droplets	- 14 -
2.3.3.	Self-Division of Active Droplets	- 15 -
2.3.5.	Suppression and Acceleration of Ostwald Ripening of Active Droplets.....	- 16 -
2.4.	Conclusion and Outlook	- 19 -
3.	Feedback Mechanisms.....	- 20 -
3.1.	Feedback Mechanisms and their Role in Living Systems	- 21 -
3.2.	Feedback in Chemically Fueled Reaction Cycles	- 23 -
3.2.1.	Feedback by Catalysis	- 23 -
3.2.2.	Feedback by Up- or Down-Concentration.....	- 28 -
3.3.	Conclusion and Outlook	- 30 -
4.	Aims of the Thesis	- 32 -
5.	Parasitic Behavior in Competing Chemically Fueled Reaction Cycles.....	- 34 -
6.	Chemically Fueled Materials with a Self-Immolative Mechanism: Transient Materials with a Fast On/Off Response.....	- 65 -
7.	Conclusion and Outlook.....	- 84 -

8. Materials and Methods	- 86 -
9. Further Publications.....	- 90 -
10. Acknowledgments.....	- 91 -
11. References	- 93 -

1. Synthesis of Life

Abstract.

Despite the marvelous progress in unraveling life's principles, the synthesis of life from inanimate matter remains extremely challenging. This chapter will give an overview of the history of the origin of life research as it is closely related to the synthesis of life. Understanding one process also means a huge step towards the other. Synthetic systems are still far from being alive, which means that new systems must be developed. I will show that life could be synthesized in the lab following either a top-down or a bottom-up approach. Chemists favor the latter as the approach aims to create a system comprised of simple molecules and precursors to reconstitute and mimic certain biological functions under simplified conditions. To decide whether a synthesized system is alive, one must be able to distinguish between the living and non-living, which requires a definition of life. However, no unambiguous definition of life exists due to its inherent complexity. Instead of defining life, scientists have to focus on the essential properties of living systems to decide if a synthetic system is alive. Any synthetic system having one or more of these essential properties could be a step towards synthesizing life.

1.1. History and Approaches

'We must either succeed in producing living matter artificially, or we must find the reason why this is impossible.' Jacques Loeb.^[1]

As expressed by Jacques Loeb in 1912, the questions of what life is and how it originated from inanimate matter have been concerning humankind ever since.^[1] In the early ages, most cultures believed that life originated from a supernatural creation.^[2] For example, in Greek mythology, people believed that men and women spring into life from the stones cast on the earth.^[3] In 384 B.C., Aristotle wrote that *'Animals sometimes arise in soil, in plants or in other animals.'*, which illustrates the belief of many ancient writers that life forms from the non-living, *i.e.*, dead matter can transform into living matter.^[2-3] The belief that living matter is spontaneously generated from inanimate matter persisted for over two centuries.

The invention of the microscope and the discovery of the cell by Hooke in 1665 revived the origin of life research.^[4] The cell was since then considered as the fundamental unit of all living systems, which narrowed the origin of life question down to how cells originated.^[4] Despite the discovery of cells and microorganisms, their emergence remained elusive, wherefore the theory of the spontaneous generation of life persisted tenaciously until the 19th century. It was only disproved in 1860 when Louis Pasteur showed that microorganisms are not produced spontaneously but rather by germs in the atmosphere.^[5] Simultaneously, Charles Darwin established the evolution theory, which made it clear that the first primitive life forms were subjected to billion years of evolution.^[6]

These new insights reinforced the question about the origin of life in the 19th century. In the 1920s, Aleksandr Oparin and John Haldane independently proposed the emergence of life after a step-by-step process from non-living matter, later referred to as the Oparin-Haldane hypothesis.^[7] Oparin and Haldane both assumed a reducing atmosphere with the sun as an energy source and reactions capable of prebiotic synthesis of organic compounds, like amino acids and nucleotides, from a dilute phase of inorganic molecules. In further reactions, these organic compounds could have formed more complex molecules, like proteins and nucleic acids, that self-assembled in a dense phase by the combination of negatively and positively charged polymers, later referred to as coacervation. They suggested that these coacervates could have up-concentrated molecules from their surroundings and thus served as an environment for replicative and self-sustaining molecules, which are crucial for the emergence of life. Shortly after, Urey and Miller showed that organic compounds could be synthesized from inorganic precursors, such as H₂O, H₂, CH₄, and NH₃.^[8] They used an electric discharge to form free radicals, which allowed them to synthesize various organic molecules, including amino acids, nucleobases, and fatty acids. In line with the Oparin-Haldane theory, Fox and

Harada reported the thermal copolymerization of amino acids to proteinoids which could self-assemble in microspheres.^[9] These results are the basis for the so-called 'peptide world' hypothesis, which considers oligopeptides as the first functional biomolecules. Due to the uncertainty of the first functional biomolecules, several analogous theories emerged based on lipids and RNA.^[10] In 2013, Szostak combined both theories and reported the non-enzymatic RNA replication inside lipid vesicles.^[11]

However, these systems are still far from being considered alive, which means that scientists must develop even more sophisticated or finely tuned approaches and systems. In general, life could be synthesized following two different approaches. One approach is to decrease the complexity of living systems in a so-called top-down approach, *e.g.*, by removing genes in cells that are unnecessary to sustain their essential properties. In other words, this approach aims to derive a minimal cell with the lowest number of genes necessary to maintain essential cellular functions.^[12] Thus, a top-down approach is suitable for biologists and biochemists. In contrast, less complex molecules and precursors are combined to reconstitute and mimic certain biological functions under simplified conditions following a bottom-up approach.^[12] The aim is to increase the complexity step by step to create a synthetic living system. Consequently, a bottom-up approach is an ideal choice for chemists to tackle the question of the origin of life and synthesize life from inanimate matter.

1.2. When is Something Alive?

Before one can synthesize life, one must be able to distinguish whether a synthetic system is alive or not. For this distinction, scientists strive for a definition of life that should cover all forms of life and allow the discrimination between the living and non-living. However, defining life with a compact and unambiguous definition remains challenging due to life's complexity and diversity.^[13] Nowadays, it is widely accepted but not yet demonstrated that life originated from inanimate matter through a lengthy, continuous process of increasing molecular complexity and organization.^[13a] At some point, a transition from physical or chemical systems to biological systems occurred, which means that attempts to discriminate between the living and non-living correspond to drawing an arbitrary line on this timeline.^[14] This means that the research focus of the corresponding person determines the position of the line, which results in differentiation at various positions. For example, during a meeting of the International Society for the Study of the Origins of Life, each participant was asked to define life, resulting in 40 pages of text and 78 different definitions.^[15] Rather than focusing on defining life, one has to agree on essential properties of living systems that a synthetic system must have to decide whether or not the system is alive.^[13b] Essential properties that delimit living systems from inanimate

matter can be concluded by considering the cell as an example because it is the essential component and building block of all living systems.^[4] For example, Yewdall *et al.* identified five essential properties which all living systems have in common (Figure 1).^[16]

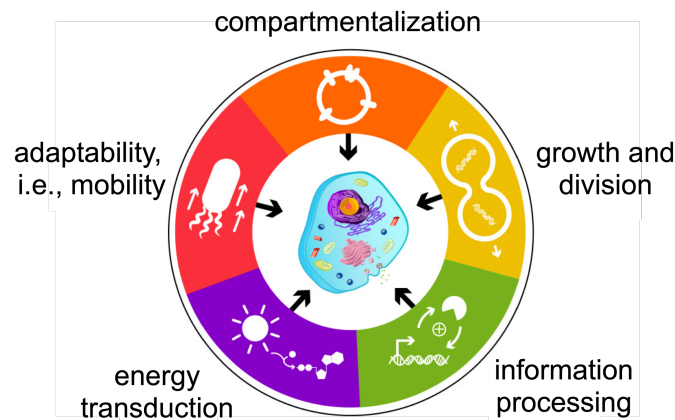


Figure 1: Essential properties of living systems that synthetic systems require to be considered alive. Figure adapted from reference [16].

An essential property of living systems is **compartmentalization**.^[16] Compartments can organize complex biochemical reactions in space and time by regulating and localizing reagents, *e.g.*, increasing, decreasing, or inhibiting reactions by up-concentration or segregation of reagents.^[17] Moreover, biological systems use compartments to avoid mutual interferences between biochemical processes, *e.g.*, by conflicting reaction pathways. Two essential properties characterize a compartment. Firstly, it must be separated from its surrounding by a boundary.^[18] Secondly, the diffusion of components in- and outwards of the compartment must be regulated in order to perform chemical reactions.^[19]

Another essential property of a living system is **energy transduction**.^[16] Generally, life operates in a far-from-equilibrium steady-state (homeostasis) that relies on the continuous consumption of energy from the surrounding.^[19-20] *'How does the living organism avoid the decay? The obvious answer is: By eating, drinking, breathing, and (in the case of plants) assimilating. The technical term is metabolism.'* Erwin Schrödinger.^[21] As Erwin Schrödinger pointed out in 1944, our body requires the constant input of energy derived from food, also referred to as metabolism. Similar to the metabolism on a macroscopic level, many cellular processes rely on non-equilibrium conditions and constant input of energy, *e.g.*, intracellular transport,^[22] cell signaling,^[23] diffusion processes,^[24] and gene transcription.^[25] This energy dependence might seem wasteful, but it endows living systems with dynamic properties, such as adaptivity, self-healing ability, as well as temporal and spatial control.^[26] To sum up,

synthetic living systems must have a metabolism to sustain their organization at the expense of nutrients/energy from the environment.^[13a, 19, 27]

Moreover, living systems require **information processing**.^[13a, 16, 27a] DNA, RNA, and protein are the three biopolymers for information processing in biological systems.^[28] DNA encodes the genetic information that is copied into complementary RNA, which is translated into a protein sequence following the genetic code.^[28] Despite these biopolymers, also the complex machinery for replication, transcription, and translation are required. Thus, for the bottom-up synthesis of life, a much simpler system to process information is required.

Another essential property of life is **growth and division** to transfer the information stored in the components of the system, *i.e.*, the system must be able to reproduce by making copies of itself.^[16, 19, 27b] Thus, systems must be able to grow, deform and divide to self-reproduce.^[16] The reproduction process must be accurate enough to maintain the species' integrity and error-prone to drive Darwinian evolution by which living systems increase their viability through various selection pressures.^[19, 27b] Moreover, self-reproduction enables thermodynamically unstable systems to persist, referred to as dynamic kinetic stability (DKS).^[29] DKS could have played a role in stabilizing intermediate stages during the emergence of life.

Lastly, a synthetic living system must respond to changes in its environment, *i.e.*, **adaptability**.^[16] Living systems show a variety of adaptable behaviors ranging from single-cell levels to populations of cells.^[16] A basic form of adaptability is mobility which is the ability to move towards an energy source that can be either chemical fuel (chemotaxis) or light (phototaxis).^[16] Ideally, the system should move towards areas of higher fuel concentration to minimize the loss of energy.

1.3. Conclusion and Outlook

What life is and how it originated remains a longstanding question. Despite the progress in understanding the principles of life, we are still far from understanding its origin and synthesizing it in the lab. Up to now, there is still no unequivocal definition of what life is. One must identify and consider essential properties of living systems as a model for the creation of synthetic analogs, *e.g.*, compartmentalization, energy transduction, information processing, growth, and division, and adaptability. Any synthetic system comprised of simple molecules and precursors with one or more of these essential properties could be a step towards the bottom-up synthesis of life.

2. Compartmentalization

Abstract

In Chapter 1, I showed that compartmentalization is essential for living systems. Compartmentalization is required to separate a system from its surroundings and control the diffusion and concentration of reagents. In this chapter, I will discuss the two types of compartments in biological systems: membrane-bound compartments and membraneless compartments. I will show that the absence of a membrane facilitates diffusion and regulation of the concentrations of reactants, which makes membraneless compartments an ideal candidate for the bottom-up synthesis of life. I will show that membraneless compartments are protein- and nucleotide-rich droplets that are thought to be primarily formed by liquid-liquid phase separation and discuss the advantages of their liquid nature. Moreover, I will show that biological systems use chemical reactions to control where and when phase separation occurs. This kinetic control can result in significantly different properties of droplets than observed under thermodynamic control. I will end this chapter with an overview of the theoretical calculations and experimental studies on chemically fueled droplets and complex properties.

2.1. Compartments in Biology

2.1.1. Membrane-Bound Compartments

In the 19th century, De Vries (1885), Pfeffer (1897), and Overton (1899) suggested that a membrane encloses the cell to separate it from its surrounding.^[30] They observed that the cell responds osmotically to changes in the external osmolarity. However, technological limitations prevented acquiring unambiguous proof for the existence of a cell membrane until the invention of analytical techniques, such as micromanipulation, X-ray diffraction, and electron microscopy, around 1930.^[30] Since then, it was found that the cell is further organized in sub-compartments, which are also enclosed by lipid membranes, such as the endoplasmatic reticulum, mitochondria, Golgi apparatus, and lysosomes.^[17a, 31] The lipid membranes physically separate the interior and exterior of these compartments. They are typically impermeable to most biological molecules and require complex membrane proteins and machinery to control the permeability of reactants.^[17a, 32] Hence, a membrane-based compartment is challenging in a bottom-up approach to synthesize life due to the complex regulation of diffusion of reactants through the lipid bilayer.

2.1.2. Membraneless Compartments

Recently, more and more compartments lacking a membrane have been identified. Examples include the Cajal bodies, nucleoli, and stress- and germ granules (Figure 2).^[17a] These so-called membraneless organelles (MLOs) can sequester biomolecules despite lacking a physical barrier to the surrounding cytoplasm. For many years, it remained unclear why these compartments could maintain their structure and not simply mix with their surroundings.^[33] Brangwynne *et al.* gained key insights in the nature of MLOs when they observed liquid-like properties of P granules from *C. elegans*, such as a spherical shape, fusion, rapid exchange of components with the surrounding, deformation by flow, viscosity, and wetting.^[33-34] These properties of P granules suggest that they are liquid droplets that are formed through liquid-liquid phase separation (LLPS) from the surrounding cytoplasm.

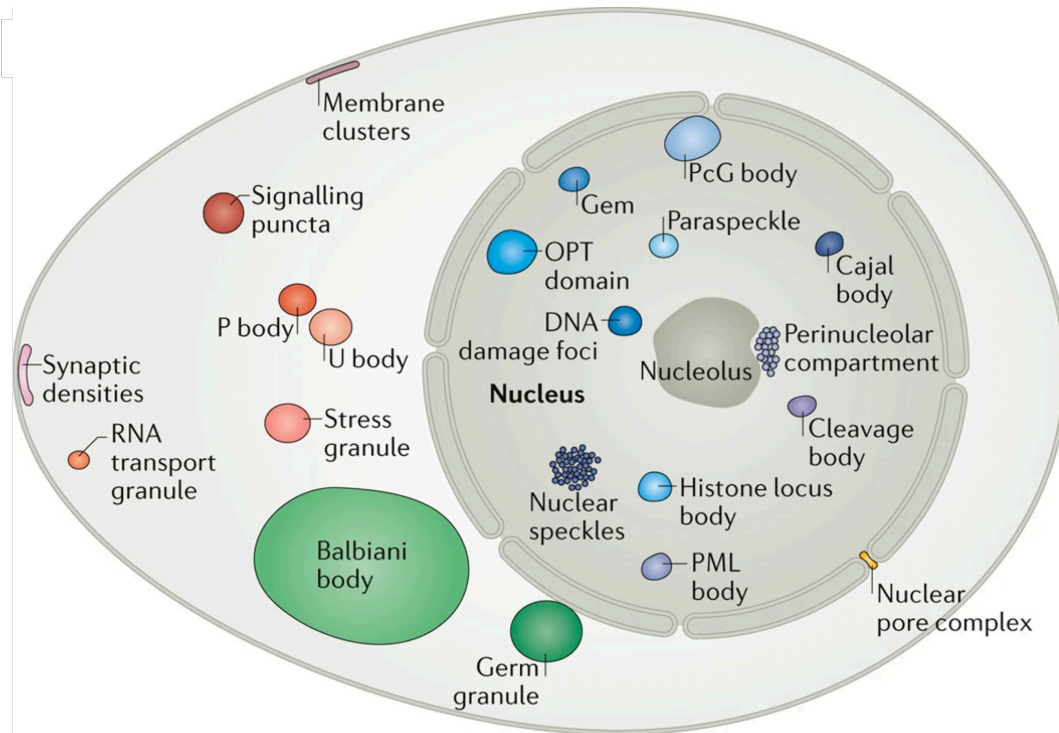


Figure 2: Schematic representation of MLOs in eukaryotic cells. Reprinted from reference [17a] by permission from the Nature Publishing Group, Copyright © 2017.

What Drives Phase Separation of MLOs?

Typically, the multivalence of their building blocks drives the phase separation of these protein- and nucleotide-rich droplets. For example, multivalent proteins have multiple functional domains/motifs and interact via different intra- or intermolecular interactions (Figure 3).^[35] Thus, phase separation is a consequence of the collective effects of their interacting domains/motifs. Another class of phase-separating proteins is proteins with intrinsically disordered regions (IDRs). These proteins lack a defined three-dimensional structure and thus do not have structural constraints. They are often repetitive in their amino acid sequence and biased in the amino acid composition, *i.e.*, enriched blocks of specific amino acid sequences and charged residues. Apart from proteins, nucleotides can drive LLPS of MLOs by base-pairing with other nucleotides and binding proteins with specific binding domains.

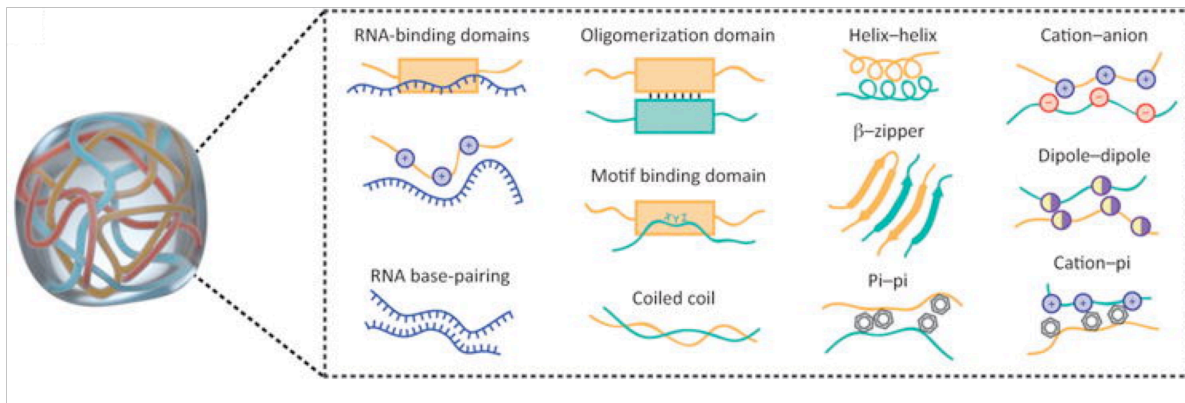


Figure 3: Schematic representation of molecular interactions driving LLPS in biology. Reprinted from reference [35] by permission from Elsevier Ltd., Copyright © 2018.

What Are the Advantages of MLOs Over Membrane-Bound Compartments?

Like membrane-bound compartments, MLOs can spatiotemporally compartmentalize biochemical compounds.^[36] However, their liquid nature allows for fast diffusion of reactants in- and outwards of the droplets without the need for complex machinery to regulate the diffusion.^[34, 37] Moreover, the composition of droplets can regulate the partitioning of molecules, which means that reagents can be selectively accumulated in a confined space. They also decelerate or accelerate biochemical reactions by down- or up-concentrating reagents inside or offering a specific catalytic microenvironment. These liquid droplets can adopt different physical states in response to external stimuli which means that LLPS can result in a wide range of compartments with different physical properties, *e.g.*, harden into gel- or glass-like states or turn into solid crystals.^[17b] Due to these combined properties of MLOs, the creation of a synthetic compartment by LLPS is probably more suitable for a bottom-up approach to synthesize life compared to membrane-bound compartments.

2.2. Regulation of Phase Separation

A system of multiple droplets is thermodynamically unstable and tends to evolve towards a system with only one large droplet driven by coalescence and Ostwald ripening.^[38] This behavior is opposite to living systems where multiple droplets with characteristic sizes coexist and increase their number by division. In conclusion, cells must somehow regulate where and when phase separation occurs. How can phase separation be regulated? To answer this question, we must consider the free energy and chemical potential of the system. The free energy $F = E - TS$ is the available energy to perform work that combines the internal energy E and the entropy S of a system.^[17a] In general, systems tend to minimize their free energy and

maximize their entropy. To explain how to regulate phase separation, we consider a simple binary system that comprises solute A and solvent B with the respective volume fractions ϕ_A and ϕ_B . In the case of no interactions between solute A and solvent B , the free energy as a function of volume fractions has one explicit minimum, *i.e.*, the free energy is unimodal (Figure 4A, red trace).^[17a, 33] The system's entropy is maximized by distributing the solute molecules homogeneously in the solvent. Moreover, the system approaches a stable thermodynamic state with minimal free energy and diffusive fluxes equalize any fluctuations. The chemical potential is the first derivative of the free energy and describes how the free energy changes when the volume fraction of the solute changes. In a case without interactions between the solute and the solvent, the chemical potential is monotonic. Each value of the chemical potential corresponds to a different volume fraction ϕ_B (Figure 4B, red trace).

In contrast, phase separation requires molecular interactions between the solute and solvent molecules. A system phase-separates when the attractive interactions between solute molecules or the repulsive interactions between solute and solvent molecules exceed the entropic tendency of the system to remain mixed.^[38] An approach to describe the free energy as a function of molecular interactions is the Flory-Huggins solution theory which was initially applied to describe the physics of phase separation of homopolymers with a length N in low molecular weight solvent.^[39] This approach models the solution as an infinite lattice with coordination number z where each lattice site can be occupied either by a solute or solvent molecule (Figure 4C). As $\phi_A + \phi_B = 1$, we can consider $\phi_B = 1 - \phi$ if ϕ_A is denoted as ϕ . Using a mean-field assumption, the Flory-Huggins free energy of mixing per lattice site can be calculated following equation (1).^[39a]

$$\frac{F}{k_B T} = \frac{\phi}{N} \ln \phi + (1 - \phi) \ln(1 - \phi) + \chi \phi(1 - \phi) \quad (1)$$

The first two terms in equation (1) represent the mean-field entropy of mixing per lattice site. The third term represents the energy of mixing per lattice site, which considers the strength of the molecular interactions. The Flory parameter χ is defined in equation (2). It quantifies the balance between homotypic (A - A and B - B) and heterotypic interactions (A - B) with the corresponding mean-field energies per site u_{AB} , u_{BB} and u_{AA} .

$$\chi = \frac{z}{k_B T} \left[u_{AB} - \frac{1}{2}(u_{BB} + u_{AA}) \right] \quad (2)$$

The magnitude of the Flory parameter χ quantifies the energetic costs of having solvent molecule B besides a lattice site occupied by a solute molecule A . Dependent on the strength of the different interactions, two different cases can occur. In the first case, the homotypic interactions (u_{BB} and u_{AA}) are weaker than heterotypic interactions (u_{AB}) which means that solute A remains dissolved in solvent B at all concentrations. However, when the homotypic

interactions are sufficiently stronger than the heterotypic interactions, the Flory parameter χ reaches a critical value and the energetic term in equation (1) will overcome the mixing entropy. This means that the free energy in Figure 4A (blue trace) becomes multimodal and thus unstable, which is resolved by separating solute A in volume fractions ϕ_s and ϕ_d (ϕ_s =volume fraction of A in solvent, ϕ_d =volume fraction of A in droplets). In other words, the solute A phase-separates from solvent B and forms a dense phase (ϕ_d) that is enriched with solute A and a dilute phase that is depleted of solute A (ϕ_s).^[17b] In this case, the chemical potential becomes non-monotonic which means that some chemical potential values correspond to the two different volume fractions ϕ_s and ϕ_d (Figure 4B, blue trace). The net diffusive flux between the phases is eliminated as the chemical potentials of the two volume fractions are equal. In other words, molecules move at equal rates in and out of the two phases. A diffusive flux equalizes any difference in chemical potential, e.g., a chemical reaction in one phase can alter the potential of that phase. A binary phase diagram shows whether the solution remains mixed or phase-separates into two phases for a given volume fraction ϕ and a temperature (Figure 4D). In conclusion, where and when phase separation occurs can be regulated by temperature, but also by tuning the attractive and repulsive interactions between solute and solvent. Because temperature within a cell is almost constant and hard to vary, chemical reactions, like post-translational modifications or binding of a ligand, are frequently used by cells to regulate the solubility, valency, or affinity of a protein. Such chemical reactions include phosphorylation, dephosphorylation, and methylation.^[17b] For example, phosphorylation can change the attractive interactions between solute molecules or the repulsive interactions between solute and solvent molecules which increases the Flory parameter χ above its critical value and thus drives phase separation. *Vice versa*, dephosphorylation can decrease the Flory parameter below its critical value, and the solute remains dissolved in the solvent.

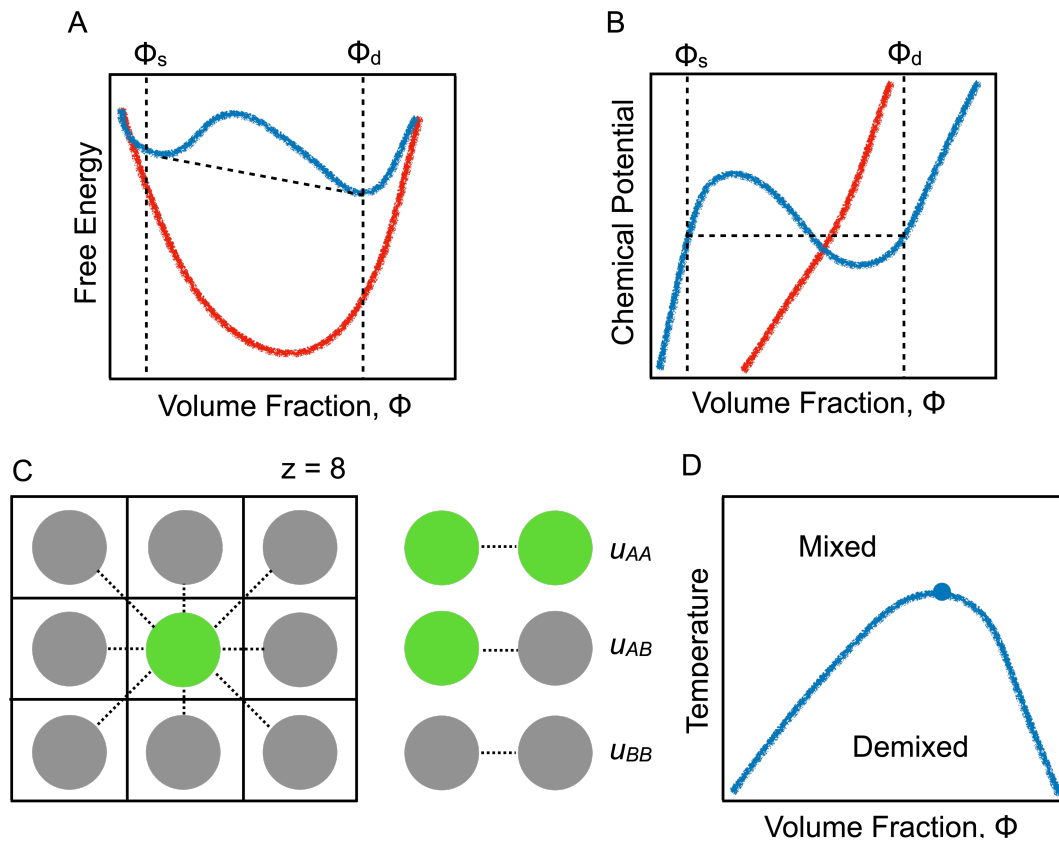


Figure 4: **A)** Free energy and **B)** chemical potential of a solution as a function of the solute concentration for non-interacting solute molecules (red line), and interacting, phase-separated solute molecules (blue line). **C)** Schematic representation of a solution of solute A in solvent B modeled as a lattice with coordination number $z = 8$ and the corresponding homotypic and heterotypic interactions (U_{AA} , U_{BB} , and U_{AB}). Adapted from reference [39a] by permission from the Nature Publishing Group, Copyright © 2015. **D)** Phase diagram of solute A in solvent B. **A)**, **B)**, and **D)** adapted from reference [33] by permission from Annual Reviews, Copyright © 2014.

2.3. Active Droplets

When phase separation is regulated by chemical reactions, like phosphorylation and dephosphorylation, which activate and deactivate droplet material, the droplets are considered chemically active.^[38] In contrast to passive droplets that are controlled by thermodynamics, these droplets are controlled kinetically by an external energy supply, e.g., by chemical fuels like ATP and GTP. The kinetic control allows regulation of properties previously constrained by thermodynamics, e.g., droplet number and size. How can a kinetic control result in different behavior than dictated by thermodynamics?

2.3.1. Regulation of Active Droplets

At least two chemical reactions regulate active droplets (Figure 5A). In the first reaction, a soluble precursor A converts into a self-assembling product B at the expense of a chemical fuel F which is converted to waste W (equation (3)). The conversion of A to B typically occurs in solution and results in an influx of phase-separating B to the product-rich droplets.



The conversion of F with high chemical potential μ_F to W with low chemical potential μ_W drives the reaction. In other words, the required energy to convert A to B is transduced by the conversion of the chemical potential $\Delta\mu_F = \mu_F - \mu_W > 0$. Thus, the precursor A acts as a catalyst for the fuel-to-waste conversion that transduces energy to B . In other words, a metabolism regulates active droplets, which is an essential property of living systems. The energy is typically stored in fuels of high chemical potential, like ATP, GTP, and NADH, and is transduced by hydrolysis or reduction to their corresponding waste products.^[40] These molecules can efficiently store energy as they hardly degrade in the absence of a catalyst.^[40] In the second reaction, B typically degrades by reacting with an ubiquitous species in the reaction solution (indicated by X) to recover the initial catalyst A (equation (4)).^[41] For example, X can be a molecule of water or a reducing agent. Thus, the regulation of active droplets by chemical reactions can be illustrated by a reaction cycle (Figure 5B). Oversimplified, this cycle is driven by the conversion of F to W . For example, the net reaction that drives microtubule polymerization is the hydrolysis of GTP ($GTP + H_2O \rightarrow GDP + P_i$).^[42]



The degradation of B can either occur inside or outside the product-rich droplets. When the degradation of B occurs inside the droplets, an efflux of A from the droplet to the solution arises (Figure 5A). The precursor may be converted again to the product that can diffuse into droplets and replenish the spontaneously degraded B inside the droplets, e.g., as in case of active coacervate droplets.^[43] In contrast, active oil droplets composed of phase-separating anhydride products require water to degrade, which these oil droplets exclude.^[44] In this case, B is degraded in solution and replenished by B from the droplets, resulting in an efflux of B from the droplets to the solution.

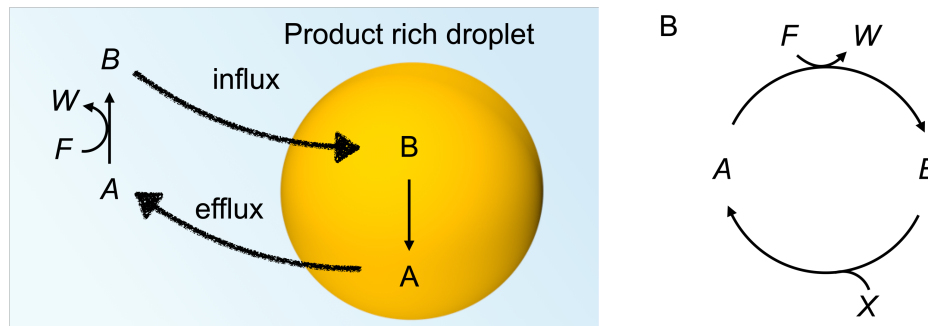


Figure 5: **A)** Schematic representation of chemical reactions and diffusive fluxes for the phase separation of product B formed from precursor A and driven by a chemical fuel F with the degradation reaction localized inside the droplets. Adapted from reference [38] by permission from IOP Publishing Ltd., Copyright © 2019. **B)** Schematic representation of the reaction cycle of precursor A which is converted into the phase-separating product B at the expense of fuel F .

2.3.2. Noise Reduction by Phase Separation of Active Droplets

The synthesis and turnover of proteins by chemical reactions can cause non-equilibrium fluctuations and noise in concentration, which is disadvantageous for biological systems. It has been shown that LLPS can reduce the noise in expressed protein concentration.^[45] The constrained concentration outside of the droplets reduces the noise. Any increase in the total protein concentration will change the number of droplets and sizes, but the concentration outside remains unaffected. Theoretical calculations show that the noise strength declines when the mean total concentration $\bar{\phi}$ approaches the threshold concentration for phase separation ϕ^* (Figure 6). After that, the noise strength settles at a certain minimum, dependent on the diffusion and chemical reactions. This minimal noise strength depends on the time scales of protein diffusion and turnover. When diffusion is much faster than protein turnover ($\tau_D \gg \tau_p$), phase separation can reduce the noise to the Poisson limit, *i.e.*, in quasi-equilibrium conditions. However, when the protein turnover rate approaches protein diffusion ($\tau_D \approx \tau_p$), the minimal noise strength increases. This means that proteins accumulate in the dilute phase due to fast synthesis and slow diffusion, which hampers the efficiency of noise reduction. In other words, phase separation most effectively reduces noise for long-living and fast-diffusing proteins. Taken together, phase-separated compartments can effectively buffer concentration oscillations, enabling them to maintain the protein concentration within a narrow concentration range. The noise reduction by phase separation could be a relevant mechanism in biological systems to enhance their robustness.

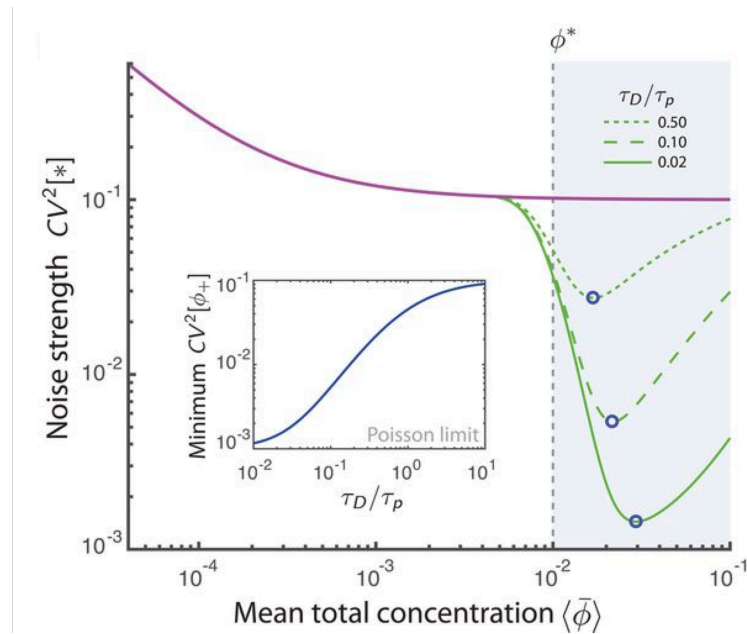


Figure 6: Noise strength in dependence on the mean total concentration for different protein diffusion times and protein lifetimes (τ_D and τ_p , respectively). The minima of the noise strength strongly depend on the ratio τ_D/τ_p (blue circle and inset). Figure from reference [45]. Reprinted with permission from AAAS.

2.3.3. Self-Division of Active Droplets

Theoretical calculations showed that the kinetic control of droplets by chemical reactions could endow them with properties that significantly differ from properties at thermodynamic equilibrium. Zwicker *et al.* showed that spherical droplets regulated by chemical reactions can grow and spontaneously split into two smaller daughter droplets of equal size, reminiscent of cellular behavior (Figure 7).^[46] These spherical droplets can undergo shape instabilities and split into two smaller droplets despite their surface tension. These shape instabilities are thermodynamically unfavored and require non-equilibrium conditions. A droplet undergoes different stages before division. At first, a droplet grows until it reaches a stationary size. After that, it elongates and forms a dumbbell shape. Finally, the dumbbell splits and divides into two smaller droplets of equal size, which can grow and self-divide again.

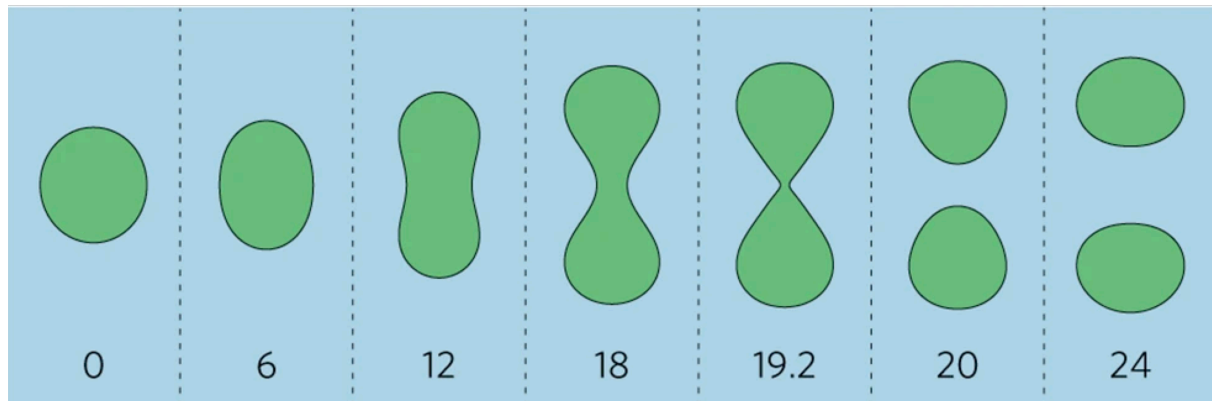


Figure 7: Sequence of stages at different times during active droplet division due to shape instabilities. Reprinted from reference [46] by permission from the Nature Publishing Group, Copyright © 2016.

The shape instabilities are dependent on the supersaturation ε and the turnover ν of the droplet material inside droplets. The supersaturation ε means the excess concentration of droplet material outside the droplet which results for $\varepsilon > 0$ in a diffusive flux towards the droplets. For a given turnover ν , a stationary state exists where the influx of the phase-separating product B due to supersaturation outside is balanced by the efflux of precursor A which is produced inside the droplets. A spherical droplet undergoes shape instability when the supersaturation increases and its radius reaches a critical value R_{div} , which depends on the reaction rates and droplet parameters. The spherical shape becomes unstable beyond that critical radius, and any shape deformation can trigger dumbbell formation through elongation of the droplet shape along one axis.

2.3.5. Suppression and Acceleration of Ostwald Ripening of Active Droplets

Stabilizing an emulsion over longer times is challenging as a system of multiple droplets is thermodynamically unstable.^[47] Droplets typically grow and fuse by droplet coalescence and Ostwald ripening until one big and stable droplet is formed. Thus, both processes have to be suppressed to stabilize emulsions over time. Zwicker *et al.* showed that Ostwald ripening can be suppressed when chemical reactions regulate droplets.^[48] Why are droplets growing, and how can chemical reactions suppress this behavior? Droplets strive to minimize their free energy, which is the smallest for droplet configurations with minimal interface area. This means that larger droplets (smaller surface-to-volume ratio) are energetically favored over multiple smaller droplets with the same total droplet volume. Ostwald ripening is driven by a diffusive flux between droplets which is caused by a difference in volume fractions ϕ_{\pm}^B of the droplet material outside of the droplets. The Laplace pressure dictates the volume fraction of product

outside a droplet, which is thus dependent on the surface tension γ and the droplet radius R (equation (5)). As shown in equation (5), the volume fraction of product outside the droplets ϕ_+^B is larger for smaller droplets, *i.e.*, smaller radius R (Figure 8A).^[44a]

$$\phi_+^B = \gamma\beta/R \quad (5)$$

In other words, the local concentration of the phase-separating product is higher around small droplets compared to bigger ones which causes a diffusive flux of droplet material from small to big droplets (Figure 8B).

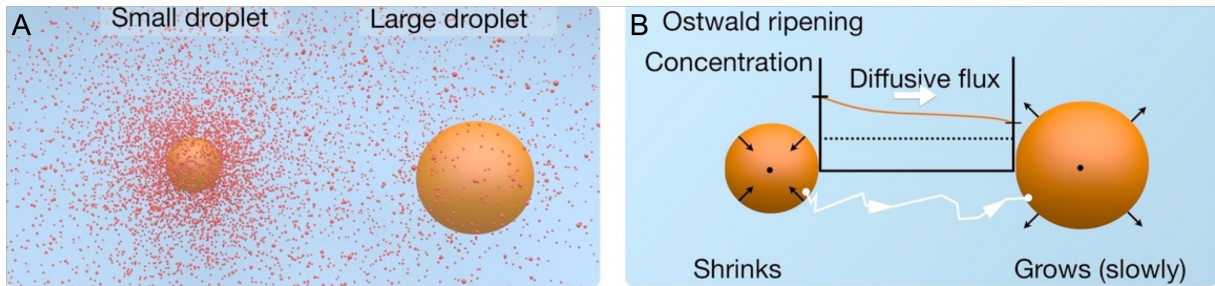


Figure 8: **A)** Schematic representation of volume fractions ϕ_+^B of phase-separating product outside the droplets for small and large droplets. **B)** Schematic representation of the diffusive flux from small to large droplets caused by the difference in volume fractions. Figures adapted from reference [44a].

Zwicker *et al.* considered a simplified system of two droplets for their calculations. They show that a steady-state with two equally sized droplets is unstable in the absence of chemical reactions as one droplet always grows at the expense of the other. In this system, only steady-states with a single droplet or without droplets are stable. In contrast, when chemical reactions regulate droplets, a steady-state with two coexisting droplets at equal sizes can be stable. The rate of relaxation to the steady-state is dependent on the degradation rate of the product k_b (equation (6)).

$$\lambda = \frac{D_B\gamma\beta}{\bar{R}^3} - \frac{2k_b}{3} \quad (6)$$

For a relaxation rate of $\lambda > 0$, the steady-state is unstable and large droplets grow at the expense of smaller droplets, which means that droplets ripen. Without chemical reactions, equation (6) simplifies to $\lambda = D_B\gamma\beta\bar{R}^{-3}$ which is always positive. Thus, Ostwald ripening will always occur in a system of passive droplets.

In contrast, for $\lambda < 0$, a steady-state with multiple droplets is stable and Ostwald ripening is suppressed. They used a single dimensionless stability number χ to predict the maximal number of stable droplets N at given parameter values (equation (7)). The number is defined

such that $\chi > 1$ corresponds to negative relaxation rates which means that a steady-state of N droplets is stable at these reaction rates.

$$\chi = \frac{V_S}{2\pi D_B \gamma \beta N} - \frac{k_f k_b}{k_f + k_b} \quad (7)$$

The dimensionless stability number shows that the number of stable droplets increases with the rate of chemical reactions. At vanishing reaction rates, droplets behave like their passive counterparts. A state with multiple stable droplets and suppression of Ostwald ripening exists for intermediate reaction rates. However, too large reaction rates result in the breakup of droplets. This means that adjusting the rate constants for chemically active droplets can control the droplet size and number of stable droplets.

In contrast, Tena-Solsona *et al.* showed that active oil droplets comprised of transient anhydride products grow orders of magnitude faster than expected for Ostwald ripening.^[44a] Moreover, the rates of the chemical reaction cycle can regulate the accelerated growth of the droplets. They observed that the deactivation rate dictates the acceleration of ripening, *e.g.*, higher acceleration of ripening for faster deactivation rates (Figure 9A). When fueled with a single batch of fuel, big droplets did not grow, wherefore the increase of average droplet volume can be attributed to an accelerated shrinkage of small droplets due to the deactivation reaction (Figure 9B). In contrast, when continuously fueled, large droplets showed accelerated growth while small droplets showed accelerated shrinkage, which explains the higher acceleration of ripening compared to batch-fueled experiments (Figure 9C).

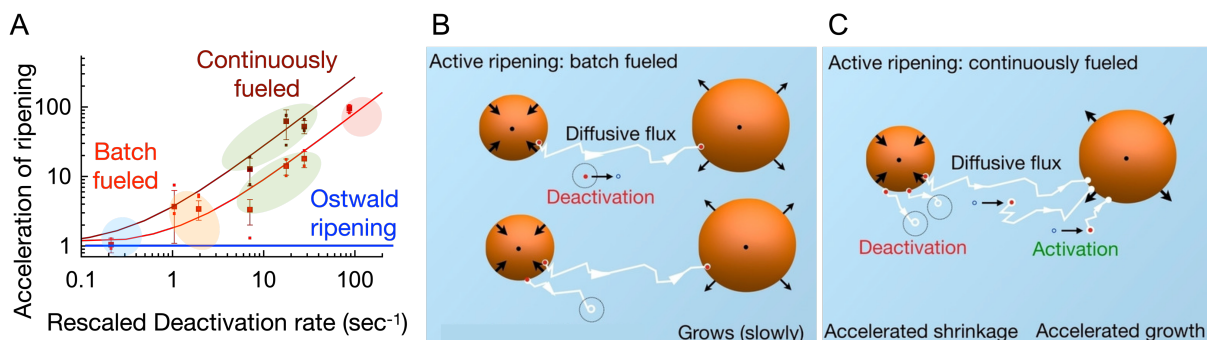


Figure 9: **A)** Acceleration of ripening as a function of the deactivation rate for batch- and continuously fueled active droplets. **B)** Schematic representation of the accelerated ripening of batch-fueled active droplets. The deactivation reaction accelerates the shrinkage of small droplets. **C)** Schematic representation of the accelerated ripening of continuously fueled active droplets resulting in accelerated shrinkage of small droplets and accelerated growth of big droplets. Figures adapted from reference [44a].

2.4. Conclusion and Outlook

Compartmentalization of living systems is crucial for their internal organization and separation from the surroundings. Compartments regulate complex biochemical reactions by increasing, decreasing, or inhibiting reactions through up-concentration or segregation of reagents. The regulation is based on diffusion of reactants in- and outwards a boundary that separates the compartment from its surroundings.

The first type of compartments in biological systems is separated by a membrane from the environment, *i.e.*, a membrane-bound compartment. However, as membranes are typically impermeable to most biological molecules, they require complex machinery to regulate the diffusion of specific reagents, which is disadvantageous in a bottom-up approach for the synthesis of life.

The other type of compartments in living systems are MLOs which lack a physical barrier to their surroundings and are thus more attractive for a bottom-up approach. MLOs have liquid-like properties, which suggest that they form through LLPS. The liquid nature of MLOs enables fast diffusion of reactants in- and outwards of the droplets and the partitioning of molecules can be regulated by the composition of the droplets. Typically, these droplets are comprised of protein and nucleotides, and multivalence between these building blocks drives their phase separation. Phase separation occurs when the attractive interactions between the building blocks or the repulsive interactions between building blocks and solvent exceed the entropic tendency of the system to remain mixed.

Biological systems use chemical reactions to tune the attractive and repulsive interactions between building blocks and the solvent to regulate where and when phase separation occurs. When chemical reactions regulate phase separation, droplets are considered active droplets. Active droplets are controlled kinetically by an external energy supply, which means that their properties are not governed by the rules of in-equilibrium thermodynamics, *e.g.*, controlled by fuels with high chemical potential like ATP and GTP. Theoretical calculations and experimental studies showed that active droplets under kinetic control could have significantly different properties than droplets controlled by thermodynamics, *e.g.*, noise reduction in building block concentrations, self-division of droplets, and acceleration or suppression of Ostwald ripening. Especially, the contrast between acceleration or suppression of Ostwald ripening for different reaction rates indicates the variety of different properties that can be observed when droplets are kinetically controlled by chemical reactions.

Even more complex behavior can be expected when not only the phase separation of active droplets is regulated by chemical reactions but also the assembly reciprocally regulates the chemical reactions. In other words, the assembly exerts feedback on its regulating reaction cycle which I will discuss in the next chapter.

3. Feedback Mechanisms

Abstract.

In Chapter 2, I described the types of different compartments in living systems and how biology regulates the phase separation of MLOs by chemical reactions. Moreover, dependent on the rates of the regulative chemical reactions, I showed that droplets under kinetic control could have significantly different properties than under thermodynamic control, *e.g.*, suppression or acceleration of Ostwald ripening and self-division of droplets. In this chapter, I will show that biological assemblies can also reciprocally regulate their chemical reaction cycles, *i.e.*, feedback of the assembly onto its reaction cycle. These feedback mechanisms are crucial for regulation and control in living systems and could result in life-like behavior in synthetic systems. For example, I will demonstrate how feedback mechanisms can control the nucleation and length of biological assemblies. After that, I will show recent examples of synthetic, chemically fueled assemblies that exert feedback on their reaction cycle and discuss their different feedback mechanisms.

Parts of this chapter are based on the following publications:

[1] P. S. Schwarz, M. Tena-Solsona, K. Dai, J. Boekhoven, *ChemComm*, **2021**, accepted.

3.1. Feedback Mechanisms and their Role in Living Systems

Chemical reactions often regulate assembly and phase separation in biological systems. *Vice versa*, biological assemblies can regulate their underlying chemical reactions, *i.e.*, the assembly exerts feedback on its reaction cycle. Living systems require feedback mechanisms to precisely regulate, control, and coordinate the interplay among the vast number of different building blocks and reaction networks. In these reaction networks, the products of one reaction can serve as the reactants for another reaction.^[37] For example, feedback mechanisms regulate metabolic reaction networks, cellular signaling systems, and other internal cellular mechanisms, which can result in complex dynamic behavior, such as bistability, hysteresis, and oscillations.^[49] A feedback mechanism is defined as a response within a system that adjusts the rate of production of the elements of a system to its state and relevant environmental variables.^[50] In other words, if a specific component within a system levels its activity, than it regulates itself *via* a feedback mechanism.^[51] This feedback mechanism can either be positive or negative depending on whether the component accelerates or decelerates its production rate. The feedback is positive when a product *B* accelerates its production from a precursor *A* (Figure 10A). An example of positive feedback in biology is the ripening of fruits. When fruits ripen, they release ethylene which accelerates the ripening of other fruits that further release ethylene.^[52] In contrast, if *B* decelerates its production rate from *A*, it exerts negative feedback on its production (Figure 10A). Biological systems use negative feedback to stabilize processes against fluctuations, changes in their surroundings, or other disturbances and as vital control mechanisms to remain homeostasis.^[37, 53] For example, negative feedback regulates the blood glucose level. When the blood glucose level increases, insulin is released into the bloodstream causing cells to store glucose as intracellular triglycerides and glycogen, thus lowering the blood glucose level.^[54]

Like these feedback mechanisms, self-assembled or phase-separated structures can also exert feedback on the reactions that produce or degrade their components. For example, the depolymerization of microtubules is dependent on their filament length.^[55] The length-dependent depolymerization of microtubules can be explained by an antenna model in which kinesin-8 and other motor proteins that depolymerize microtubules randomly bind along their length (Figure 10B). These motor proteins have a high processivity that funnels them to the plus end of the microtubules. The high processivity results in an increasing concentration gradient of motor proteins towards the plus end, *i.e.*, almost all motor proteins reach the plus end of the microtubule. As the number of landings is proportional to the length of the microtubule, longer microtubules depolymerize faster than shorter microtubules. In summary,

the higher the processivity of the motor proteins, the more pronounced is the length-dependent depolymerization of the microtubules.

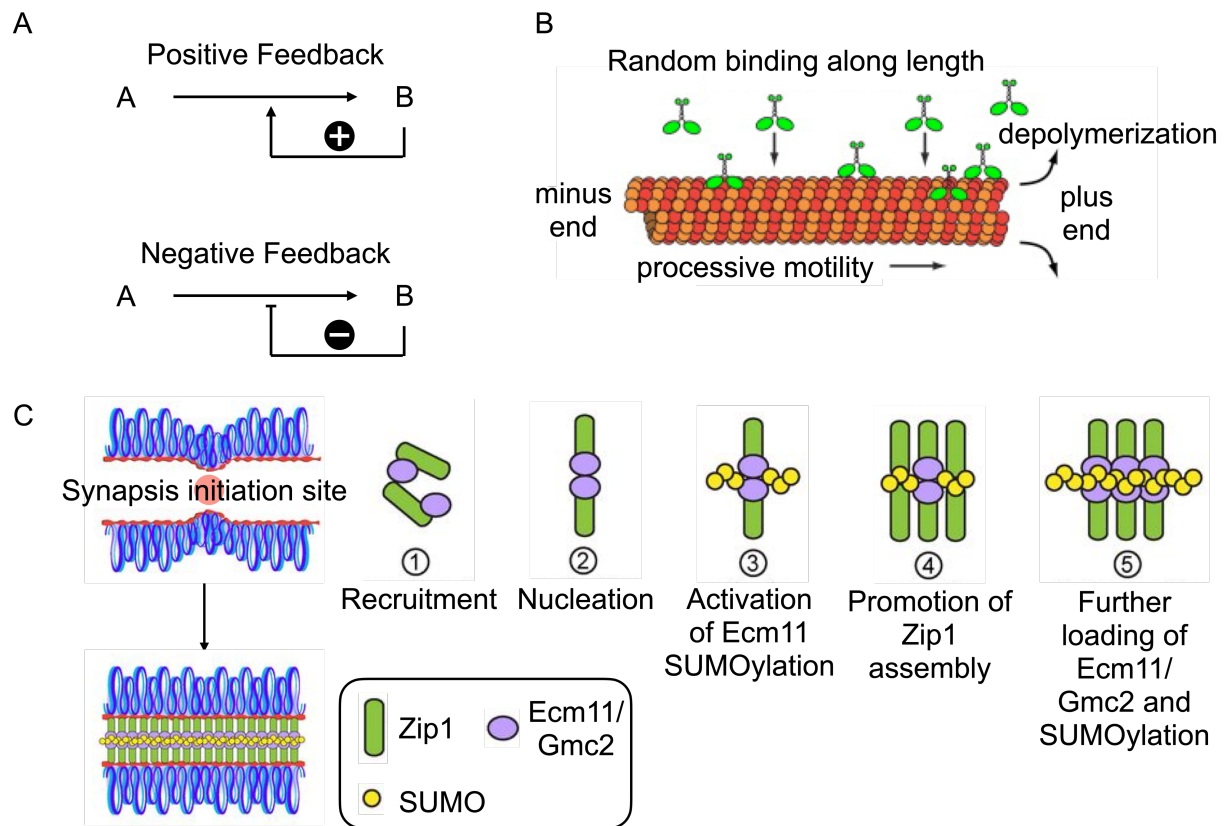


Figure 10: **A)** Schematic representation of positive and negative feedback of a component *B* on its production from precursor *A*. **B)** Antenna model of microtubule depolymerization. Longer microtubules depolymerize faster due to the higher probability of motor proteins landing on the microtubule lattice. Adapted from reference [55a] by permission from Elsevier Ltd., Copyright © 2009. **C)** Positive feedback regulation of the synaptonemal complex between polySUMOylation of Ecm11 and transverse filament assembly. Figure adapted from reference [56].

The synaptonemal complex (SC) is also a feedback-regulated self-assembled structure. The SC connects the homologous chromosomes along their lengths via polymeric arrays of transverse filaments (TFs) during meiotic prophase I. Thus, the control of TF polymerization is crucial for the self-assembly of the SC. Leung *et al.* found that positive feedback regulates the self-assembly of the synaptonemal complex (Figure 10C).^[56] In the first phase, the TF protein of budding yeast (Zip1) and protein components of the SC (Ecm11 and Gmc2) are recruited to synapsis initiation sites. In the second phase, Zip1 nucleates in association with Ecm11/Gmc2. They found that the *N*-terminus of Zip1 activates the SUMOylation of Ecm11.

The SUMO chains facilitate the recruitment and assembly of more Zip1, which further activates Ecm11 for SUMOylation, *i.e.*, polymerization of the SC is based on a positive feedback loop.

3.2. Feedback in Chemically Fueled Reaction Cycles

In the previous section, I discussed the role of feedback control and regulation in biological systems. In particular, the design of feedback mechanisms of self-assembled or phase-separated structures on the chemical reactions that produce and destroy their components could be a step towards the bottom-up synthesis of life. The combination of a compartment that is regulated by chemical reactions and feedback mechanisms of the assembly onto the regulating chemical reactions could result in other essential properties of life, such as self-replication and adaptability. In the following section, I will discuss recent examples of feedback mechanisms of synthetic assemblies that are regulated by chemical reactions. These assemblies exert feedback on regulating chemical reactions *via* two different mechanisms: catalysis, and up- or down-concentration.

3.2.1. Feedback by Catalysis

Self-assembled structures can be catalytically active and increase the rate constant or decrease the activation energy of a chemical reaction that regulates the assembly, *i.e.*, the assembly catalyzes its reaction cycle. One mechanism by which the assembly can catalyze a reaction of the regulating reaction cycle is by changing the microenvironment of the reactants. For example, Bal *et al.* reported that histidine moieties in self-assembled amphiphiles (C18H) can catalyze the activation and deactivation in EDC-driven reaction cycles (Figure 11).^[57] They fueled C18H with EDC in the presence of *p*-nitrophenol (NP), resulting in the formation of C18H-NP ester and a rapid gel formation. The reactive histidine group cooperatively catalyzes the assembly and disassembly process. On one hand, it serves as a base and enables the ester formation of alcohol and carboxylic acid. However, in this case, the activation reaction can also be catalyzed by non-assembling peptides which means that the catalysis is not related to self-assembly. On the other hand, histidine influences the local pH in the self-assembled state and thus catalyzes the hydrolysis of the kinetically stable ester bond. They showed that the histidine group as well as the microenvironment of the self-assembled fibers are crucial for the disassembly and gel-to-sol transition as the ester hydrolyzes only in the presence of fibers. They also showed that the concept of cooperative catalysis of histidine is applicable for other systems, *e.g.*, amyloid peptides.^[58]

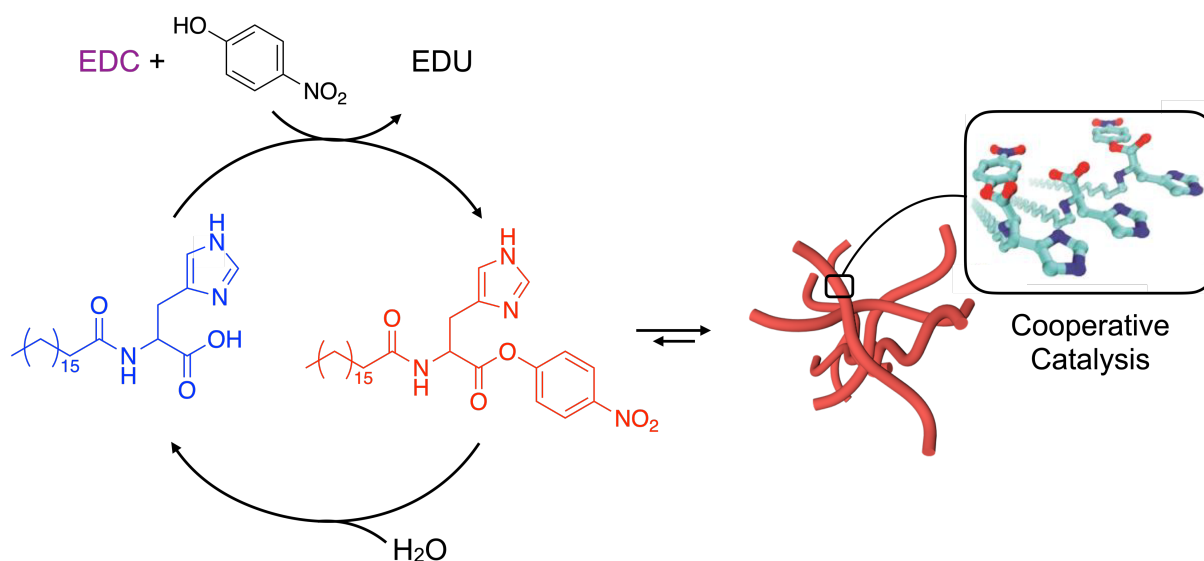


Figure 11: Schematic representation of the EDC-driven reaction cycle of a C18H precursor, resulting in the transient formation of C18H-NP nanofibers in the presence of *p*-nitrophenol (NP). The nanofibers cooperatively catalyze the assembly and disassembly process. Adapted from reference [57] by permission from the Wiley-VCH Verlag GmbH, Copyright © 2019.

Recently, Kriebisch *et al.* showed that regulating reaction cycles and self-assembly of peptide nanofibers can be reciprocally coupled (Figure 12).^[59] They also found that the emerging assemblies change the microenvironment of their components which accelerates both the activation and deactivation pathway in EDC-driven reaction cycles. Upon addition of fuel, the Fmoc-AVD precursor assembles in peptide fibers which are comprised of precursor and anhydride products. The hydrophobic microenvironment of the assembly increases the pK_a of co-assembled precursors, which changes the activation pathway from a stepwise proton transfer to a concerted proton transfer. The concerted proton transfer is drastically faster and results in a roughly five times higher fuel consumption rate. Moreover, the deactivation rate of the anhydride product is increased in the presence of assemblies which is likely due to β -sheet hydrogen bonding interactions. These interactions significantly increase the carbonyl carbon's electrophilicity, wherefore the nucleophilic attack of water molecules is favored.

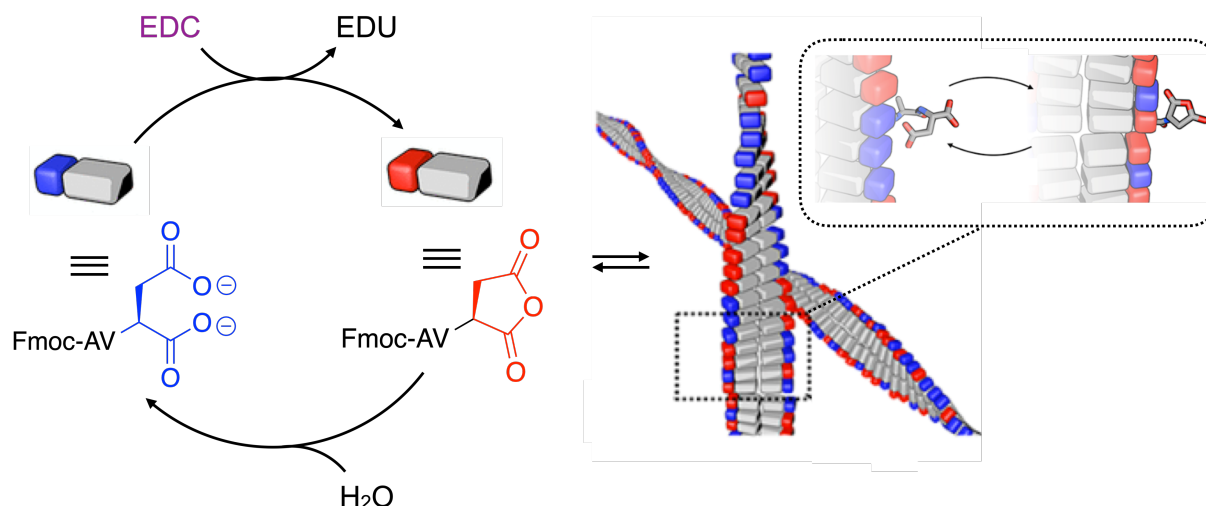


Figure 12: Schematic representation of the EDC-driven self-assembly of a Fmoc-AVD precursor in peptide nanofibers. The assembly is reciprocally coupled to the reaction cycle as self-assembly is regulated by activation and deactivation which both are catalyzed in the assembly's hydrophobic microenvironment. Adapted with permission from reference [59], Copyright © 2020 American Chemical Society.

Borsley *et al.* showed that differences in the microenvironment of a catalytic carboxylate on a rotaxane precursor can result in kinetic gating and thereby drive a molecular information ratchet (Figure 13).^[60] They used a rotaxane precursor with a catalytic carboxylate group and two fumaramide (prox- and dist-co-conformers) binding sites for a benzylic amide macrocycle. An *N*-acyl pyridinium barrier for the ring movement is formed at the catalytic carboxylate group upon the addition of DIC and pyridine. The addition of the chemical fuel changes the ratio of the macrocycle's prox:dist equilibrium population from roughly 1:1 to 1:12. The equilibrium population changes because both fuel addition and waste production are kinetically gated, *i.e.*, activation and deactivation favor the forward stepping of the machine. The activation is kinetically gated as the barrier formation for the dist-rotaxane is twice as fast as for the prox-rotaxane due to steric hindrance of the macrocycle. The deactivation is kinetically gated as hydrogen bonds between the macrocycle and the activated ester increase the hydrolysis rate of the prox-rotaxane's barrier by an 8-fold compared to the dist-rotaxane. The doubly kinetic gating of the rotaxane drives the significant shift in the population of the two binding sites. After depletion of the fuel, the hydrolysis of the barrier restores the equilibrium population of 1:1.

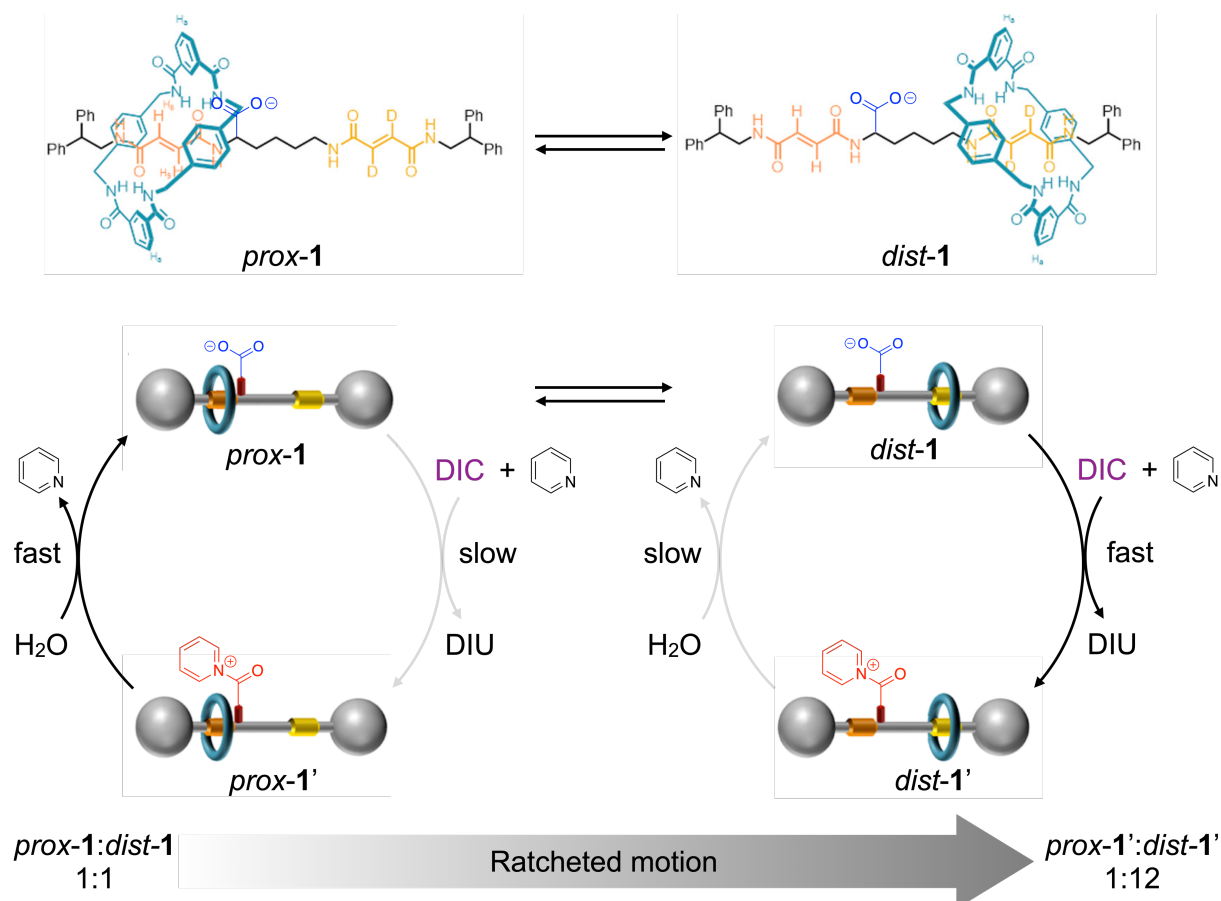


Figure 13: Schematic representation of a chemically fueled, doubly kinetically gated information ratchet. Activation and deactivation in the reaction cycle favor the machine's forward stepping, which drives the significant shift in the population of the two binding sites from 1:1 to 1:12. Adapted with permission from reference [60], Copyright © 2021 American Chemical Society.

Apart from changing the microenvironment of reactants, an assembly can also catalyze a reaction of its regulating reaction cycle by replication which can occur *via* two different mechanisms. In the first mechanism, the replicator is composed of two different components, and self-replication occurs by binding these components and templating their conversion into a single replicator, *e.g.*, self-replicating systems of DNA and RNA oligomers.^[27b, 61] So far, these systems remain irreversible, and thus a regulation by chemical reactions has not yet been realized. The second mechanism of self-replication is based on supramolecular polymerization. In a supramolecular polymerization, the assembly catalyzes the ligation of components and thus results in the formation of replicator stacks.^[27b] In this case, exponential replicator growth is observed when stacks are constantly broken, *e.g.*, by mechanical force through stirring. Upon breaking, the number of replicative ends of the stacks increases resulting in exponential growth by a breaking-nucleation-elongation mechanism.

For example, Yang *et al.* reported a chemically fueled supramolecular polymerization based on the oxidation of a dithiol precursor driven by a sodium perborate fuel (Figure 14).^[62] Upon oxidation, a mixture of cyclic disulfides of different ring sizes emerges from which trimers and hexamers self-assemble into fiber stacks. Mechanical induced breaking of the stacks increases the number of ends resulting in exponential growth of the replicator. They observed that the replication rate of the hexamer is significantly lower than the rate of the trimer which means that most precursor is consumed by the trimer. The difference in replication rate is most likely related to a higher fragility of trimer fibers which results in a trimer-dominated population. In contrast, the reducing agent TCEP as a fuel for the deactivation of the macrocycles enabled a steady-state with an out-of-equilibrium population of hexamer, which accounted for 60 – 70% of the precursor. Reduction with TCEP regenerates the precursor, which can be re-oxidized to a macrocycle. The population change is most likely caused by a lower reduction rate of the hexamer compared to the trimer. This means that in the absence of fuel, the population reverts to the trimer-dominated population. In summary, the combination of oxidant and reductant mediate the re-population of high-energy states, which enables populating molecularly more complex replicators.

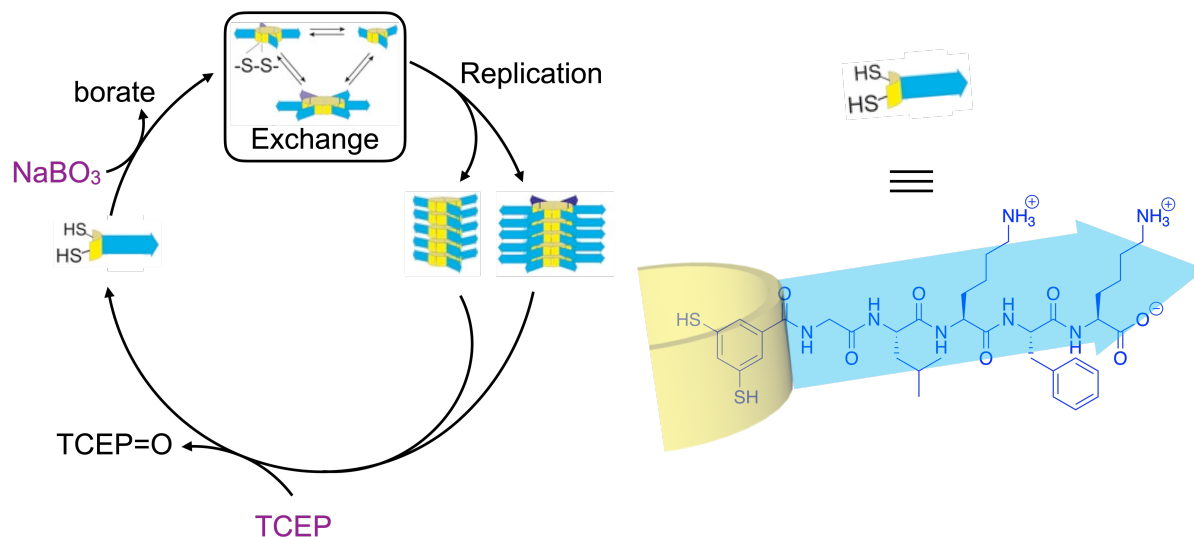


Figure 14: Chemically fueled self-assembly of a dithiol precursor in replicator stacks (trimer vs. hexamer) driven by oxidation with sodium perborate and reduction with TCEP. Adapted from reference [62] by permission from the Wiley-VCH Verlag GmbH, Copyright © 2021.

Another example for catalysis by replication is the chemically fueled cooperative polymerization of a perylene diimide (PDI) derivative reported by Leira-Iglesias *et al.*

(Figure 15).^[63] They used $\text{Na}_2\text{S}_2\text{O}_4$ as a chemical fuel to reduce the neutral PDI to mostly monomeric PDI^{2-} . Oxidation by atmospheric oxygen converts the monomeric PDI^{2-} to neutral PDI. The neutral PDI undergoes cooperative supramolecular polymerization to micrometer-sized colloidal assemblies. Similar to the previous example, fragmentation of the supramolecular polymers results in positive feedback due to a breaking-nucleation-elongation mechanism. Moreover, the supramolecular polymer exerts negative feedback on its disassembly as the reductant reacts with the colloidal assembly's outer shell, which means that larger assemblies have slower reduction rates. The cooperative nature of the polymerization enabled them to control the spatiotemporal behavior, e.g., traveling fronts and patterns, by seeding with assembled PDI. Moreover, the system oscillated dependent on the rate constants k_{red} and k_{ox} .

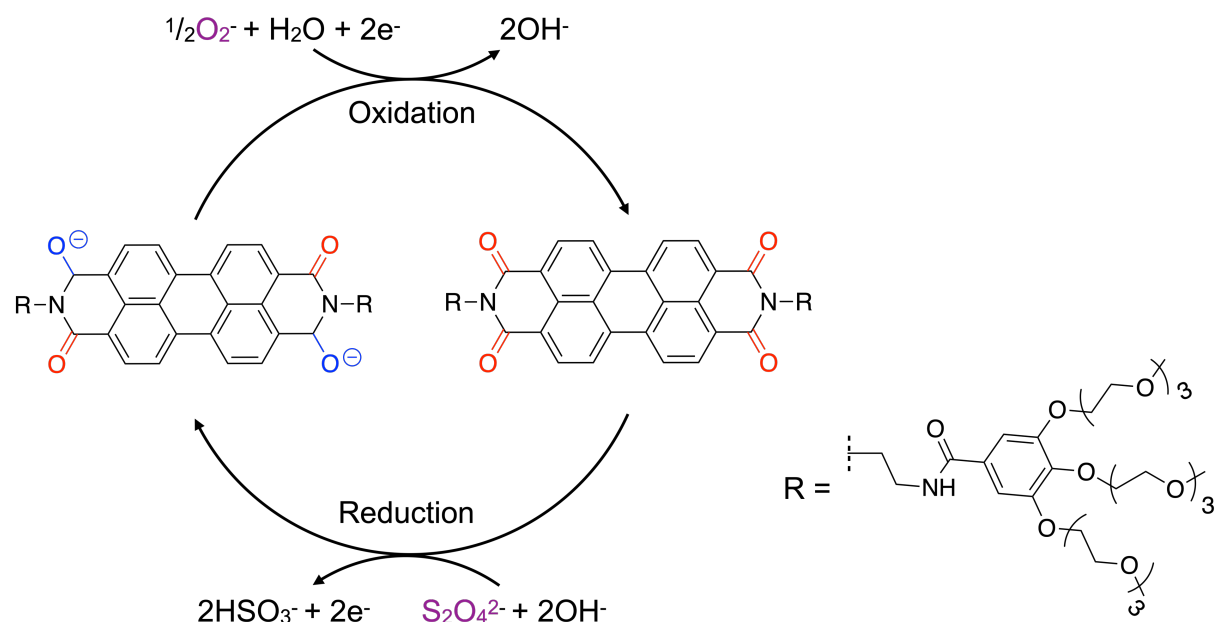


Figure 15: Schematic representation of the redox-fueled reaction cycle of monomeric PDI^{2-} . Adapted from reference [63] by permission from Springer Nature Ltd., Copyright © 2018.

3.2.2. Feedback by Up- or Down-Concentration

Another mechanism by which self-assembled structures can exert feedback on their regulating chemical reactions is by up- or down-concentration of reactants. An up- or down-concentration of reactants influences their availability for the chemical reactions and thus increases or decreases their rates. In contrast to catalytic feedback, an up- or down-concentration is not changing a rate constant.

For example, Morrow *et al.* reported a chemically fueled system that self-replicates due to an up-concentration of reagents (Figure 16).^[64] The system is based on two phase-separated precursors which react to a surfactant product under the formation of one equivalent of a thermodynamic byproduct. The surfactant product forms micelles above its CMC, which solubilize and up-concentrate the hydrophobic precursor in the aqueous phase and thus accelerate the rate of surfactant product formation. Thiol-disulfide exchange with the precursor deactivates the replicator, resulting in the formation of another equivalent of the thermodynamic byproduct and a non-functional waste. They used the oxidizing agent H_2O_2 as a chemical fuel to regenerate the high-energy precursor *in-situ* from the non-functional waste.

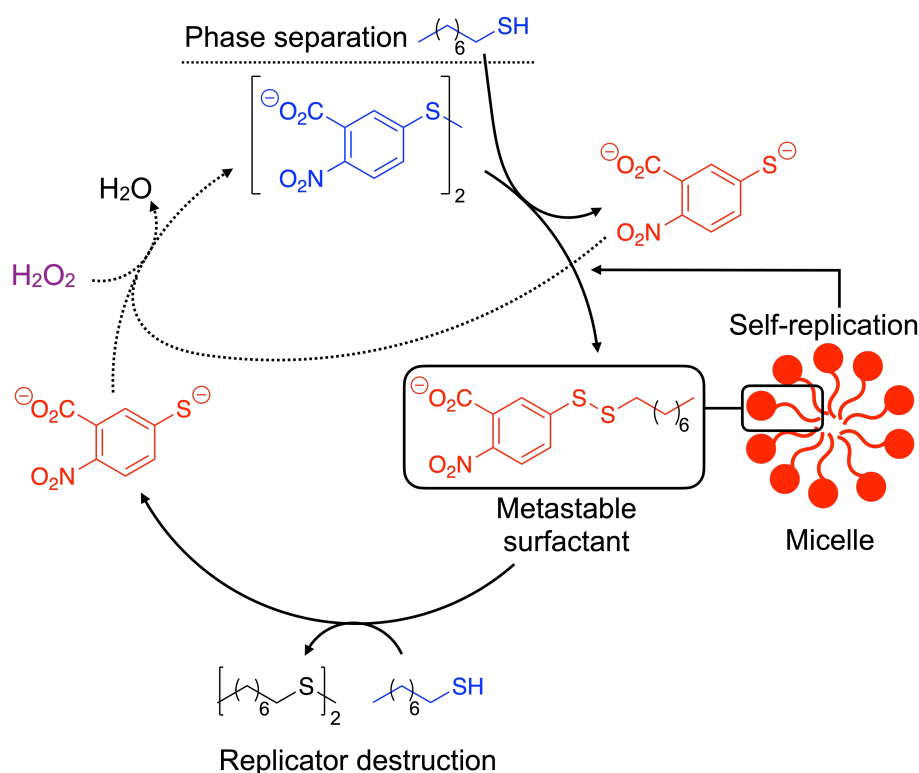


Figure 16: Schematic representation of a chemically fueled reaction cycle of two phase-separated precursors which form a surfactant product. The surfactant product forms micelles above its CMC, which catalyze the formation of its building blocks and thus self-replicates. Adapted from reference [64].

Another example for feedback of the assembly onto its reaction cycle by up- or down-concentration is reported by Tena-Solsona *et al.* (Figure 17).^[44b] They found that fueling aliphatic carboxylic acids with EDC resulted in transient anhydride formation and phase separation in micron-sized droplets. Phase separation in droplets down-concentrates the anhydride in the aqueous phase that hydrolyzes, *i.e.*, droplets protect anhydride molecules inside from deactivation. The fraction of anhydride that hydrolyzes is equal to its solubility,

resulting in a characteristic zeroth-order deactivation due to a constant hydrolysis rate. Tena-Solsona *et al.* used the protection mechanism to select certain non-equilibrium products over others when propionic acid (C_3 , $n=1$) and valeric acid (C_5 , $n=3$) precursors competed for EDC.^[44b] They found that the anhydride products C_3C_3 and C_3C_5 are soluble in the aqueous media. In contrast, the most hydrophobic product C_5C_5 is insoluble. The protection mechanism enabled C_5C_5 to survive starvation periods. Thus, phase separation selects C_5C_5 over the other products, as it down-concentrates the fraction of anhydride that hydrolyzes. Moreover, due to the constant zeroth-order deactivation of the anhydride, Wanzke *et al.* used the protection mechanism of oil droplets for the controlled linear release of hydrophobic drugs.^[65]

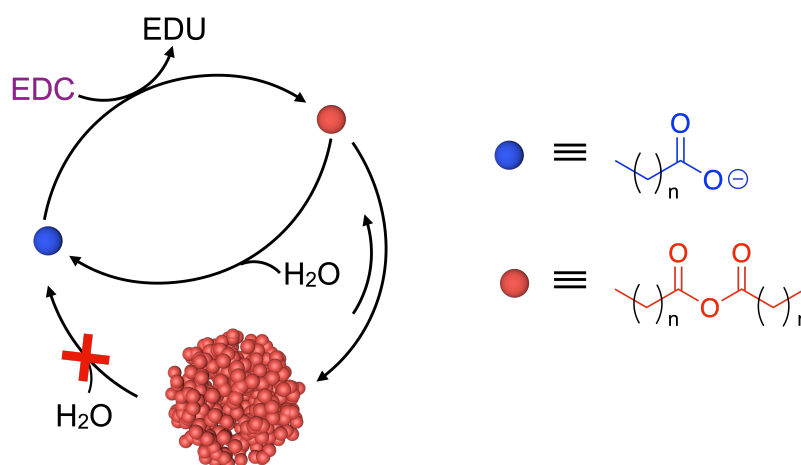


Figure 17: Phase-separated anhydride products in EDC-driven reaction cycles exert negative feedback on their deactivation as droplets down-concentrate the fraction of anhydride that is susceptible to hydrolysis. Adapted from reference [44b].

3.3. Conclusion and Outlook

Feedback mechanisms play an essential role in the regulation and control processes of biological systems. In a feedback mechanism, a component influences or levels its activity which can either be positive or negative depending on whether it accelerates or decelerates its production rate. For example, living systems control the length and nucleation of biological assemblies by feedback mechanisms. Thus, the design of feedback mechanisms in synthetic systems could be a step towards the bottom-up synthesis of life. Recently, several examples of synthetic chemically fueled assemblies are reported which exert feedback on their reaction cycles, *e.g.*, feedback based on replication, catalysis, and up-or-down concentration of reagents. Such self-assembled structures could serve as metabolically active compartments which means that these systems already have two essential properties of living systems. Consequently, feedback mechanisms in such systems are exciting as they could result in other

Feedback Mechanisms

essential properties, like adaptability or self-replication. So far, the chemically fueled oil droplets reported by Tena-Solsona *et al.* are the only example of phase-separated active droplets that exert feedback on their reaction cycle which is why I chose them for the following experimental part of the thesis.

4. Aims of the Thesis

The overarching goal of this thesis was to design a synthetic system comprised of simple molecules and precursors that shows some life-like behavior. Such a system could be relevant as a model system to gain insights into life's origin or could be applied as a life-like material.

In Chapter 1, I discussed essential properties of biological systems, which a synthetic system must have to be considered alive, such as energy transduction, compartmentalization, information processing, growth and division, and adaptability. Chapter 2 showed that membraneless compartments are ideal to create a synthetic living system as the absence of a membrane and their liquid nature facilitate the diffusion in- and outwards of the compartment. As a starting point for designing a system with life-like behavior, I thus chose chemically regulated droplets as they already combine two essential properties of life, namely compartmentalization, and energy transduction. Despite the impressive progress in chemically fueled self-assembly, these systems are still far from being alive. Other essential properties of living systems could be observed when the assembly also regulates the reaction cycle's kinetics via feedback mechanisms as discussed in Chapter 3.

To create a synthetic system with some life-like behavior, the first aim of the thesis is to investigate how the negative feedback of oil droplets in Chapter 3 affects the kinetics of the products when multiple, simultaneously operating reaction cycles compete for fuel. In general, the competition of metabolic reaction cycles for a common nutrient causes lower product yields and lifetimes. In other words, both reaction cycles suffer as they have to share the resources. However, in Chapter 5, we found a counterintuitive behavior where the success of a succinate derivative can increase when competing with a more hydrophobic succinate derivative, *e.g.*, by more prolonged survival or reduced concentration oscillations in the presence of periodic fueling. When one product phase-separates, the other product can co-phase-separate and exploit the protective environment of the droplets. This behavior is reminiscent of parasitic behavior in biology and shows that life-like behavior can be observed in simple non-equilibrium systems.

Next, we wanted to demonstrate that feedback offers new ways to control materials. Thus, we aimed to design an opposing feedback mechanism that rapidly dissolves the oil droplets once a certain threshold is reached. As described in Chapter 6, I aimed to improve the off-response of the emulsion to gain precise control over the material properties. Typically, these emulsions decay via zeroth-order kinetics and the material properties constantly decrease over their entire lifetime, which is disadvantageous for applications. We found that micelles formed by the surfactant precursor can trigger the solubilization of oil droplets. The surfactant precursor

Aims of the Thesis

accelerates the deactivation of the anhydride product, which releases more surfactant and further accelerates the deactivation, *i.e.*, a self-immolation mechanism. Moreover, we designed the system such that the trigger for the self-immolation is released *in-situ* by the reaction cycle. Unlike common self-immolative materials, these materials switch off themselves through a rapid self-amplifying decay without an external trigger. We applied this self-immolative emulsion as a self-expiring ticket and drug delivery platform, which could serve as a cornerstone for more sophisticated, life-like materials.

In conclusion, this thesis aims to investigate the impact of a negative feedback mechanism on a network of fuel-driven reaction cycles, *i.e.*, how feedback mechanisms affect the products of the reaction cycles. Moreover, I aim to demonstrate that feedback offers new ways of controlling materials, *e.g.*, by an opposing feedback mechanism that enables the precise control over the material properties.

5. Parasitic Behavior in Competing Chemically Fueled Reaction Cycles

Abstract.

In this work, we investigated how the negative feedback mechanism of chemically fueled, phase-separated anhydride droplets described in Chapter 3 affects the kinetics of products when competing for fuel. We created a library of precursors of different hydrophobicity that compete for a common fuel. In the absence of phase separation, we found that the lifetimes of both products decrease due to competition for the common resources. However, the success of a soluble product drastically increases when the product of the competitor phase-separates, *i.e.*, it shows increased persistence and fewer concentration variations in consecutive fueling rounds. We explain this behavior by co-phase separation of the soluble product with droplets formed by the competitor's product. Like a parasite, the soluble product competes with the host for a common nutrient. It exploits its protective environment, which shows that life-like behavior can already emerge in simple networks of chemically fueled reaction cycles. We believe that this mechanism could be a tool to control concentrations of downstream chemical reactions of competitors and that the system could serve as a model system for feedback regulation in networks of reaction cycles.

This work has been published:

Title: Parasitic Behavior in Competing Chemically Fueled Reaction Cycles
Authors: Patrick S. Schwarz, Sudarshana Laha, Jacqueline Janssen, Tabea Huss, Prof. Dr. Job Boekhoven, Dr. Christoph A. Weber
First published: 28. April 2021
Journal: *Chem. Sci.*, **2021**, 12, 7554-7560.
Publisher: Royal Society of Chemistry
DOI: 10.1039/D1SC01106E

Reprinted with permission from *Chem. Sci.* **2021**. Copyright 2021 Royal Society of Chemistry.

This section states the individual work of each author in the publication above. P. S. Schwarz and S. Laha contributed equally. J. Boekhoven and P. S. Schwarz designed the experiments. P. S. Schwarz and T. Huss carried out the experiments. S. Laha, J. Janssen and C. A. Weber worked out the theory. S. Laha and J. Janssen performed the numerical studies and the fitting to the experimental data. P. S. Schwarz, S. Laha, J. Boekhoven and C. A. Weber wrote the manuscript. All authors have given approval to the final version of the manuscript.

Cite this: *Chem. Sci.*, 2021, 12, 7554

All publication charges for this article have been paid for by the Royal Society of Chemistry

Parasitic behavior in competing chemically fueled reaction cycles[†]Patrick S. Schwarz,[‡] Sudarshana Laha,[†] Jacqueline Janssen,^{bc} Tabea Huss,^a Job Boekhoven^{*ad} and Christoph A. Weber^{*bc}

Non-equilibrium, fuel-driven reaction cycles serve as model systems of the intricate reaction networks of life. Rich and dynamic behavior is observed when reaction cycles regulate assembly processes, such as phase separation. However, it remains unclear how the interplay between multiple reaction cycles affects the success of emergent assemblies. To tackle this question, we created a library of molecules that compete for a common fuel that transiently activates products. Often, the competition for fuel implies that a competitor decreases the lifetime of these products. However, in cases where the transient competitor product can phase-separate, such a competitor can increase the survival time of one product. Moreover, in the presence of oscillatory fueling, the same mechanism reduces variations in the product concentration while the concentration variations of the competitor product are enhanced. Like a parasite, the product benefits from the protection of the host against deactivation and increases its robustness against fuel variations at the expense of the robustness of the host. Such a parasitic behavior in multiple fuel-driven reaction cycles represents a lifelike trait, paving the way for the bottom-up design of synthetic life.

Received 24th February 2021
Accepted 28th April 2021DOI: 10.1039/d1sc01106e
rsc.li/chemical-science

Introduction

In chemically fueled systems, the propensity of molecules to form assemblies is regulated by a chemical reaction cycle. In the cycle, a precursor is activated at the expense of a chemical fuel.^{1–8} Simultaneously, a deactivation reaction spontaneously reverts the product to its precursor state. Thus, a population of transient product molecules emerges whose properties are regulated kinetically. In recent years, examples of such reaction cycles have been introduced that regulate the ability of molecules to assemble or phase-separate, resulting in dynamic structures like colloids,^{9,10} fibers,^{10–16} supramolecular polymers,^{17–19} oil-based droplets,^{20,21} coacervate-based droplets,^{22,23} vesicles,^{24–26} micelles,²⁷ particle clusters,^{28–31} macrocycles³² and DNA-based nanostructures.^{33,34} Due to the transient nature of these building blocks, these assemblies are endowed with properties typically absent at thermodynamic equilibrium. For example, fibrils that spontaneously self-divide,³³ temporary

hydrogels,^{10,35–37} or oil-based emulsions of which ripening is accelerated.² Moreover, the theory on active emulsions suggests that droplets can self-divide.^{38,39} More recently, examples of assemblies were observed that exert feedback over their chemical reaction cycle.^{11,27,40,41} The underlying mechanisms can result in exciting behavior like the spontaneous emergence of switches between the morphologies or the ability of molecules to persist while others decay.^{9,20} All these developments in the field are incremental steps towards the synthesis of life, and a living system essentially represents a complex non-equilibrium assembly of molecules that is regulated by chemical reaction cycles.^{42–44} However, in living systems, a vast number of reaction cycles operate simultaneously and interact in intricate networks through feedback mechanisms. While such systems show interesting and complex emergent properties in a close-to-equilibrium context,^{45–50} the behavior of multiple reaction cycles in fuel-driven synthetic systems has been underexplored. In particular, competition and feedback are expected to lead to interesting emergent behavior in such systems. For example, oil droplets showed that selection and inhibition can occur in systems competing for a common fuel.⁵¹

In this work, we show an unexpected behavior in phase-separated emulsions that are regulated by chemical reaction cycles and compete for a fuel. Counterintuitively, the lifetime of a transient product can be vastly prolonged even when resources have to be shared. The underlying mechanism is based on co-phase separation which protects products against

^aDepartment of Chemistry, Technical University of Munich, Lichtenbergstraße 4, 85748 Garching, Germany. E-mail: job.boekhoven@tum.de

^bBiological Physics, Max Planck Institute for the Physics of Complex Systems, Nöthnitzer Straße 38, 01187 Dresden, Germany. E-mail: weber@pks.mpg.de

^cCenter for Systems Biology Dresden, Pfotenhauerstraße 108, 01307 Dresden, Germany

^dInstitute for Advanced Study, Technical University of Munich, Lichtenbergstraße 2a, 85748 Garching, Germany

[†] Electronic supplementary information (ESI) available. See DOI: 10.1039/d1sc01106e

[‡] P. S. S. and S. L. contributed equally.



deactivation, and it shows similarity to how a parasite benefits from the presence of a host.

Results and discussion

We used a chemical reaction cycle that is driven by the hydration of the condensing agent EDC (fuel, 1-ethyl-3-(3-dimethylaminopropyl)carbodiimide). In the activation reaction, the fuel condenses a succinate derivative into its corresponding anhydride product (Fig. 1A). In the aqueous media, the corresponding anhydride rapidly hydrolyses to the initial succinate derivative. We refer to this reaction step as the deactivation. Similar to the fuel-driven reaction cycles in biological systems, the energy obtained from the hydrolysis of EDC is used for the transient activation of the succinate derivative. The population of anhydride product can thus only be maintained when the rate of activation equals the rate of deactivation.⁵²

In this study, we used three succinate derivatives: 2-buten-1-ylsuccinate, which we refer to as precursor, succinate (competitor 1) and 2-hexen-1-ylsuccinate (competitor 2, Fig. 1B). We observed that the addition of fuel to competitor 2 made the solution turn turbid due to the presence of oil-droplets which we verified *via* confocal microscopy (Fig. 1C), and is in line with previous work.⁵³ However, the emergence of droplets could not be observed for the precursor and competitor 1.

In order to determine the kinetics of the three reaction cycles, we fueled 50 mM of each succinate derivative with 100 mM EDC and quantified the corresponding anhydride product concentration by means of high-performance liquid chromatography (HPLC). When we fueled 50 mM precursor

with 100 mM EDC, we found that the precursor is immediately converted to roughly 25 mM of the product and, after the depletion of the fuel, degraded rapidly with a first-order decay within 24 minutes (Fig. 1D). Next, we fueled 50 mM of competitor 1 with 100 mM EDC and observed a similar yield and lifetime (Fig. 1E). In contrast, under the same conditions, fueling competitor 2 resulted in 45 mM anhydride product which lasted for over an hour (Fig. 1F). We explain the increased yield and lifetime of the droplet-forming anhydride product of competitor 2 by a previously described self-protection mechanism, *i.e.*, the phase separated anhydride product is shielded from water and thus protected from hydrolysis.^{9,20,53} Consequently, hydrolysis occurs only on the anhydride molecules in solution which we refer to as the outside equilibrium concentration of the anhydride product (c_{out}). The hydrolysis rate can then be calculated by $r = k_d c_{\text{out}}$, where k_d is the hydrolysis rate constant. Since both k_d and c_{out} are constant, the effective hydrolysis rate is constant leading to a linear decay of the total anhydride product concentration when all fuel is consumed. Indeed, when using this equation in a theoretical kinetic model, we can accurately predict the concentration of fuel, succinate derivative and anhydride product for all three chemical reaction cycles (solid lines in Fig. 1D–F).

We tested how the kinetics of the reaction cycles are affected when the precursor competes with either competitor 1 or competitor 2 for fuel. We were particularly interested in how the anhydride products influence each other's activation and deactivation reactions and thereby determine their lifetimes. When we mixed equal concentrations of the precursor with

Open Access Article. Published on 28 April 2021. Downloaded on 12/10/2021 10:24:53 AM.
 This article is licensed under a Creative Commons Attribution 3.0 Unported Licence.

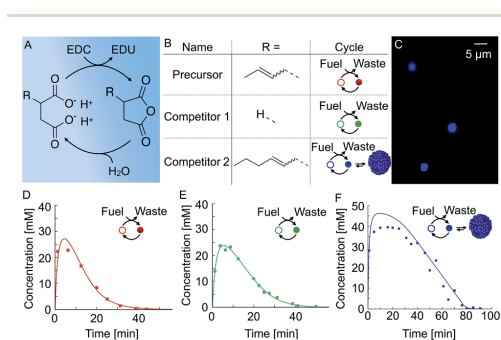


Fig. 1 The design of chemically fueled reaction cycles. (A) The chemically fueled reaction cycle used in this work. Succinate derivatives are converted into their corresponding transient anhydrides. (B) Molecular structures of the precursor, competitor 1, and competitor 2. The cycle column shows a schematic representation of the cycle with the succinate derivative as an open circle and the anhydride as a closed circle. Competitor 2 can form droplets. (C) Confocal microscopy of 50 mM competitor 2 fueled with 100 mM EDC. The corresponding anhydride product phase-separates into micron-sized oil droplets. (D–F) The anhydride product concentration profile of 50 mM precursor (D), competitor 1 (E), and competitor 2 (F) fueled with 100 mM EDC. Markers represent HPLC data; solid lines represent data calculated using the theoretical kinetic model.

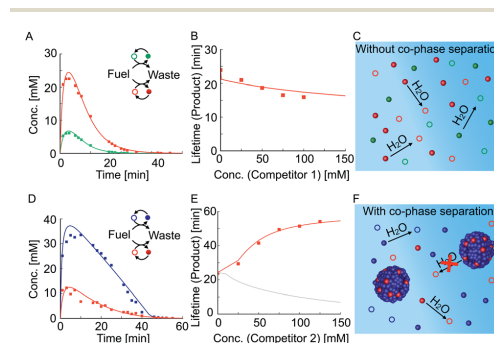


Fig. 2 Competition between reaction cycles for a shared fuel. (A) The anhydride concentration profiles when 50 mM precursor (red) and 50 mM competitor 1 (green) compete for 100 mM fuel. (B) The lifetime of the product against the concentration of competitor 1. The lifetime decreases with increasing competition. (C) Schematic representation of the hydrolysis of anhydrides in the experiment in (A). (D) The anhydride concentration profiles when 50 mM precursor (red) and 50 mM competitor 2 (blue) compete for 100 mM fuel. (E) The lifetime of the product against the concentration of competitor 2 (red). Using the theoretical kinetic model, we show that for the same system, but in the absence of co-phase separation, the lifetime decreases (gray line). (F) Schematic representation of the hydrolysis of anhydrides in the presence of droplets. Markers represent HPLC data; solid lines represent data calculated using the theoretical kinetic model.

competitor 1 and fueled with 100 mM EDC, we found lower yields and shorter reaction cycles for each of the anhydrides compared to their respective non-competing reaction cycles (Fig. 2A *versus* Fig. 1D and E). In order to quantify this effect, we measured the lifetime of the product as a function of competitor 1 concentration, keeping the precursor concentration fixed at 50 mM (Fig. 2B). The lifetime is defined as the time period during which the average product concentration exceeds a chosen threshold of 2 mM (see ESI Section 4† for a discussion on the robustness of the results for different threshold values). Briefly, the threshold concentration of 2 mM was chosen as it is equal to the c_{out} of competitor 2 which means that droplets dissolve below this threshold. Moreover, the threshold value is not in the tailing regime of the exponential decay of the anhydrides allowing to capture the effects of phase separation on product lifetime (ESI Fig. 11†). We find that the lifetime decreases with increasing the concentration of competitor 1, given the fact that the precursor and competitor 1 now have less fuel at their disposal compared to their corresponding non-competing reaction cycles (ESI Fig. 7†). The anhydrides of both reaction cycles are present side by side and hydrolyze in the aqueous media (Fig. 2C). In summary, both reaction cycles suffer from the competition for fuel.

The relation between the lifetime and amount of competitor 2 was very different when the precursor competed with competitor 2, which can phase-separate. Despite the competition for fuel, the lifetime of the product increased with increasing competitor 2 concentration (Fig. 2D and E). When 50 mM of competitor 2 was added, the lifetime of the product increased to 43 minutes and the decay suddenly differed from the previously observed first-order decay (Fig. 2D). The increased lifetime is particularly surprising considering that the maximum yield of the product decreased from roughly 25 mM to 10 mM when competitor 2 was added (Fig. 1D *versus* Fig. 2D). In contrast, the lifetime of the product of competitor 2 decreased from 77 minutes when on its own to 43 minutes when competing with the precursor for fuel (Fig. 1F *versus* Fig. 2D). Moreover, we found that the maximum yield of the product of competitor 2 decreased from roughly 45 mM to 35 mM when competing with the precursor for fuel. In summary, the product of competitor 2 suffers whilst the product benefits from the competition for fuel between the reaction cycles. Interestingly, both anhydrides had the same lifetime indicating a coupling between the two reaction cycles. When we further increased the concentration of competitor 2 while fixing the precursor concentration, the lifetime of the product increased even further (Fig. 2E and ESI Fig. 9†). We hypothesize that the counterintuitive behavior is related to the ability of the product to co-phase separate with the product of competitor 2. Thus, the product benefits from the self-protection mechanism of the droplets formed by the product of competitor 2 (Fig. 2F). In other words, co-phase separation decreases the concentration of the product in the aqueous phase and thereby its deactivation rate.

We investigated the composition of the oil phase during the reaction cycle by centrifugation and HPLC. We found that the product is indeed part of the oil phase (ESI Fig. 13A–C†). Moreover, when we increased the concentration of competitor

2, we found that the composition of the oil phase changed, which suggests that the composition of the oil phase is dictated by the two reaction cycles. We also measured the composition of the aqueous phase after 16 minutes in the reaction for various competitor 2 concentrations (ESI Fig. 2A and B†). Assuming that the system is close to local phase separation equilibrium (see ESI Section 2† for an estimate supporting this assumption), the concentrations of the anhydrides in the aqueous phase are approximately equal to their outside equilibrium concentration c_{out} . We found an almost constant c_{out} of roughly 2 mM for the anhydride product of competitor 2 in the presence or absence of the precursor (ESI Fig. 2A†). In other words, the c_{out} of the product of competitor 2 was hardly affected by the presence of the product. In contrast, we found that the c_{out} of the product decreased drastically, ranging from roughly 28 mM without competition to 0.6 mM with 125 mM concentration of competitor 2 (ESI Fig. 2B†).

The results described above suggest that co-phase separation takes place and that co-phase separation protects both anhydride products from hydrolysis. Thus, the product of competitor 2 serves as a host for the product and protects it from hydrolysis-driven deactivation. We assumed that competition affects the co-phase separation as it results in an increased total droplet volume and a decreased hydrolysis rate of the product (Fig. 3A). To understand the full implications of this relation, we

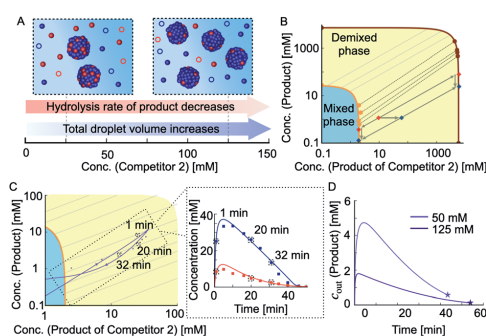


Fig. 3 Mechanism of co-phase separation and increased lifetime. (A) Schematic representation of how increasing concentration of competitor 2 affects co-phase separation and thereby the hydrolysis rate of the product. (B) Ternary phase diagram depicting the equilibrium concentrations of the product and the product of competitor 2. The circles correspond to the experimental data and the solid lines represent the theoretical binodal and tie lines. The dashed black lines represent the experimental tie lines. (C) The trace of total concentrations of product and product of competitor 2 in the phase diagram during the reaction cycle when 50 mM precursor and 50 mM competitor 2 compete for 100 mM fuel. The arrows depict the direction in which the total concentrations move with time. Markers represent HPLC data; solid lines represent data calculated using the theoretical kinetic model. (D) The outside equilibrium concentration c_{out} of the product over time for 50 mM and 125 mM competitor 2. The course of the c_{out} of the product is dictated by the shape of the orbital in the phase diagram and the tie lines it crosses. The stars denote the point of dissolution of the droplets.



derived a model that accounts for the interplay between the chemical reaction kinetics and the physics of phase separation. The latter is determined by the phase diagram of the co-phase separating anhydride components (Fig. 3B and C). Since diffusion is fast compared to the hydrolysis of both anhydrides, changes in their total concentrations due to chemical reactions are slow enough such that phase separation can equilibrate quasi-instantaneously (see ESI Section 2†). Thus, the non-equilibrium chemical kinetics changes the average product concentrations leading to an orbit in the equilibrium phase diagram.

To determine the phase diagram in the experimental system, we measured the total anhydride concentrations at 16 minutes into the cycle and subtracted the previously determined concentrations in the aqueous phase to find the amount of each anhydride in the oil droplets (Fig. 3B and ESI Fig. 2A–C, see ESI Tables 4 and 5† and Methods). Together with the molecular volumes, we can thus calculate the concentrations of both anhydrides in the oil phase. In other words, for each set of total anhydride concentrations in the system corresponding to different initial competitor 2 concentrations, we calculated the anhydride concentrations in the aqueous phase and the oil phase (Fig. 3B, markers on the orange and dark red line, respectively). The measured concentrations which correspond to the coexisting phases in the phase diagram can be connected by tie lines (Fig. 3B, dashed lines between the orange and dark red line). We fitted the ternary Flory–Huggins model to the experimentally determined values.⁵⁴ We found good agreement between the experimentally measured tie lines and the theoretically calculated ones (Fig. 3B). The theoretical phase diagram also interpolated between the experimentally measured data points. With this interpolation, we could determine the anhydride concentrations inside and outside of the droplets (oil phase) for any total concentration of anhydrides. As an example, when the total concentrations in the system were measured to be 1 mM product and 10 mM product of competitor 2, the tie line connects to concentrations of the anhydrides in the aqueous phase of 0.5 mM of product and 2 mM of the product of competitor 2 (Fig. 3B, red marker). In other words, under these conditions, roughly half of the product was protected. The phase diagram also showed that if the total concentration of product of competitor 2 increased (total concentration of product remaining constant at 1 mM), the system shifted to another tie line, and the c_{out} of the product decreased further (Fig. 3B, blue marker).

In the following, we extend the previously described kinetic model for two competing reaction cycles⁵³ and account for the physics of co-phase separation characterized by the phase diagram. The kinetic model determines the time-dependent concentrations of fuel, succinate derivatives and anhydride products at each second of the reaction cycle *via* a set of five differential equations. The extended kinetic model in addition takes into account the concentrations in the aqueous phase and the oil phase and considers that activation and deactivation only take place in the aqueous phase. Solving the underlying kinetic equations of the extended model, we found that the calculated data was in good agreement with the concentrations

measured by HPLC (Fig. 2D and ESI Fig. 2†). The model also allowed to represent the theoretical data and the HPLC data as points along orbits in the phase diagram (Fig. 3C). Each data point on such an orbit can be decomposed into concentrations of the anhydrides in the aqueous and in the oil phase. If an orbit lies parallel to a tie line, the anhydride concentrations in the aqueous phase remain almost constant over time. This implies that both anhydrides hydrolyze *via* kinetics close to zeroth-order as long as droplets are present. However, if the orbit evolves through several tie lines, the product concentration in the aqueous phase changes with time. In other words, the c_{out} of the product of competitor 2 in the aqueous phase barely changes and is independent of the shape of the orbit, *i.e.*, hydrolysis occurs *via* zeroth-order kinetics with or without the product.

In contrast, the c_{out} of the product changed drastically with the amount of competitor 2, and its time-dependent evolution depends on the shape of the orbit through the phase diagram. The extended kinetic model allowed us to calculate the outside equilibrium concentration c_{out} of the product as a function of time for different competitor 2 concentrations (Fig. 3D). For low concentration of competitor 2, the c_{out} of the product varied drastically from roughly 5 mM to 0.7 mM over the course of the reaction cycle. In contrast, for high concentration of competitor 2, the c_{out} varied only from roughly 2 mM to 0.5 mM. In summary, we showed that the shape of the orbit is influenced by the amount of competitor 2, *i.e.*, the more competitor is present, the more parallel the orbits are oriented with respect to the tie lines (ESI Fig. 14A–F†). However, due to adding fuel only at the beginning of the kinetics, all systems show a single orbit that

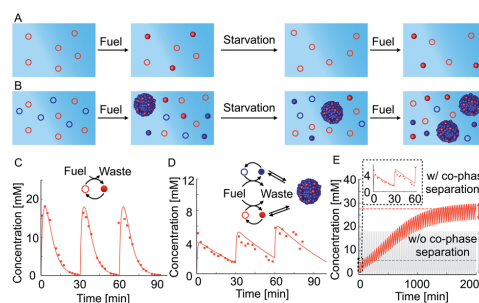


Fig. 4 Co-phase separation facilitates the survival of the product in repetitive fueling starvation experiments. (A and B) Schematic representation of the precursor in periodic fueling and starvation periods without (A) and with (B) competitor 2. (C) 50 mM precursor fueled with an amplitude of 60 mM every 30 minutes. (D) 50 mM precursor and 100 mM competitor 2 fueled with an amplitude of 60 mM every 30 minutes. Markers represent HPLC data; solid lines represent data calculated using the theoretical kinetic model. (E) Calculation using the theoretical kinetic model of long-time kinetics of the reaction cycle of the experiments in (C) and (D). The gray and red dashed lines represent the mean concentrations achieved at pseudo steady state without and with co-phase separation, respectively. Inset shows the first three refueling steps. Note that the oscillations around the pseudo steady state concentration are severely damped with co-phase separation.



enters and leaves the domain of co-phase separation in the phase diagram.

We tested how co-phase separation is affected when the system is subject to periodic fueling and starvation periods. We chose the amount of fuel and fueling frequency such that the product is depleted during each starvation period (Fig. 4A). We hypothesize that competition with competitor 2 under the exact same conditions let the product survive starvation (Fig. 4B). Indeed, when we periodically fueled 50 mM precursor every 30 minutes with 60 mM of fuel, we found that the corresponding product completely hydrolyzed after each starvation period (Fig. 4C). In contrast, when we periodically fueled 50 mM precursor and 100 mM competitor 2 with the same amplitude and frequency, we observed that co-phase separation protected the product from hydrolysis and thereby helped it to survive starvation (Fig. 4D and ESI Fig. 15A†). Despite the competition and lower anhydride yield, the survival of the product during the starvation period resulted in a drastically increased yield over fueling and starvation periods compared to a system without competitor 2 which did not show an increased yield. We used our theoretical kinetic model to calculate the response of the system to hundreds of cycles (Fig. 4E and ESI Fig. 15B–D†). We found that co-phase separation of the product with the anhydride product of competitor 2 resulted in a pseudo-steady state of the product in which the concentration oscillated around roughly 27 mM (red dashed line in Fig. 4E). In contrast, in the absence of competitor 2, the product oscillated around a mean concentration of roughly 6 mM and did not show any increase in concentration over time (gray solid line in Fig. 4E). These observations support the idea that the product of competitor 2 acts as a host and that the product of the precursor thus survives longer, benefitting like a parasite.

Besides the anticipated result of survival in the presence of a host, we found a surprising new behavior, *i.e.*, we observed that the oscillation in the concentrations in pseudo steady state due to fueling and starvation was dependent on the amount of competitor in the system (Fig. 4E). Specifically, in the first experiment, the concentration oscillated between a maximum of 18 mM and a minimum of 0 mM, *i.e.*, the concentration variation is $\Delta = 18$ mM (Fig. 4C and gray solid line in Fig. 4E). In the experiment with competitor 2, this Δ had drastically decreased to just 3 mM when pseudo steady state was reached (red solid line in Fig. 4E). The concentration variation Δ was quantified by the theoretical kinetic model for increasing competitor 2 concentrations and tended to decrease (Fig. 4E and ESI Fig. 16†). In other words, co-phase separation protects the products from hydrolysis and buffers against fuel-driven oscillations. A reminiscent observation was recently reported in a population of *Hela* cells where phase separation was shown to buffer different expression levels.³⁵

Conclusions

In general, when metabolic reaction cycles compete for a common nutrient, both suffer because they need to share a common, scarce resource. In this work, we found a surprising behavior where competition can increase the success of one of

the precursors, *i.e.*, it can survive longer or show reduced concentration oscillations in the presence of oscillatory fueling. The reason for this success relies on co-phase separation as a mechanism where droplets composed of both anhydrides create a protective environment. This behavior shows analogies to parasitic behavior in biology. The parasite competes with the host for resources and thereby decreases the lifetime of the host. Furthermore, the parasite exploits the protective environment of the host which increases its lifetime. This property could be crucial for the control of downstream chemical reactions of the competitors. Our results demonstrate that parasitic behavior can already emerge in a simple non-equilibrium system that can phase separate and is controlled by fuel-driven chemical reaction cycles. Our understanding of the underlying mechanism can be a step toward the design of more complex, synthetic life-like systems. In the future, we will explore how co-phase separation affects the selection of a large number of chemically active molecules.

Materials and methods

Materials

We purchased (*E/Z*)-2-buten-1-ylsuccinic anhydride (product) and (*E/Z*)-2-hexenyl-1-ylsuccinic anhydride (product of competitor 2) from TCI chemicals. Succinic acid (competitor 1), succinic anhydride (product of competitor 1), Nile Red, 1-ethyl-3-(3-dimethyl-aminopropyl)carbodiimide hydrochloride (EDC), trifluoroacetic acid (TFA) and 2-(*N*-morpholino)ethane sulfonic acid (MES buffer) were purchased from Sigma-Aldrich. All chemicals were used without any further purification unless otherwise indicated. High performance liquid chromatography (HPLC) grade acetonitrile (ACN) was purchased from VWR.

Synthesis of the succinate precursors

(*E/Z*)-2-Buten-1-yl-succinic anhydride (product) and (*E/Z*)-2-hexenyl-1-ylsuccinic anhydride (product of competitor 2) were dispersed in 30 mL MQ water and stirred for 3 days. Subsequently, the reaction mixture was freeze-dried, and the corresponding succinates (precursor and competitor 2) were stored at -20 °C until further usage.

HPLC

We used a ThermoFisher Dionex Ultimate 3000 analytical HPLC with a Hypersil Gold 250 \times 4.6 mm C18 column (5 μ m pore size) to monitor the concentration profiles of each reactant of the chemical reaction network. We prepared 1.0 mL samples according to the sample preparation protocol described above into a screw cap HPLC vial. Samples were injected directly from the HPLC vial without any further dilution. We injected 25 μ L for the detection of the succinates and anhydrides and 1 μ L for the detection of EDC. We used a UV/Vis detector at 220 nm for the detection. A linear gradient of MQ water : ACN with 0.1% TFA was used to separate the compounds. We used a linear gradient from 98 : 2 to 2 : 98 in 10 minutes followed by 2 minutes at 2 : 98 for the separation. The column was equilibrated for 2 minutes after each gradient. We performed



calibration curves of the compounds in triplicates. Calibration values and retention times are given in ESI Tables S1 and S2.†

Confocal fluorescence microscopy

We imaged the droplets using a Leica SP8 confocal microscope with a 63× oil immersion objective. Samples were prepared as described above but with 0.1 μM Nile Red added before EDC addition. We added 5 μL sample to a silicon grease reservoir on a PEG-coated glass slide covered with a 12 mm diameter coverslip. The samples were excited with a 543 nm laser and imaged at 580–700 nm.

Droplet composition experiments

We prepared 5 mL samples as described above to guarantee a sufficient droplet phase volume after centrifugation. After the depletion of the fuel, the reaction mixture was centrifuged at 4 °C for 3 minutes (rpm = 5000). We used an Eppendorf pipette to take a 1 μL sample of the droplet pellet which we diluted in 200 μL ACN in a HPLC screw cap vial. We analyzed the ratio of product to product of competitor 2 with HPLC.

Supernatant composition experiments

We prepared 1 mL samples as described above in 1.5 mL Eppendorf reaction vessels. After 16 minutes, the samples were centrifuged at 25 °C for 1 minute (rpm = 13 500). We directly analyzed the concentrations of the corresponding anhydrides in the supernatant of the sample with HPLC (see ESI Tables S4 and S5†).

Calculation of respective concentrations inside the droplets

We calculated the corresponding anhydride concentrations inside the droplets using the relation $n^I = n^{\text{total}} - n^{\text{II}}$ and their molecular volumes, respectively (see ESI Tables S3, S5–S7†). The superscripts I and II represent the droplet phase and aqueous bulk phase, respectively. The total volume of the droplets is represented as V^I .

Author contributions

J. B. and P. S. S. designed the experiments. P. S. S. and T. H. carried out the experiment. S. L., J. J. and C. A. W. worked out the theory. S. L. and J. J. performed the numerical studies and the fitting to the experimental data. P. S. S., S. L., J. B. and C. A. W. wrote the manuscript. All authors have given approval to the final version of the manuscript.

Conflicts of interest

There are no conflicts to declare.

Acknowledgements

Funded by the Deutsche Forschungsgemeinschaft (DFG, German Research Foundation) – Project-ID 364653263 – TRR 235 (CRC 235). This research was conducted within the Max

Planck School Matter to Life supported by the German Federal Ministry of Education and Research (BMBF) in collaboration with the Max Planck Society. J. B. and P. S. S. are grateful for the funding by the European Research Council (ERC starting grant 852187). S. L. and J. J. thank the IMPRS-CellDevoSys for support.

References

- G. Wang and S. Liu, *ChemSystemsChem*, 2020, **2**, e1900046.
- N. Singh, G. J. M. Formon, S. De Piccoli and T. M. Hermans, *Adv. Mater.*, 2020, **32**, 1906834.
- R. Merindol and A. Walther, *Chem. Soc. Rev.*, 2017, **46**, 5588–5619.
- S. De and R. Klajn, *Adv. Mater.*, 2018, **30**, 1706750.
- F. Della Sala, S. Neri, S. Maiti, J. L. Chen and L. J. Prins, *Curr. Opin. Biotechnol.*, 2017, **46**, 27–33.
- L. S. Kariyawasam, M. M. Hossain and C. S. Hartley, *Angew. Chem., Int. Ed.*, 2020, DOI: 10.1002/anie.202014678.
- G. Ragazzon and L. J. Prins, *Nat. Nanotechnol.*, 2018, **13**, 882–889.
- A. Mishra, S. Dhiman and S. J. George, *Angew. Chem., Int. Ed.*, 2021, **60**, 2740–2756.
- B. Riefl, C. Wanzke, M. Tena-Solsona, R. K. Grötsch, C. Maity and J. Boekhoven, *Soft Matter*, 2018, **14**, 4852–4859.
- M. Tena-Solsona, B. Riefl, R. K. Grötsch, F. C. Löhner, C. Wanzke, B. Käs Dorf, A. R. Bausch, P. Müller-Buschbaum, O. Lieleig and J. Boekhoven, *Nat. Commun.*, 2017, **8**, 15895.
- B. A. K. Kriebisch, A. Jussupow, A. M. Bergmann, F. Kohler, H. Dietz, V. R. I. Kaila and J. Boekhoven, *J. Am. Chem. Soc.*, 2020, **142**, 20837–20844.
- K. Dai, J. R. Fores, C. Wanzke, B. Winkeljann, A. M. Bergmann, O. Lieleig and J. Boekhoven, *J. Am. Chem. Soc.*, 2020, **142**, 14142–14149.
- J. Boekhoven, A. M. Brizard, K. N. Kowłgi, G. J. Koper, R. Eelkema and J. H. van Esch, *Angew. Chem.*, 2010, **122**, 4935–4938.
- S. Bal, K. Das, S. Ahmed and D. Das, *Angew. Chem.*, 2019, **131**, 250–253.
- W. A. Ogden and Z. Guan, *ChemSystemsChem*, 2020, **2**, e1900030.
- J. Boekhoven, W. E. Hendriksen, G. J. M. Koper, R. Eelkema and J. H. van Esch, *Science*, 2015, **349**, 1075–1079.
- K. Jalani, A. D. Das, R. Sasmal, S. S. Agasti and S. J. George, *Nat. Commun.*, 2020, **11**, 3967.
- S. Dhiman, R. Ghosh and S. J. George, *ChemSystemsChem*, 2020, **2**, e1900042.
- G. Panzarasa, A. L. Torzynski, T. Sai, K. Smith-Mannschott and E. R. Dufresne, *Soft Matter*, 2020, **16**, 591–594.
- M. Tena-Solsona, C. Wanzke, B. Riess, A. R. Bausch and J. Boekhoven, *Nat. Commun.*, 2018, **9**, 2044.
- M. Tena-Solsona, J. Janssen, C. Wanzke, F. Schnitter, H. Park, B. Riefl, J. M. Gibbs, C. A. Weber and J. Boekhoven, *ChemSystemsChem*, 2021, **3**(2), e2000034.
- C. Donau, F. Späth, M. Sosson, B. A. K. Kriebisch, F. Schnitter, M. Tena-Solsona, H.-S. Kang, E. Salibi,



- M. Sattler, H. Mutschler and J. Boekhoven, *Nat. Commun.*, 2020, **11**, 5167.
- 23 E. te Brinke, J. Groen, A. Herrmann, H. A. Heus, G. Rivas, E. Spruijt and W. T. S. Huck, *Nat. Nanotechnol.*, 2018, **13**, 849–855.
- 24 C. Wanzke, A. Jussupow, F. Kohler, H. Dietz, V. R. I. Kaila and J. Boekhoven, *ChemSystemsChem*, 2020, **2**, e1900044.
- 25 S. Maiti, I. Fortunati, C. Ferrante, P. Scrimin and L. J. Prins, *Nat. Chem.*, 2016, **8**, 725.
- 26 P. Solís Muñana, G. Ragazzon, J. Dupont, C. Z.-J. Ren, L. J. Prins and J. L.-Y. Chen, *Angew. Chem., Int. Ed.*, 2018, **57**, 16469–16474.
- 27 S. M. Morrow, I. Colomer and S. P. Fletcher, *Nat. Commun.*, 2019, **10**, 1011.
- 28 R. K. Grötsch, A. Angi, Y. G. Mideksa, C. Wanzke, M. Tena-Solsona, M. J. Feige, B. Rieger and J. Boekhoven, *Angew. Chem., Int. Ed.*, 2018, **57**, 14608–14612.
- 29 R. K. Grötsch, C. Wanzke, M. Speckbacher, A. Angi, B. Rieger and J. Boekhoven, *J. Am. Chem. Soc.*, 2019, **141**, 9872–9878.
- 30 D. Manna, T. Udayabhaskararao, H. Zhao and R. Klajn, *Angew. Chem.*, 2015, **127**, 12571–12574.
- 31 B. G. P. van Ravensteijn, W. E. Hendriksen, R. Eelkema, J. H. van Esch and W. K. Kegel, *J. Am. Chem. Soc.*, 2017, **139**, 9763–9766.
- 32 M. M. Hossain, J. L. Atkinson and C. S. Hartley, *Angew. Chem., Int. Ed.*, 2020, **59**, 13807–13813.
- 33 E. Del Grosso, L. J. Prins and F. Ricci, *Angew. Chem., Int. Ed.*, 2020, **59**, 13238–13245.
- 34 L. Heinen and A. Walther, *Sci. Adv.*, 2019, **5**, eaaw0590.
- 35 B. Zhang, I. M. Jayalath, J. Ke, J. L. Sparks, C. S. Hartley and D. Konkolewicz, *Chem. Commun.*, 2019, **55**, 2086–2089.
- 36 N. Singh, B. Lainer, G. J. M. Formon, S. De Piccoli and T. M. Hermans, *J. Am. Chem. Soc.*, 2020, **142**, 4083–4087.
- 37 L. Heinen, T. Heuser, A. Steinschulte and A. Walther, *Nano Lett.*, 2017, **17**, 4989–4995.
- 38 D. Zwicker, R. Seyboldt, C. A. Weber, A. A. Hyman and F. Jülicher, *Nat. Phys.*, 2017, **13**, 408–413.
- 39 C. A. Weber, D. Zwicker, F. Jülicher and C. F. Lee, *Rep. Prog. Phys.*, 2019, **82**, 064601.
- 40 S. Yang, G. Schaeffer, E. Mattia, O. Markovitch, K. Liu, A. S. Hussain, J. Ottelé, A. Sood and S. Otto, *Angew. Chem., Int. Ed.*, 2021, DOI: 10.1002/anie.202016196.
- 41 E. A. Post and S. P. Fletcher, *Chem. Sci.*, 2020, **11**, 9434–9442.
- 42 A. Pross and V. Khodorkovsky, *J. Phys. Org. Chem.*, 2004, **17**, 312–316.
- 43 A. J. Lotka, *J. Phys. Chem.*, 2002, **14**, 271–274.
- 44 I. Colomer, A. Borissov and S. P. Fletcher, *Nat. Commun.*, 2020, **11**, 176.
- 45 M. Altay, Y. Altay and S. Otto, *Angew. Chem., Int. Ed.*, 2018, **57**, 10564–10568.
- 46 H. Duim and S. Otto, *Beilstein J. Org. Chem.*, 2017, **13**, 1189–1203.
- 47 Z. Dadon, N. Wagner, S. Alasibi, M. Samiappan, R. Mukherjee and G. Ashkenasy, *Chem.–Eur. J.*, 2015, **21**, 648–654.
- 48 Y. Altay, M. Altay and S. Otto, *Chem.–Eur. J.*, 2018, **24**, 11911–11915.
- 49 J. W. Sadownik, E. Mattia, P. Nowak and S. Otto, *Nat. Chem.*, 2016, **8**, 264–269.
- 50 E. Mattia and S. Otto, *Nat. Nanotechnol.*, 2015, **10**, 111–119.
- 51 E. A. J. Post and S. P. Fletcher, *Chem. Sci.*, 2020, **11**, 9434–9442.
- 52 R. Pascal and A. Pross, *J. Syst. Chem.*, 2014, **5**, 3.
- 53 C. Wanzke, M. Tena-Solsona, B. Riefs, L. Tebcharani and J. Boekhoven, *Mater. Horiz.*, 2020, **7**, 1397–1403.
- 54 S. Krüger, C. A. Weber, J.-U. Sommer and F. Jülicher, *New J. Phys.*, 2018, **20**, 075009.
- 55 A. Klosin, F. Oltsch, T. Harmon, A. Honigmann, F. Jülicher, A. A. Hyman and C. Zechner, *Science*, 2020, **367**, 464–468.



Electronic Supplementary Material (ESI) for Chemical Science.
This journal is © The Royal Society of Chemistry 2021

Supporting Information

Parasitic Behavior in Competing Chemically Fueled Reaction Cycles

Patrick S. Schwarz,^{†1} Sudarshana Laha,^{‡2,3} Jacqueline Janssen,^{2,3} Tabea Huss,¹ Job Boekhoven,^{*1,4} Christoph A. Weber^{*2,3}

¹ Department of Chemistry, Technical University of Munich, Lichtenbergstrasse 4, 85748 Garching, Germany.

² Biological Physics, Max Planck Institute for the Physics of Complex Systems, Nöthnitzer Straße 38, 01187 Dresden, Germany.

³ Center for Systems Biology Dresden, Pfotenhauerstrasse 108, 01307 Dresden, Germany.

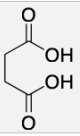
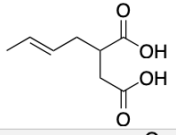
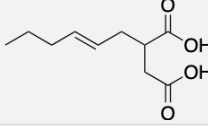
⁴ Institute for Advanced Study, Technical University of Munich, Lichtenbergstrasse 2a, 85748 Garching, Germany.

Supporting Information

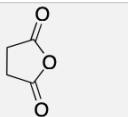
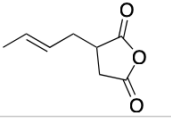
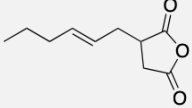
In the Supporting Information, we provide Supporting Tables with the characterization of succinate derivatives and anhydrides and with the concentrations of the anhydrides in the aqueous and oil droplet phase, respectively which is used for the construction of phase diagram. We describe our kinetic model and compare the experimental data with the theory. We tabulate the reaction rate constants as obtained from fitting routines. We also calculate the droplet composition for different competitor 2 concentrations. Furthermore, we provide additional data for the co-phase separation mechanism, periodic fueling and buffer capacity.

1. Supporting Tables

Supporting Table S1: Characterization of succinate derivatives (xx = detection not possible).

Name	Structure	Mass calc. [g/mol]	Mass observed [g/mol]	Retention time [min]	Calibration value [mAU/mM]
Competitor 1		118.0 C ₄ H ₆ O ₄	117.1 [Mw-H] ⁻	xx	xx
Precursor		172.1 C ₈ H ₁₂ O ₄	171.1 [Mw-H] ⁻	8.24	2.78
Competitor 2		200.1 C ₁₀ H ₁₆ O ₄	199.1 [Mw-H] ⁻	9.61	2.78

Supporting Table S2: Characterization of anhydrides.

Name	Structure	Mass calc. [g/mol]	Mass observed [g/mol]	Retention time [min]	Calibration value [mAU/mM]
Product of competitor 1		100.0 C ₄ H ₄ O ₃	101.1 [Mw+H] ⁺	4.91	1.03
Product		154.1 C ₈ H ₁₀ O ₃	155.2 [Mw+H] ⁺	8.24	4.78
Product of competitor 2		182.1 C ₁₀ H ₁₄ O ₃	183.1 [Mw+H] ⁺	4.58	5.19

Supporting Table S3: Parameters required for ternary phase diagram construction.

Name	Density [g/cm ³]	Molar volume [cm ³ /mol]	Molecular volume [cm ³]	Volume ratio with respect to water
H ₂ O	1.0	18.02	2.99E-23	1.0
Product	1.13	136.43	2.27E-22	7.57
Product of Competitor 2	1.07	170.30	2.83E-22	9.45

Supporting Table S4: Concentration outside of the droplet phase (solubilities) of the product for different initial competitor 2 concentrations.

Experiment	$c^{II,eq}(\text{Product})$ [mmol/L]	Deviation [mmol/L]
100 mM Precursor, 200 mM EDC	27.80	0.15
50 mM Precursor, 25 mM Competitor 2 100 mM EDC	3.88	0.09
50 mM Precursor, 50 mM Competitor 2 100 mM EDC	1.91	0.25
50 mM Precursor, 75 mM Competitor 2 100 mM EDC	0.87	0.08
50 mM Precursor, 100 mM Competitor 2 100 mM EDC	0.61	0.05
50 mM Precursor 100 mM Competitor 2	0	0

Supporting Table S5: Concentration outside of the droplet phase (solubilities) of the product of competitor 2 for different initial competitor 2 concentrations.

Experiment	$c^{II,eq}(\text{Product of Competitor 2})$ [mmol/L]	Deviation [mmol/L]
100 mM Precursor, 200 mM EDC	0	0
50 mM Precursor, 25 mM Competitor 2 100 mM EDC	1.97	0.07
50 mM Precursor, 50 mM Competitor 2 100 mM EDC	2.28	0.12
50 mM Precursor, 75 mM Competitor 2 100 mM EDC	1.94	0.10
50 mM Precursor, 100 mM Competitor 2 100 mM EDC	2.04	0.08
50 mM Precursor 100 mM Competitor 2	2.01	0.1

Supporting Table S6: Amount of substance and droplet volume for the product and product of competitor 2 for different initial competitor 2 concentrations.

Experiment	n^I (Product) [mmol]	n^I (Product of competitor 2) [mmol]	v^I [L]
100 mM Precursor, 200 mM EDC	5.85E-03	0	8.0E-07
50 mM Precursor, 25 mM Competitor 2 100 mM EDC	5.87E-03	1.30E-02	3.0E-06
50 mM Precursor 50 mM Competitor 2 100 mM EDC	4.81E-03	2.71E-02	5.3E-06
50 mM Precursor, 75 mM Competitor 2 100 mM EDC	3.98E-03	3.46E-02	6.4E-06
50 mM Precursor, 100 mM Competitor 2 100 mM EDC	3.20E-03	3.83E-02	7.0E-06
50 mM Competitor 2 100mM EDC	0	4.29E-02	7.3E-06

Supporting Table S7: Concentrations inside the droplets for the product and product of competitor 2 for different initial competitor 2 concentrations.

Experiment	$c^{I,eq}$ (Product) [mmol/L]	$c^{I,eq}$ (Product of competitor 2) [mmol/L]
100 mM Precursor, 200 mM EDC	7.32E+03	0
50 mM Precursor, 25 mM Competitor 2 100 mM EDC	1.95E+03	4.30E+03
50 mM Precursor 50 mM Competitor 2 100 mM EDC	8.37E+02	5.19E+03
50 mM Precursor, 75 mM Competitor 2 100 mM EDC	6.64E+02	5.33E+03
50 mM Precursor, 100 mM Competitor 2 100 mM EDC	4.66E+02	5.49E+03
50 mM Competitor 2 100mM EDC	0	5.87E+03

2. Theoretical kinetic model for co-phase separation and chemical reactions competing for fuel

Fuel driven chemical reactions

Our system is composed of four different types of molecules: fuel, succinate derivatives, intermediate and anhydride molecules. The fuel molecule *EDC* is abbreviated by the letter *F*. We consider three types of succinate derivatives which we refer to as precursor (A_P), competitor 1 (A_{C_1}) and competitor 2 (A_{C_2}), respectively, and abbreviate each derivative as A_i with $i = P, C_1, C_2$. The succinate derivatives used experimentally are (*E/Z*)-2-buten-1-ylsuccinic acid (precursor), succinic acid (competitor 1) and (*E/Z*)-2-hexen-1-ylsuccinic acid (competitor 2). The intermediate molecule, AF_i , is composed of fuel and the respective succinate derivative. There are three corresponding anhydrides, abbreviated as B_i , and referred to as product, product of competitor 1 or product of competitor 2. The anhydrides used experimentally are (*E/Z*)-2-buten-1-ylsuccinic anhydride (product), succinic anhydride (product of competitor 1) and (*E/Z*)-2-hexen-1-ylsuccinic anhydride (product of competitor 2). In our systems, the solvent is water (*w*).

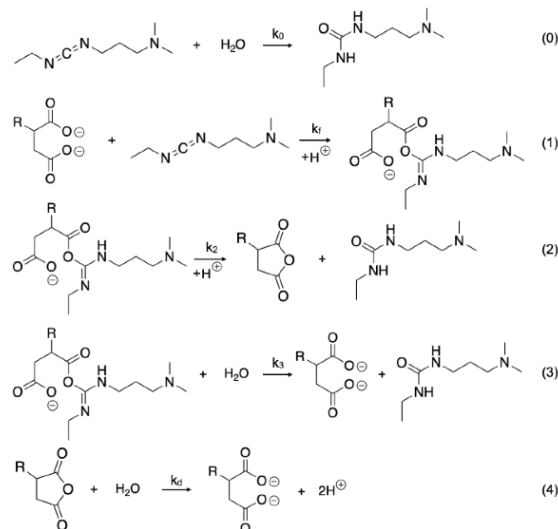
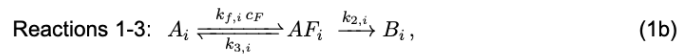


Figure 1: Chemical reactions considered in the kinetic model. Reaction (0) corresponds to the direct hydrolysis of EDC to waste, EDU. Reaction (1) shows the activation reaction of the succinate derivative with EDC to form the intermediate molecule. Reaction (2) is the intramolecular anhydride formation reaction. Reaction (3) depicts the direct hydrolysis of the intermediate molecule. Reaction (4) shows the hydrolysis of the anhydride to the initial succinate derivative.

The fuel F can undergo two chemical reactions: F can get slowly hydrolysed to waste W with a rate constant k_0 (reaction 0, Eq. (1a)), or, the fuel F drives the transition from the succinate derivative A_i to the intermediate AF_i with a chemical flux that is proportional to the fuel concentration c_F with a rate constant $k_{f,i}$ (reaction 1, second order chemical reaction). This intermediate molecule, AF_i can spontaneously hydrolyse back to A_i with a rate constant $k_{3,i}$, or irreversibly turn over to the anhydride B_i (reactions 1-3, Eq. (1b)). The turn-over to the anhydride (reaction 2) occurs spontaneously as an intramolecular reaction with a rate constant $k_{2,i}$ (first-order reaction). In aqueous media, this anhydride hydrolyses and thereby turns over to the initial succinate derivative (Eq. (1c)), which we shortly refer to as deactivation step. Considering a constant pH and approximately dilute conditions relative to water, deactivation follows a first order chemical reaction with a deactivation rate constant $k_{d,i}$. All reactions (0)-(4) as shown in Fig. 1 can be summarised by the following reaction schemes:



Co-phase separation of anhydride molecules

At concentrations larger than their respective solubilities (Supporting Table S4, S5), each anhydride B_i (product and product of competitor 2) can phase separate from the water-rich solvent w and form oil-like droplets that are rich in anhydride. Since fuel F , the succinate derivatives A_i (precursor and competitor 2) and intermediate molecules AF_i , are well soluble in water, the droplets dominantly contain the rather hydrophobic anhydrides B_i with concentrations inside compared to the outside similar to oil drops in water. Here, we study the interplay of the product (P) and the product of competitor 2 (C_2), which co-phase separate. To estimate the co-phase separation properties of these two anhydrides with respect to the solvent, we consider the limit of fuel excess. In this case, the system is mostly composed of the two anhydrides, solvent and fuel. Due to the hydrophilic property of the fuel, we neglect its effects on phase separation. Thus, we can determine a ternary phase diagram for the remaining three molecules (product and product of competitor 2, and solvent w). As a model for this phase diagram, we consider a ternary, incompressible Flory-Huggins free energy density,

$$f = \frac{k_B T}{\nu_w} \left(\sum_i \frac{\phi_i}{r_i} \ln \phi_i + \sum_{i,j:i \neq j} \frac{\chi_{ij}}{2} \phi_i \phi_j \right), \quad (2)$$

where the summation index $i, j = P, C_2, w$, runs over all three types of molecules, i.e., product, product of competitor 2 and water as the solvent, respectively. Moreover, $r_i = \nu_i / \nu_w$, where ν_i is the molecular volume of component i and ν_w is the molecular volume of water. Incompressibility implies that all molecular volumes are constant and that the volume fractions ϕ_i obey, $1 - \phi_w = \phi_P + \phi_{C_2}$. These volume fractions are related to concentrations, $c_i = \phi_i / \nu_i$. Both hetero- and homotypic interactions between molecules i and j are accounted for by the interaction parameter χ_{ij} . Our

model for the phase diagram has 5 parameters: the molecular volumes of the two anhydrides, ν_P and ν_{C_2} , the interaction parameters between each anhydride and solvent, $\chi_{P,w}$ and $\chi_{C_2,w}$, and the effective interaction parameter between the two anhydrides, χ_{P,C_2} . The ternary phase diagram is obtained from the free energy density (Eq. (2)) by a Maxwell construction, where the volume fractions in droplet phase (I), $\phi_P^{I,eq}$ and $\phi_{C_2}^{I,eq}$, coexist with the volume fractions in aqueous phase (II), $\phi_P^{II,eq}$ and $\phi_{C_2}^{II,eq}$. The volume fractions fulfil the equilibrium conditions for phase coexistence:

$$\bar{\mu}_P(\phi_P^{I,eq}, \phi_{C_2}^{I,eq}) = \bar{\mu}_P(\phi_P^{II,eq}, \phi_{C_2}^{II,eq}), \quad (3a)$$

$$\bar{\mu}_{C_2}(\phi_P^{I,eq}, \phi_{C_2}^{I,eq}) = \bar{\mu}_{C_2}(\phi_P^{II,eq}, \phi_{C_2}^{II,eq}), \quad (3b)$$

$$\Pi(\phi_P^{I,eq}, \phi_{C_2}^{I,eq}) = \Pi(\phi_P^{II,eq}, \phi_{C_2}^{II,eq}), \quad (3c)$$

where the exchange chemical potentials $\bar{\mu}_i = \nu_i \partial f / \partial \phi_i$ and the osmotic pressure $\Pi = -f + \sum_i \mu_i \phi_i / \nu_i$ can be calculated from the free energy density (Eq. (2)), and $i = P, C_2$. In the Maxwell construction for a ternary, incompressible mixture, we have two more conditions, namely the conservation laws for the total volume fraction for each anhydride, $\bar{\phi}_i = (V^I \phi_i^{I,eq} + (V - V^I) \phi_i^{II,eq}) / V$. The equilibrium volume fractions in both phases for each anhydride ($\phi_i^{I,eq}, \phi_i^{II,eq}$), together with the droplet volume V^I , give us five unknowns and we have five equations determining these unknowns.

Obtaining interaction parameters from the experimental phase diagram

Using the observed molar masses (Supporting Table S1), we find for the product (P) and the product of competitor 2 (C_2), $m_P/m_w = 8.56$ and $m_{C_2}/m_w = 10.11$, respectively. To fit the experimental phase diagram, we used the molecular masses relative to water as initial guesses for the fractions of the molecular volumes, i.e., $r_i = \nu_i/\nu_w \simeq m_i/m_w$, where m_i denotes the molecular mass of molecule i . Given the experimental equilibrium concentrations of the anhydride molecules i ($\phi_i^{I,eq}, \phi_i^{II,eq}$), in their respective binary system, i.e., product (P) with solvent (w) and product of competitor 2 (C_2) with solvent (w), we can solve Eq. (3) for $\chi_{P,w}, \nu_P, \chi_{C_2,w}$ and ν_{C_2} . In the main text $\phi^{II,eq}$ is referred to as c_{out} .

Thus, for the fraction of molecular volumes $r_i = \nu_i/\nu_w$, we obtain $r_P = 6.44$ and $r_{C_2} = 8.35$ which are in good agreement with the mass fraction (see previous paragraph). The obtained interaction parameters in the respective binary system are $\chi_{P,w} = 1.63$ and $\chi_{C_2,w} = 1.76$ (in units of $k_B T$). Keeping these interaction parameters and the molecular volume fractions fixed, we have only one undetermined parameter left, namely χ_{P,C_2} . This parameter is obtained by finding the best agreement with the binodal lines and tie line slopes. Very good agreement is obtained for the value $\chi_{P,C_2} = 0$, see Fig 2. A zero χ_{P,C_2} parameter is consistent with the homotypic interactions and heterotypic interactions between the two anhydrides being approximately of the same magnitude; a scenario that is reasonable due to similarity of the molecular structures of the two anhydrides.

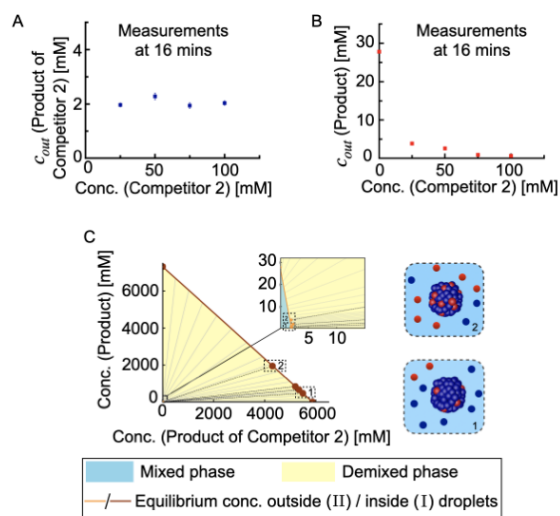


Figure 2: Ternary phase diagram. A) The concentration of the product of competitor 2 in the aqueous phase as function of competitor 2 concentration. The value remains nearly constant around 2 mM. B) The concentration of the product in the aqueous phase as function of competitor 2 concentration. In the absence of competitor 2, the value is 27.8 mM (solubility) and it decreases with increasing competitor 2 concentration. The measurements are performed at 16 mins into the reaction cycle. C) Linear representation of the ternary phase diagram, highlighting that it spans over 3 orders of magnitude in concentration values. The circles denote the experimental data points and the solid lines represent theoretically determined binodal lines and tie lines obtained from solving Eq. (3). The dashed black lines are the experimental tie lines. In the inset, we show the equilibrium concentrations in the aqueous phase (II). The compositions of the aqueous phase and oil droplet phase differ depending on which tie line the total anhydride concentrations lie.

Kinetic model for phase separation of products and fuel-driven chemical reactions

To describe the kinetics of all the reacting molecules in the system, we introduce the concentrations of the two anhydrides (product P and product of competitor 2 C_2) inside the droplet phase (I) as $c_{B_i}^I$, where $i = P, C_2$ and the concentrations of all other molecules outside the droplet as c_j , where $j = F, A_i, AF_i, B_i$ denotes fuel, succinate derivatives (precursor and competitor 2), intermediate molecules, and anhydrides (product and product of competitor 2), respectively. Within our model, these components can undergo chemical reactions as described in Eq. (1), and the anhydrides (product and product of competitor 2) can phase-separate. Supported by the experimental observation that droplets form very quickly on the experimentally relevant time scales of minutes, we propose a simplified model for the total concentrations within the demixed region of the phase diagram. This model relies on fast phase separation and partitioning kinetics of the anhydrides

relative to their chemical reactions. Specifically, this model is valid if the inter-droplet distances do not exceed the reaction-diffusion length scale $\sqrt{D_i/k_{d,i}}$ for both anhydrides. Using experimental values, this reaction-diffusion length scale is in the order of a few hundreds μm , while inter-droplet distances are about a few tenths of μm , supporting the validity of this approximation. Thus, the reaction-partitioning equations for the kinetics of all molecules outside the droplets (II) and the kinetics of the total anhydride concentrations read:

$$\partial_t c_F = - \sum_{i=P,C_2} k_{f,i} c_F c_{A_i} - k_0 c_F, \quad (4a)$$

$$\partial_t c_{A_i} = -k_{f,i} c_F c_{A_i} + k_{3,i} c_{AF_i} + k_{d,i} c_{B_i}, \quad (4b)$$

$$\partial_t c_{AF_i} = k_{f,i} c_F c_{A_i} - (k_{3,i} + k_{2,i}) c_{AF_i}, \quad (4c)$$

$$\partial_t c_{B_i} = k_{2,i} c_{AF_i} - k_{d,i} c_{B_i}, \quad (4d)$$

$$\partial_t \bar{c}_{B_i} = (1 - V^I/V) (k_{2,i} c_{AF_i} - k_{d,i} c_{B_i}). \quad (4e)$$

Under the valid assumption of fast partitioning kinetics compared to the slow chemical reactions outside the droplets, the total concentrations of the two anhydrides, $\bar{c}_{B_i}(t)$ determine their equilibrium concentrations (via Maxwell construction using Eq. (2) in Eqs. (3)) and the volume of the dense phase at each time point t :

$$\text{Maxwell construction: } \bar{c}_{B_i}(t) \rightarrow c_{B_i}^{I,\text{eq}}(t), c_{B_i}^{II,\text{eq}}(t), \quad (4f)$$

$$\text{Volume dense phase: } V^I(t) = V \frac{\bar{c}_{B_i}(t) - c_{B_i}^{II,\text{eq}}(t)}{c_{B_i}^{I,\text{eq}}(t) - c_{B_i}^{II,\text{eq}}(t)}, \quad (4g)$$

for $i = P, C_2$ and V is the total volume of the system which is a constant ($V = 1.05$ mL).

In summary, in our model which considers the limit of fast phase separation compared to chemical reactions, the chemical reactions affect the total concentrations of both anhydrides, leading to instantaneous changes of their respective equilibrium concentrations. These equilibrium concentrations varying with time modify the concentration levels in both phases (I and II) via partitioning and thereby in turn affect the chemical reactions. Due to this feedback between chemical reactions and phase separation, the total concentrations move on a specific path in the two dimensional phase diagram which is unique to the initial succinate derivative and fuel concentrations (see Fig. 3E in main text). The total concentrations of the anhydrides, i.e., $\bar{c}_{B_i}(t)$, can also lie outside the demixed region during the reaction cycle, implying that phase separation is absent and the system is homogeneous (mixed phase). In that case, there is no partitioning and $V^I = 0$, such that only the kinetic equations, i.e., Eqs. (4a) (4b) (4c), and Eq. (4e), are to be solved.

When we study the competition system between product and product of competitor 1, we also apply the aforementioned approach to the case where phase separation of anhydrides is absent and the system is always homogeneous.

3. Obtaining reaction rate constants for the kinetic model

We study three succinate derivatives, which we label as P, C_1 and C_2 and their corresponding anhydrides. We fit the experimental measurements with the kinetic traces of each of the reaction

cycles to determine the rate constants (Figs 3, 4 and 5).

Systems with one succinate derivative

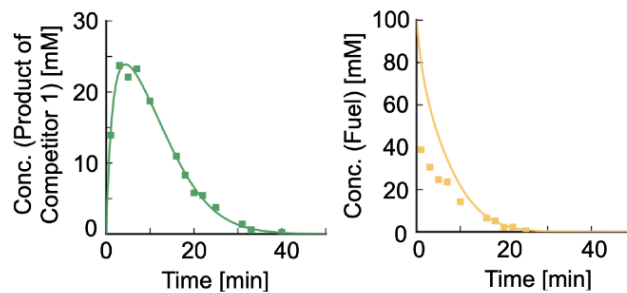


Figure 3: First order deactivation and short lifetime of product of competitor 1. 50 mM competitor 1 fuelled with 100 mM *EDC*. The two curves, corresponding to the time trace of the product of competitor 1 and fuel concentration respectively, are globally fitted to obtain the reaction rate constants. The concentration profile of product of competitor 1 shows an exponential decay as it is not able to phase separate due to its high solubility of roughly 3000 mM. Markers represent HPLC data; solid lines represent data calculated using the theoretical kinetic model.

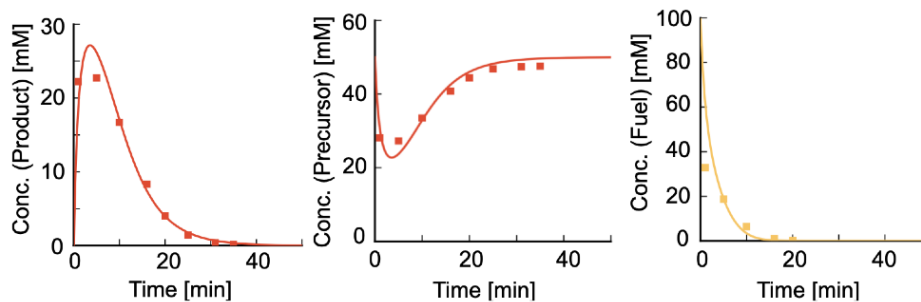


Figure 4: First order deactivation and short lifetime of product. 50 mM precursor fuelled with 100 mM *EDC*. The three curves, corresponding to the time trace of the product, precursor and fuel concentration respectively, are globally fitted to obtain the reaction rate constants. The product concentration profile shows an exponential decay as it is not able to phase separate due to its high solubility of roughly 27 mM. Markers represent HPLC data; solid lines represent data calculated using the theoretical kinetic model.

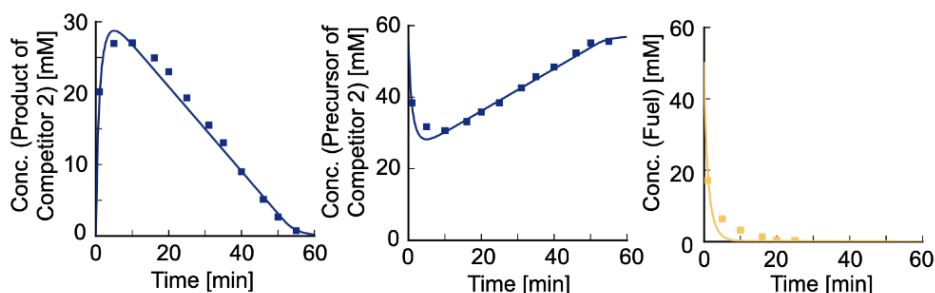


Figure 5: Zeroth order deactivation and long lifetime of product of competitor 2. 50 mM competitor 2 fuelled with 50 mM *EDC*. The three curves, corresponding to the time trace of the product of competitor 2, competitor 2 and fuel concentration respectively, are globally fitted to obtain the reaction rate constants. The concentration profile of product of competitor 2 shows a linear decay as it is able to phase separate due to its low solubility of roughly 2 mM. Markers represent HPLC data; solid lines represent data calculated using the theoretical kinetic model. The concentration of competitor 2 had to be re-adjusted to 57 mM in the theoretical kinetic model for the fitting procedure due to inaccuracies in the stock solution.

System with two competing succinate derivatives

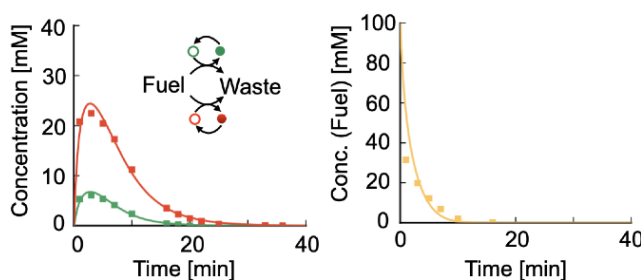


Figure 6: First order deactivation for the product and product of competitor 1. 50 mM precursor and 50 mM competitor 1 fuelled with 100 mM *EDC*. The three curves, corresponding to the time trace of two anhydrides and fuel concentration respectively, are globally fitted to obtain the reaction rate constants. The concentration profiles of product and product of competitor 1 both show exponential decay as neither is able to phase separate, and competition for fuel results in reduced yields for both anhydrides. Markers represent HPLC data; solid lines represent data calculated using the theoretical kinetic model.

Having obtained the reaction rate constants from the above fits in Fig. 6, we proceed to see how the traces change with changing competitor 1 (C_1) concentration and using fixed precursor (P) and *EDC* concentrations (Fig. 7).

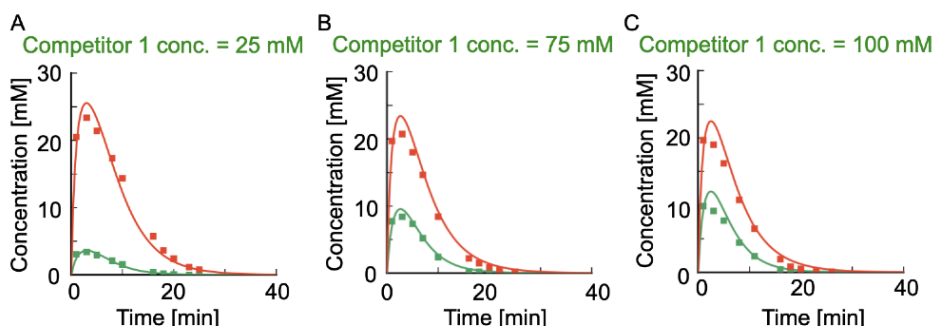


Figure 7: Competitor 1 reduces the yield and lifetime of the product. A) 25 mM C_1 , B) 75 mM C_1 , C) 100 mM C_1 , and 50 mM P fuelled with 100 mM EDC . Increasing the competitor 1 concentration reduces the maximum yield of the product and also its lifetime. Markers represent HPLC data; solid lines represent data calculated using the theoretical kinetic model.

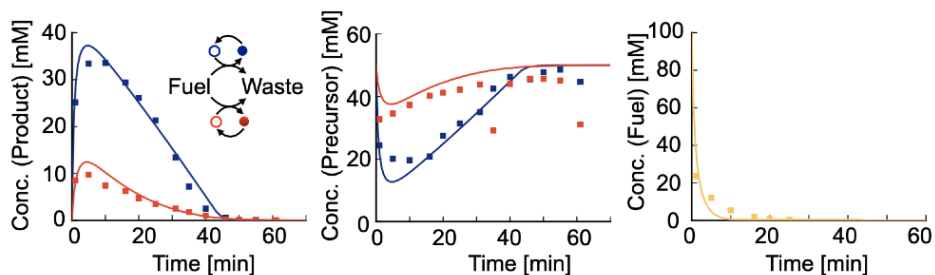


Figure 8: Non-linear and linear deactivation for the product and product of competitor 2 respectively. 50 mM precursor (P) and 50 mM competitor 2 (C_2) fuelled with 100 mM EDC . We globally fit five curves corresponding to the time trace of two anhydrides, two succinate derivatives and fuel concentration, respectively, to obtain the reaction rate constants. The two outlier points in the precursor concentration trace are omitted however. The linear decay of product of competitor 2 shows that it phase separates and the non-linear decay of the product implies that it partitions in the droplets, which we refer to as co-phase separation. Markers represent HPLC data; solid lines represent data calculated using the theoretical kinetic model.

Having obtained the reaction rate constants from the above fits in Fig. 8, we proceed to see how the traces change with changing competitor 2 (C_2) concentration and using fixed precursor (P) and EDC concentrations (Fig. 9).

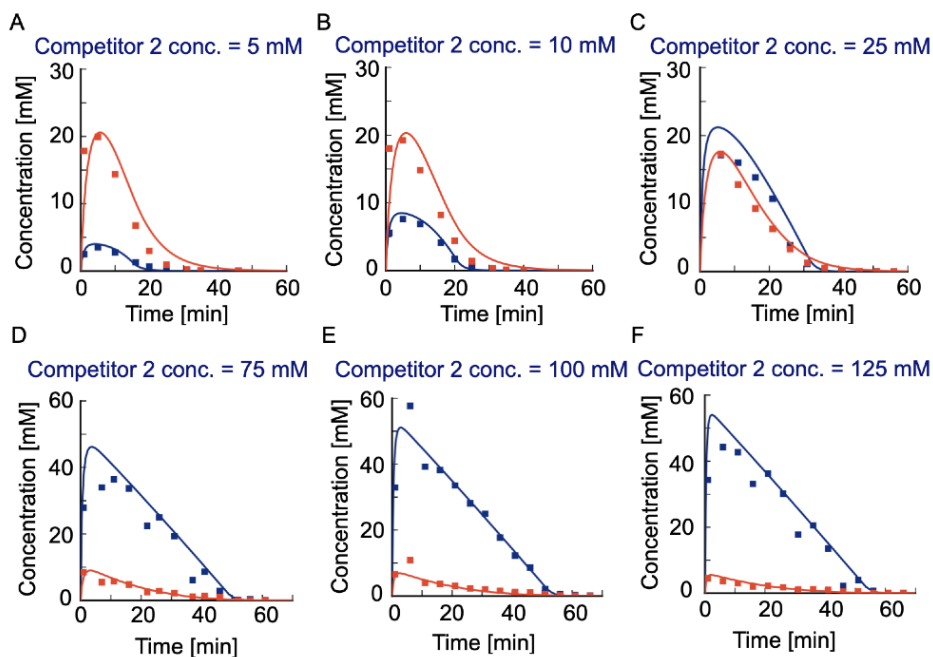


Figure 9: Competitor 2 reduces the yield but increases lifetime of the product. A) 5 mM C_2 , B) 10 mM C_2 , C) 25 mM C_2 , D) 75 mM C_2 , E) 100 mM C_2 , F) 125 mM C_2 and 50 mM P fuelled with 100 mM EDC . Increasing competitor 2 concentration reduces the maximum yield of the product, but prolongs its lifetime, allowing us to label competitor 2 as *host* and precursor as *parasite*. Markers represent HPLC data; solid lines represent data calculated using the theoretical kinetic model.

Summary of reaction rate constants

Name	Condition	k_0 [s ⁻¹]	k_f [M ⁻¹ s ⁻¹]	k_2 [s ⁻¹]	k_3 [s ⁻¹]	k_d [s ⁻¹]
Competitor 1	Single	1.35e-5	0.085	0.52	0.11	3.7e-3
	w/ Precursor		0.037	0.58	0.23	4.2e-3
Precursor	Single	1.35e-5	0.20	0.63	0.52	2.7e-3
	w/ Competitor 1		0.21	0.37	0.28	3.2e-3
	w/ Competitor 2		0.10	0.30	0.32	1.0 - 2.3e-3
Competitor 2	Single	1.35e-5	0.35	0.50	0.26	4.9 - 6.8e-3
	w/ Precursor		0.35	0.50	0.26	8.8e-3

Figure 10: Reaction rate constants. Readout for the chemical reaction rate constants used in the kinetic model as obtained from the global fits.

We summarise the reaction rate constants obtained from fits as mentioned above (Figs. 3, 4, 5, 6 and 8). We observed that in general there are only little differences in the deactivation rate constants of the single precursor system and to the system where two components compete about fuel. However, a noticeable effect is the reduction in the activation pathway rate constant, primarily k_f of competitor 1 (C_1) in the competition system with precursor (P) and that of the precursor (P) in the competition system with competitor 2 (C_2). For both single and competition studies we keep the solubilities of the product and product of competitor 2 unchanged to values, 2.01 mM and 27.8 mM, respectively. We thus assumed that competition for the fuel affects the availability of fuel for specific succinate derivatives. For periodic fueling studies, the lower value k_d was used for the product. For the Fig. 5 we use the lower value of k_d and for Fig. 1F in the main text, we use the higher value of k_d for product of competitor 2 as it was obtained from fitting routine.

4. Lifetime and half lifetime measurements for the product

The lifetime of the anhydrides is defined phenomenologically by threshold concentrations. The lifetime corresponds to the time period when the anhydride concentration is above this threshold. A threshold concentration can lose robustness against experimental measurements if it lies in the tailing regime of an exponential decay. It also becomes an injudicious choice if set to a high concentration value which is unachieved during the course of the experiment. Therefore, we choose threshold concentration values as described below such that the aforementioned difficulties are circumvented.

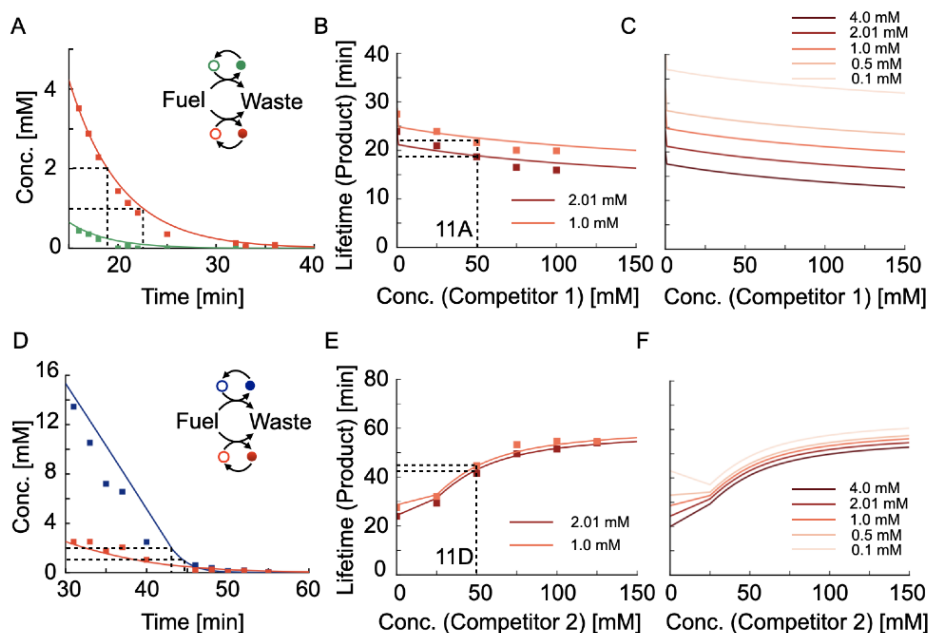


Figure 11: Co-phase separation allows longer survival of the product due to protection inside droplets from hydrolysis. A) The anhydride concentration profiles in the low concentration regime when 50 mM precursor and 50 mM competitor 1 compete for 100 mM fuel. The black dashed lines denote how the lifetimes are measured corresponding to threshold conc. values 2.01 mM and 1.0 mM. B) The lifetime of product measured for threshold concentrations of 2.01 mM and 1.0 mM. C) Trend of lifetime is robust against different threshold choices (4 mM, 2.01 mM, 1 mM, 0.5 mM and 0.1 mM). The lifetime of product decreases with increasing competitor 1 concentration. D) The anhydride concentration profiles in the low concentration regime when 50 mM precursor and 50 mM competitor 2 compete for 100 mM fuel. The black dashed lines denote how the lifetimes are measured corresponding to threshold conc. values 2.01 mM and 1.0 mM. E) The lifetime of product measured for threshold concentrations of 2.01 mM and 1.0 mM. F) Trend of lifetime is robust against different threshold choices (4 mM, 2.01 mM, 1 mM, 0.5 mM and 0.1 mM). The lifetime of product increases with increasing competitor 2 concentration. Markers represent lifetimes calculated using HPLC data; solid lines represent data calculated using the theoretical kinetic model.

We have performed two sets of competition experiments where precursor competes with competitor 1 and competitor 2, respectively. The important difference between the two competitors is that competitor 2 has a significantly lower solubility of about 2 mM compared to competitor 1 which has solubility of roughly 3000 mM, and therefore the former is capable of phase separation in the

working concentration ranges. The lifetime measurements, corresponding to Fig. 3B in the main text, are done by tracking a threshold concentration of 2.01 mM for the product. Similarly, corresponding to Fig. 3E in the main text, the lifetime measurement of the product is done by tracking the threshold concentration 2.01 mM for the product of competitor 2, as it highlights the lifetime of the droplets. We believe that the lifetimes of both the host (product of competitor 2) and parasite (product) are the same in this case. However this form of measurement is undefined for small concentration values of competitor 2 since droplets are short-lived and the product survives after droplet dissolution. In these concentration ranges we track the threshold concentration for the product instead of the product of competitor 2. We therefore choose to measure the half lifetime of the product which has a robust definition in either competition system.

The half lifetime is measured as the time difference between the time points of the maximum value and the half maximum value of the product concentration, respectively. In the experimental data, we locate the maximum value of the product concentration, calculate its halved value and determine the time point by linearly interpolating between the immediate high and low value around the half maximum. Refer to Fig. 12 for visualisation.

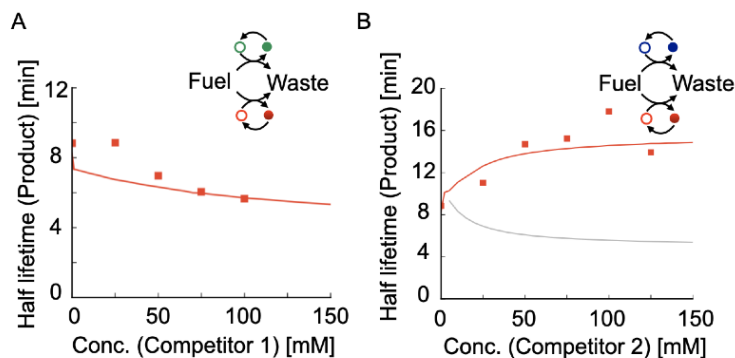


Figure 12: Half lifetime of product as a measure of survival in presence of competition. A) Half lifetime of product as a function of competitor 1 concentration. The half lifetime reduces due to competition for fuel in the system. B) Half lifetime of product as a function of competitor 2 concentration. The half lifetime increases due to protection in droplets from hydrolysis, but approaches saturation owing to a fixed fuel concentration of 100mM. The gray line denotes that in absence of co-phase separation in the competition system with competitor 2, the half lifetime would decrease solely due to competition for the fuel. Markers represent half lifetime calculated using HPLC data; solid lines represent data calculated using the theoretical kinetic model.

5. Composition of droplets

We quantified the percentage of the droplet material composed of the product for three different conditions with increasing competitor 2 concentration.

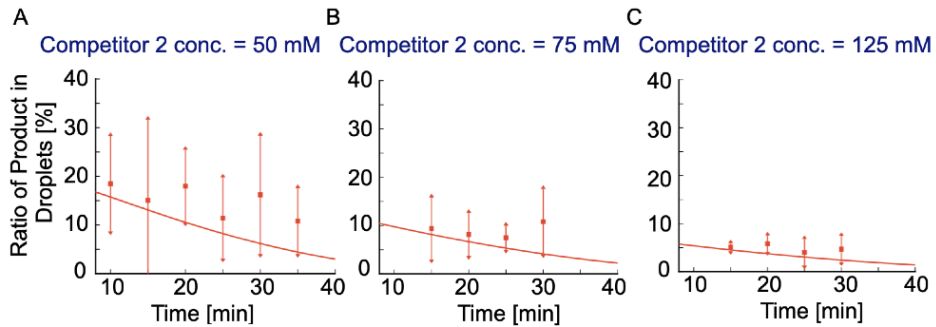


Figure 13: Reduction in composition of the product (parasite) in the droplets with increasing product of competitor 2 (host) concentration. A) 50 mM, B) 75 mM, C) 125 mM, respectively. Increasing concentration of the host reduces the maximum concentration of the parasite in the droplets. Also the maximum value of product monotonically decreases with time as the total volume of droplets keeps decreasing. Markers represent ratio calculated using HPLC data; solid lines represent data calculated using the theoretical kinetic model.

6. Mechanism of Co-phase separation

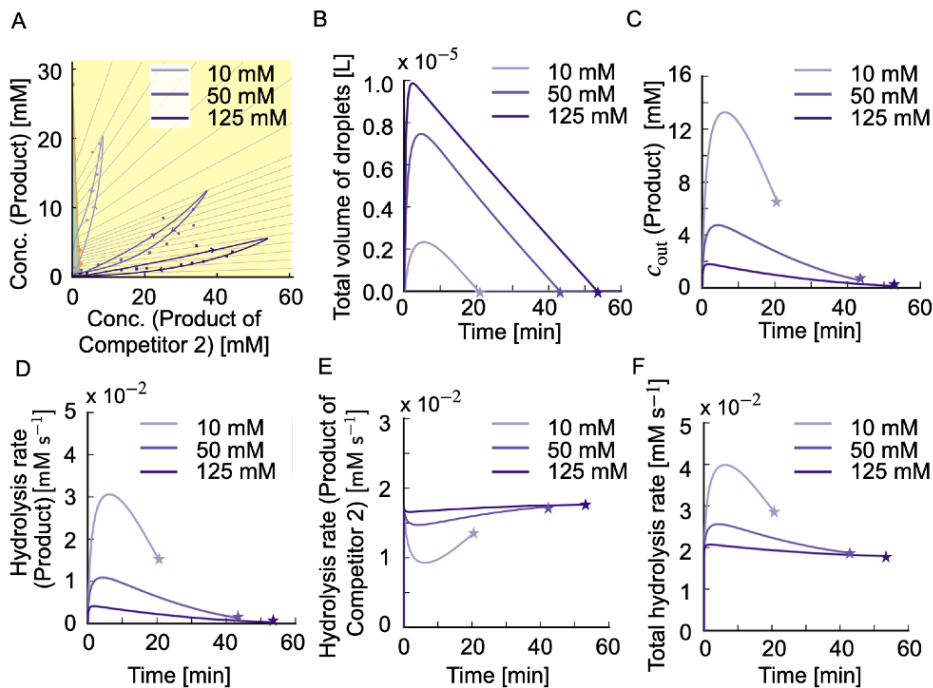


Figure 14: Total droplet volume increases and total hydrolysis rate decreases in the dilute phase allowing longer survival of the parasite. A) The kinetic orbits corresponding to different concentrations of competitor 2. The kinetic orbit crosses fewer tie lines at maximal competitor 2 concentration (125 mM), suggesting the solubility change is not drastic and allows nearly zeroth order decay for both anhydrides. Markers represent HPLC data; solid lines represent data calculated using the theoretical kinetic model. B) The total droplet volume increases with increasing the competitor 2 concentration and the product of competitor 2 starts acting like a host to protect the parasite inside the droplets from hydrolysis. C) The equilibrium concentration of the product in the aqueous phase, c_{out} , decreases with increasing competitor 2 concentration. D) The hydrolysis rate of the product in the dilute phase decreases with increasing competitor 2 concentration. E) The hydrolysis rate of the product of competitor 2 in the aqueous phase sets the offset of the total hydrolysis rate, and it increases with increasing competitor 2 concentration. F) The total hydrolysis rate of both anhydrides outside the droplets. The stars in B, C, D, E and F denote the time-point of dissolution of droplets.

7. Co-phase separation with periodic fuelling

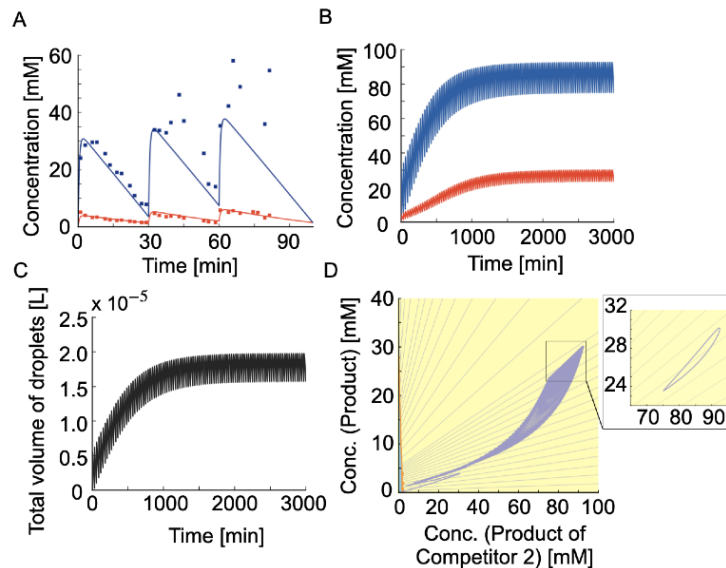


Figure 15: Survival and consequent enrichment of both the product of competitor 2 (host) and the product (parasite) due to co-phase separation. A) The time traces of both anhydrides (host and parasite with initial concentrations 100 mM and 50 mM, respectively), for periodic fuelling at the rate of 60 mM every 30 minutes. Markers represent HPLC data; solid lines represent data calculated using the theoretical kinetic model. Disagreement between the experimental data and the data calculated from the kinetic model for the host is more prominent after the first cycle of fuelling due to the formation of multiple droplets that settled at the bottom of the HPLC screw cap vial. B) The time traces of the host and the parasite under the experimental fuelling conditions to highlight the long-time behavior using the kinetic model. We observe the emergence of a non-equilibrium steady state for both the host and the parasite. C) The total volume of droplets also achieves a non-equilibrium steady state. D) The time trace representation in the phase diagram shows the oscillatory behavior and approach to a non-equilibrium steady state. The inset depicts the limit cycle in the phase diagram achieved due to the emergence of non-equilibrium steady states for both the host and the parasite (in the inset: last 3 cycles).

8. Buffer capacity in presence of periodic fuelling

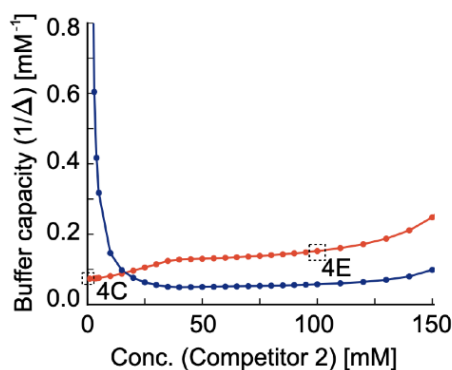


Figure 16: The buffer capacity against fuel oscillations increases for the parasite with increasing host concentration. The buffer capacity defined as inverse of the deviation in concentration, i.e., (Δ^{-1}) increases for the parasite with the increasing competitor 2 (host) concentration. The propensity to co-phase separate increases in the system with increasing the host concentration which allows for more protection of the parasite and thus less degradation. It leads to smaller deviations around mean pseudo-steady state concentration. The host's buffer capacity decreases, making it more susceptible to fluctuations. The blue and red solid line represent buffer capacity of host and parasite respectively. Initially the buffer capacity of the host is high due to lower mean concentration of the host and hence less deviation. As the mean concentration increases, the deviation around it also increases, thus reducing its buffer capacity. The opposite trend occurs for the parasite, upto 40 mM, following which the mean concentration of the product also increases due to the protection from the host droplets. The highlighted values of buffer capacity are corresponding to the data shown in the main text Figs. 4C and 4E, respectively.

9. Effects of activation rate constants on host-parasite identity

We have shown that the kinetic orbit of the average product concentrations in the phase diagram determines the lifetimes of the products and the composition inside droplets. The shape of the orbit is also affected by the rate constants. To illustrate this aspect we considered, precursor concentration of 50 mM and competitor 2 concentration of 100 mM fuelled with 100 mM *EDC*, as the experimental reference and swapped the rate constants related to the activation reaction pathway (Fig. 17).

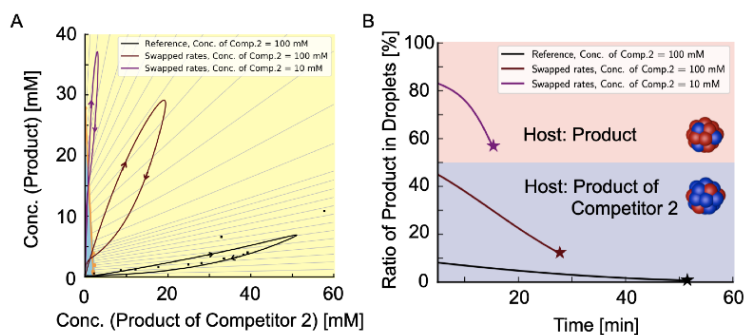


Figure 17: Host and parasite identity depends on the solubilities of the components and initial precursor concentrations. A) Kinetic orbits in the phase diagram corresponding to three different parameter sets in which we swapped the rate constants of the fuel-driven activation pathway (i.e., all rate constants except for the deactivation rate constants) and considered different concentrations of competitor 2 at a fixed *EDC* concentration of 100 mM and precursor concentration of 50 mM. Markers represent HPLC data; solid lines represent data calculated using the theoretical kinetic model. B) The ratio of product of precursor in droplets over time shows that the identity of host and parasite can change with swapped rates. Due to the higher solubility, the product is typically the parasite, except when it is at excess. In this case, the product starts as a host and transits to a parasite, as long as droplets do not dissolve beforehand. The star markers denote the time-point of droplet dissolution.

6. Chemically Fueled Materials with a Self-Immolative Mechanism: Transient Materials with a Fast On/Off Response

Abstract. In this work, we wanted to demonstrate that feedback offers new ways to control materials. We designed an opposing feedback mechanism that counteracts the negative feedback mechanism of phase-separated anhydride oil droplets described in Chapter 3 and Chapter 5 to rapidly dissolve them above a certain threshold. We found that the surfactant precursor can form micelles above its CMC and rapidly dissolve the emulsion. The micelles accelerate the hydrolysis rate, resulting in the release of more surfactant precursor, which further accelerates the hydrolysis rate, *i.e.*, a self-immolation mechanism. In contrast to common self-immolative materials, which require the addition of an external trigger to initiate their degradation, we designed the system such that the trigger for self-immolation is released *in-situ* by the reaction cycle. This mechanism offered precise control over the material properties and enabled us to significantly improve its off-response, *i.e.*, the time the material requires to switch off. We showcase our findings with applications of the self-immolative emulsion as a self-expiring ticket and a drug delivery platform with a unique linear-then-burst release profile. We believe that these preliminary results could serve as a basis for developing more sophisticated, life-like materials.

This work has been published:

Title: Chemically fueled materials with a self-immolative mechanism: transient materials with a fast on/off response

Authors: Patrick S. Schwarz, Laura Tebcharani, Julian E. Heger, Peter Müller-Buschbaum, Job Boekhoven

First published: 21. June 2021

Journal: *Chem. Sci.*, **2021**, 12, 9969-9976.

Publisher: Royal Society of Chemistry

DOI: 10.1039/D1SC02561A

Reprinted with permission from *Chem. Sci.* **2021**. Copyright 2021 Royal Society of Chemistry.

This section states the individual work of each author in the publication above. P. S. Schwarz, J. Boekhoven and P. Müller-Buschbaum designed the experiments. P. S. Schwarz, L. Tebcharani and J. E. Heger performed the experiments. P. S. Schwarz and J. Boekhoven wrote the manuscript. All authors have given approval to the final version of the manuscript.



Cite this: *Chem. Sci.*, 2021, 12, 9969

All publication charges for this article have been paid for by the Royal Society of Chemistry

Received 10th May 2021
 Accepted 19th June 2021

DOI: 10.1039/d1sc02561a

rsc.li/chemical-science

Chemically fueled materials with a self-immulative mechanism: transient materials with a fast on/off response†

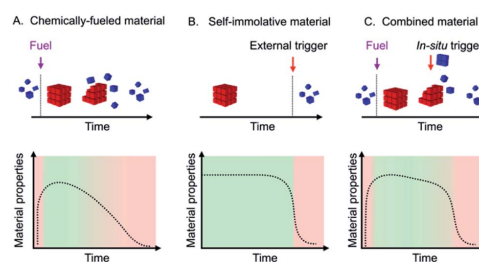
Patrick S. Schwarz,^a Laura Tebcharani,^a Julian E. Heger,^b Peter Müller-Buschbaum^{b,c} and Job Boekhoven^{b,*ad}

There is an increasing demand for transient materials with a predefined lifetime like self-erasing temporary electronic circuits or transient biomedical implants. Chemically fueled materials are an example of such materials; they emerge in response to chemical fuel, and autonomously decay as they deplete it. However, these materials suffer from a slow, typically first order decay profile. That means that over the course of the material's lifetime, its properties continuously change until it is fully decayed. Materials that have a sharp on-off response are self-immulative ones. These degrade rapidly after an external trigger through a self-amplifying decay mechanism. However, self-immulative materials are not autonomous; they require a trigger. We introduce here materials with the best of both, *i.e.*, materials based on chemically fueled emulsions that are also self-immulative. The material has a lifetime that can be predefined, after which it autonomously and rapidly degrades. We showcase the new material class with self-expiring labels and drug-delivery platforms with a controllable burst-release.

Introduction

Transient materials retain their function over a defined period and dissolve or resorb when their task is fulfilled.¹ They are particularly powerful in medicine, *i.e.*, as a scaffold that aids the body to regenerate lost tissue or as a delivery system for therapeutics.² They have also gained popularity in electronics as temporary circuits that disintegrate after a predefined time.^{1,3} These materials degrade by a range of structure-dependent biodegradation processes.⁴ A different approach for the generation and degradation of transient materials is through chemically fueled materials. These materials are regulated by a fuel-driven chemical reaction cycle, *i.e.*, in the cycle, building blocks for the materials are activated at the expense of chemical fuel, and the building blocks spontaneously deactivate. When a finite amount of fuel is added to such a system, a material emerges, and it autonomously decays when it runs out of fuel.⁵ The building blocks of these materials are typically self-assembling molecules and yield supramolecular materials like fibers,⁶

vesicles,⁷ micelles,⁸ colloids,⁹ oil-or coacervate based droplets,¹⁰ nanoparticles,¹¹ hybridized DNA¹² and others. We and others applied chemically fueled assemblies as transient materials, *e.g.*, as self-erasing inks,^{6c,13} drug delivery platforms,^{10d} solutions containing macrocycles,¹⁴ transient hydrogels,^{6a-c,12a,15} supramolecular polymers,¹⁶ transient emulsions,^{10a-d} transient photonics¹⁷ and temporary nanoreactors.^{7c,8a,18} These fuel-driven supramolecular materials, but also other approaches towards transient materials, typically decay *via* first- or zeroth-order kinetics. The material and its properties will thus decay over its entire lifetime (Scheme 1A). Such a constant decay profile can be disadvantageous for applications that require a fast on-off response, *i.e.*, materials in which the period of



Scheme 1 Schematic representations of a chemically fueled material (A), a self-immulative material (B), and a combined material (C) with their respective evolutions of material properties.

^aDepartment of Chemistry, Technical University of Munich, Lichtenbergstraße 4, 85748 Garching, Germany. E-mail: job.boekhoven@tum.de

^bLehrstuhl für Funktionelle Materialien, Physik Department, Technische Universität München, James-Frank-Str. 1, 85748 Garching, Germany

^cHeinz Maier-Leibnitz Zentrum (MLZ), Technische Universität München, Lichtenbergstr. 1, 85748 Garching, Germany

^dInstitute for Advanced Study, Technical University of Munich, Lichtenbergstraße 2a, 85748 Garching, Germany

† Electronic supplementary information (ESI) available. See DOI: 10.1039/d1sc02561a



switching off is only a fraction of the total lifetime of the material. For example, a transient electronic circuit that is operational for its entire lifetime and then rapidly dissolves is more useful than one that decays gradually after its emergence. Similarly, it would be desirable that self-degrading packaging retains its material properties and rapidly decays when its lifetime is over.

Self-immolation partly addresses this challenge by making use of a self-amplifying decay mechanism which found widespread application in hydrogels,¹⁹ drug delivery,²⁰ antibiotics,²¹ fluorescent labels,²² temporary linkers,²³ microcapsules and membranes,²⁴ degradable plastics,²⁵ sensors²⁶ and responsive polymers.²⁷ However, self-immolative materials do not decay autonomously but instead require an external trigger that initiates the self-amplifying cascade (Scheme 1B).

In this work, we thus explore materials that make use of the best of both: we describe the synthesis of chemically fueled materials with self-amplifying decay mechanisms to accelerate their off-response (Scheme 1C). We make use of two simultaneously operating feedback mechanisms of the material on its regulatory kinetics: one feedback mechanism ensures that the material decays slowly with linear kinetics, while a second feedback mechanism ensures a rapid autocatalytic decay once a threshold level is reached. In contrast to self-immolative materials, the trigger for the degradation is released *in situ* by the reaction cycle. In other words, the addition of a trigger is not necessary as the autocatalytic decay occurs as soon as the *in situ* release of the trigger reaches the aforementioned threshold. The result is a set of materials, turbid emulsions, self-erasing labels, and drug-releasing hydrogels that autonomously decay after their lifetime with a very fast, autocatalytic response. Specifically, the decay time is less than 10% of the total material's lifetime.

Results and discussion

The basis of our autonomous self-immolative material is a transient emulsion formed by a chemically fueled reaction cycle (Fig. 1A). The reaction cycle uses a condensing agent (1-ethyl-3-(3-dimethylaminopropyl)carbodiimide hydrochloride (EDC or fuel) as a chemical fuel to convert the 2-decen-1-ylsuccinate (precursor) into its corresponding anhydride (activation reaction). The anhydride is unstable in the aqueous media and hydrolyzes back to the precursor (deactivation reaction). Thus, when a finite amount of fuel is added, the anhydride emerges and decays again as fuel is depleted. Above its solubility, the anhydride phase separates into micron-sized oil droplets, which results in the formation of a turbid emulsion (see ESI, Fig. 1†).^{10a,10b,10d} As the anhydride deactivates, the total droplet material does too, resulting in a decrease in turbidity until a transparent solution is obtained (Fig. 1B). Thus, the loss of turbidity can serve as a measure for the state of the material. The anhydride hydrolysis proceeds with a characteristic zero-order decay because the droplets protect the anhydride molecules from hydrolysis.^{9,10d} Consequently, hydrolysis only occurs on the fraction in solution, which is constant and equal to the anhydride's solubility.

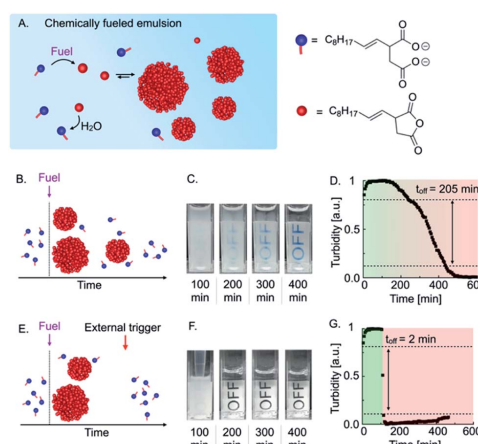


Fig. 1 Triggered self-immolation of a chemically fueled, active emulsion. (A) Schematic representation of a chemically fueled reaction cycle based on 2-decen-1-ylsuccinic acid as precursor and EDC as chemical fuel. (B) Schematic representation of the temporal course of a chemically fueled emulsion. (C) Webcam images of 7.5 mM precursor fueled with 2 mM EDC. (D) Grey-value analysis of 7.5 mM precursor fueled with 2 mM EDC. (E) Schematic representation of the temporal course a self-immolative emulsion that rapidly degrades in response to the addition of the surfactant precursor as an external trigger. (F) Webcam images of 7.5 mM precursor fueled with 2 mM EDC and triggered with 20 mM precursor after 100 min. (G) Grey-value analysis of 7.5 mM precursor fueled with 2 mM EDC and triggered with 20 mM precursor after 100 min.

When we added 2 mM EDC to 7.5 mM precursor, the solution immediately turned turbid (Fig. 1C). Over the course of roughly 400 min, the turbidity of the emulsion decreased continuously, which we quantified by measuring the grey value of the time-lapsed photographs in selected areas and found a characteristic constant decay of the emulsion's turbidity (Fig. 1D). We considered the material as "turbid" above a grey value of 0.8 and "optically clear" below 0.1. Using this definition, we could calculate that the material spends roughly 205 min transitioning from turbid to optically clear. We refer to this value as the "off-response," *i.e.*, the time it takes to switch off the material.

In order to obtain a sharper off-response, like self-immolative materials, we tested whether the addition of an external trigger could induce the degradation of the material (Fig. 1E). We hypothesized that the addition of a surfactant could increase the solubility of the anhydride and thereby accelerate its deactivation through hydrolysis.²⁸ For common and inverse micelles, a micelle-catalyzed formation of micelle-forming components results in an autopoietic micellar system, *i.e.*, the micelles catalyze the formation of their own building blocks.²⁹ Analogously, we hypothesized that the precursor at high concentrations could act as a surfactant that forms micelles and helps to dissolve the anhydride which accelerates the hydrolysis and results in the release of more



surfactant. Indeed, by means of Nile Red assay and DLS measurements, we found that the precursor could form micelles of roughly 7 nm in diameter in the absence of oil droplets above a critical micelle concentration of roughly 1 mM (CMC, see ESI, Fig. 2 and 3†). A CMC typically increases in the presence of oil droplets as the surfactant first saturates the surface of the droplets before forming micelles.³⁰ Thus, we also measured indirectly the CMC in the presence of oil droplets. Indeed, we found a CMC of roughly 11 mM precursor when samples were fueled with 2 mM EDC (see ESI, Fig. 4 and notes†). We hypothesized that the addition of precursor as an external trigger could result in an increase in the anhydride solubility. That increase would accelerate the hydrolysis that further releases precursor, which is the basis of a self-immolative cascade. To prove whether the precursor can be used as an external trigger, we fueled 7.5 mM precursor with 2 mM EDC and added a concentrated solution of precursor after 100 min (Fig. 1F). In contrast to the experiment without the addition of a trigger, we observed that the emulsion almost immediately turned transparent. We quantified the self-immolation by measuring the grey values of a selected area in the images and calculated an off-response of 2 min (Fig. 1G). From these findings, we conclude that the excess of precursor can form micelles that solubilize the anhydride oil resulting in its rapid hydrolysis. Thus, the addition of excess of precursor can serve as a trigger for self-immolation.

As the trigger for self-immolation of the emulsion is also produced by the deactivation reaction of the reaction cycle, we tested if we could design it such that the trigger is generated *in situ* (Fig. 2A). In our design, we start with a solution of precursor above its CMC, *i.e.*, a micellar precursor solution. To this solution, we add fuel to induce droplet formation. As the micelle-

forming precursor is partly converted into droplet-forming product, the micellar solution turns into a turbid emulsion without micelles. As the deactivation of the anhydride proceeds, the concentration of the precursor in the solution with droplets increases until it reaches the CMC of roughly 11 mM. At that point, the micelles will reappear and act as an *in situ* generated trigger for the solubilization of the emulsion.

Indeed, when we fueled 20 mM precursor with 9 mM EDC, the turbidity remained mostly constant, but, after 400 min, suddenly and rapidly decreased (Fig. 2B). Quantification of the grey value showed that the off-response took 10 min, which equals only 2.5% of the total lifetime (Fig. 2C). In other words, the emulsion retains its original properties 97.5% of the time, and then it rapidly degrades.

To quantitatively understand the mechanisms at play, we performed high-performance liquid chromatography (HPLC) of our transient emulsions (7.5 mM precursor with 8 mM EDC) and quantified the anhydride and EDC concentration profiles (Fig. 2D and ESI, Fig. 5†). Under these conditions, the precursor is not able to form micelles when droplets are present. We found that the anhydride concentration increased rapidly in the first 30 min at the expense of EDC, which is consumed within the same timeframe. From there on, the anhydride concentration decayed linearly until no more anhydride was detected after roughly 1400 min. We can explain the linear decay of the anhydride with a self-protection mechanism which was described in previous work.^{9,10c} In this mechanism, the anhydride phase separates into droplets and is thereby physically separated from the aqueous phase. Thus, hydrolysis can only take place on the fraction that remains in the aqueous solution, which results in a linear decay of the anhydride until all droplets are dissolved. This relation implies that the decay rate of the emulsion is dependent on the anhydride solubility, which is constant. Indeed, we were able to fit and accurately predict the kinetics of our reaction cycle with a kinetic model that takes into account this self-protection mechanism (see ESI, Fig. 6, notes, and ESI, Table 2†).

When we fueled a solution of 20 mM precursor with the same amount of fuel, *i.e.*, a solution of precursor that contained micelles, we found a similar rapid increase in anhydride concentration until all fuel has been depleted (Fig. 2D, green trace). Then, the anhydride concentration decays linearly, which implies that the self-protection mechanism is also present in this experiment. However, after 300 min, the negative slope of the anhydride concentration as a function of time started to increase and deviate from a linear decay. The acceleration of the hydrolysis rate kept on increasing until no more anhydride was detected, pointing towards an autocatalytic hydrolysis mechanism.

We explain the autocatalytic behavior by the following mechanism. Before the addition of fuel, the solution of the precursor contains micelles. The conversion of the precursor into its corresponding anhydride decreases the precursor concentration in solution to values below its CMC. Consequently, shortly after the addition of fuel, the solution contains droplets and most likely no micelles. As the reaction cycle proceeds, the anhydride concentration decays linearly, and thus

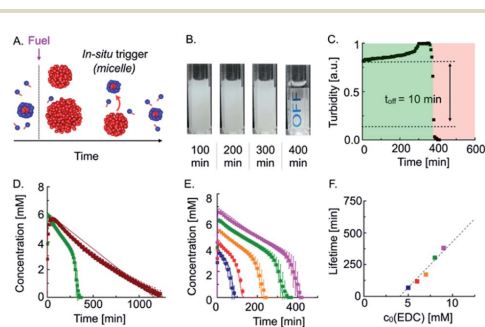


Fig. 2 Autonomous self-immolation based on an *in situ* trigger release. (A) Schematic representation of an autonomous self-immolative material. (B) Webcam images of 20 mM precursor fueled with 9 mM EDC. (C) Grey-value analysis of 20 mM precursor fueled with 9 mM EDC. (D) Anhydride concentration profiles of 7.5 mM (burgundy red) and 20 mM precursor (green) fueled with 8 mM EDC. (E) Anhydride concentration profile of 20 mM precursor fueled with different amounts of EDC. Markers represent HPLC data; solid lines represent data calculated by the kinetic model. (F) Lifetime of the turbidity against initial fuel concentration (markers). The dashed line is added to guide the eye.

the concentration precursor increases *vice versa*. After 300 min, the precursor reaches its CMC, and micelles start to form, which act as a phase-transfer catalyst and solubilize the anhydride which significantly increases the anhydride hydrolysis rate. Similar to reported models of micellar phase-transfer catalysis, it is likely that mixed micelles composed of precursor and anhydride are formed.³¹ However, the hydrolysis reaction of the anhydride does not occur at or in the micelles but in the bulk solution.^{31,32} As the anhydride hydrolysis rate increases, the concentration of micelles further increases, thereby further accelerating the hydrolysis rate. This mechanism explains (1) the sudden onset of acceleration of the hydrolysis and (2) the ever-increasing hydrolysis rate due to autocatalysis.

To quantitatively verify our proposed mechanisms, we wrote a kinetic model that describes the activation reaction, deactivation reaction, and the self-protection mechanism, which is activated when the anhydride passes its solubility of 0.025 mM in the absence of micelles (see ESI, Fig. 6, Table 2 and notes[†]). The model captures the evolution of the anhydride in the absence of micelles very well. Then, we adjusted the kinetic model to also describe the autocatalytic behavior. Autocatalytic micellar systems have been well described with kinetic models relying on classical micellar catalysis³³ as well as on phase-transfer catalysis.^{31,32,34} We found good agreement with the experimental data using a phase-transfer catalysis model in which micelles enable the insoluble anhydride the transition in the aqueous phase. We observed that the autocatalytic decay initiated when the concentration precursor reached a threshold concentration of 16.5 mM, which we considered as the CMC of the system under these conditions. Thus, in our kinetic model, we described that above 16.5 mM, every additional precursor molecule released by hydrolysis increases the solubility of the anhydride. We found that we could fit the data well by defining an effective solubility (S_{eff}) above the CMC. It is calculated based on the constant solubility of the anhydride below the CMC (S_0) and increases as a function of the amount of precursor above the CMC. This increase scales with a factor of 0.1, which we refer to as the solubilization capacity (SC) of the surfactant precursor. The effective solubility can then be calculated following the equation $S_{\text{eff}} = S_0 + SC \times ([\text{precursor}] - \text{CMC})$ (see ESI, notes[†]). For example, if the precursor concentration was 17.5 mM, *i.e.*, 1 mM above its CMC, the effective anhydride solubility increased from 0.025 mM to 0.125 mM. The increase in solubility accelerates the hydrolysis, which again increases the precursor release rate. The solubilization capacity $SC = 0.1$ implies that roughly ten precursor molecules are used to solubilize a molecule of anhydride. Our kinetic model calculated that the maximum acceleration of the hydrolysis rate towards the end of the self-immolation regime was 10-fold higher compared to the chemically fueled material without self-immolation (see ESI, Fig. 7[†]).

Excited by the accurate prediction of the data by our kinetic model, we tested the system for different initial amounts of fuel, *i.e.*, 5–9 mM EDC (Fig. 2E). With an increasing amount of fuel, the maximum anhydride concentration increased. The subsequent slope of the hydrolysis was nearly equal for all experiments and we slightly adjusted our kinetic model by adjusting

the anhydride solubility S_0 (see ESI, Table S3[†]). Interestingly, the onset of the autocatalysis occurred at roughly the same precursor threshold (16.5 mM) and resulted in the complete hydrolysis of the anhydride within 20 min. The kinetic model allowed us to accurately fit the anhydride concentration profiles for different fuel concentrations, further validating the mechanism through micellar autocatalysis. Moreover, we demonstrated the autocatalytic nature of the micelles by the addition of different amounts of the precursor as a seed which resulted in an earlier acceleration of the hydrolysis rate and shorter lifetime (see ESI, Fig. 8[†]). We were able to tune the lifetime of the cycle from 60 min up to 400 min (Fig. 2E), and we found that the lifetime of the turbidity scaled linearly with the initial fuel concentration (Fig. 2F and ESI, Fig. 9[†]).

The quantitative understanding of the mechanism allowed us to test the autonomous self-immolative emulsion in two materials. First, we designed a transient label that self-erased after fueling it (Fig. 3A). For the chemically fueled label without self-immolation, we embedded 7.5 mM precursor in a 15% polyacrylamide hydrogel and used a spray gun to coat these gels with 200 μL of a 3 M EDC stock solution. Upon spray-coating, the hydrogel became turbid, indicating that the droplets emerged in the polymer hydrogel. Thus, we imaged the evolution of the turbidity using a webcam set-up (Fig. 3B). We observed that the turbidity of the gel constantly decreased, and the label became transparent after roughly 900 min (Fig. 3B). To implement the self-immolation mechanism in the label, we increased the precursor concentration to 35 mM. When we fueled this label, we observed that it remained turbid for roughly 1100 min, after which the turbidity suddenly disappeared from one edge to the other, and the label became

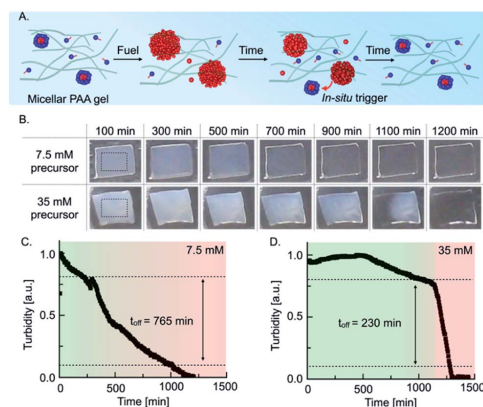


Fig. 3 Self-immolative emulsion embedded in a polyacrylamide gel and its application as a self-expiring label. (A) Schematic representation of a self-immolative emulsion immobilized in a polyacrylamide (PAA) hydrogel. (B) Time-evolution of 15% PAA hydrogels containing 7.5 mM and 35 mM precursor spray-coated with 200 μL of a 3 M EDC stock solution. Rectangles in the first images represent the region of interest (ROI) considered for the grey value analysis. Grey value analysis of (C) 7.5 mM and (D) 35 mM precursor in 15% PAA hydrogels.



transparent. We assumed that the deactivation from one side to the other was caused by an inhomogeneous distribution of the fuel on the surface of the gel, *i.e.*, the turbidity in a region with less fuel is expected to degrade earlier as micelles reappear earlier. Grey value analysis of the turbidity validated that the turbidity of the common chemically fueled label containing 7.5 mM precursor constantly decreased with an off-response of 765 min which, corresponds to roughly 70% of its lifetime (Fig. 3C). In contrast, the combined material with the self-immolation mechanism (35 mM precursor) was constantly turbid for roughly 1100 min followed by a sharp decay with an off-response of 230 min, which corresponds to a degradation time of roughly 20% of its lifetime (Fig. 3D). From these findings, we can conclude that the self-immolation of the emulsion by the formation of micelles remains function in a polymer hydrogel. We observed that the self-immolation is slightly slower, but the off-response still remains roughly 3.5-fold faster than in a common chemically fueled material. Such materials could find application as self-expiring labels, *e.g.*, an expiration date for perishable food or as an entrance- or bus ticket.

Next, we tested whether our self-immolative materials could be used to alter the profile of the release of hydrophobic drugs. Emulsions are frequently used for the sustained release of drugs, and we reported recently that droplets of a hydrolyzable oil could release drugs with zeroth-order kinetics.^{10d} In the self-immolative system, we expected a similar linear release of the drug followed by a sudden burst release when self-immolation commences (Fig. 4A). We prepared the drug delivery platform by embedding 15 mM anhydride droplets loaded with 25 μ M of the hydrophobic drug Nimesulide (a common nonsteroidal anti-inflammatory drug) in an agar-agar gel (see ESI, Fig. 10†). To implement the self-immolation mechanism in the drug delivery platform, we added 9 mM of the precursor to the hydrogel and supernatant. Next, we measured the cumulative drug release with analytical HPLC (Fig. 4B) which showed a drug

release with zero-order (linear) kinetics for the first 300 min. After 300 min, the trend suddenly accelerated, and the remaining 45% of the drug was released over the course of roughly 50 min. The triplicate measurement of the cumulative drug release showed increased deviations in the burst release regime (see ESI, Fig. 11† for the individual traces). We explain this behavior by small concentration inaccuracies which significantly influence the time of the burst release due to the autocatalytic nature of the mechanism. After 350 min, the drug concentration remained stable at an approximate cumulative release of roughly 70%. We assumed that the time of the burst release could be tuned by a variation of the initial precursor concentration in the gel and supernatant. Indeed, we found that an increase in the initial precursor concentration, *e.g.*, from 9 mM to 11 mM, reduced the time of the burst release from roughly 300 min to 125 min (see ESI, Fig. 12†). Moreover, we found that the time of the burst release shows a linear dependence on the initial precursor concentration (Fig. 4C). This relation enables us to predict the timepoint of the burst release for any initial precursor concentration using our kinetic model. In summary, the designed drug delivery platform releases the loaded hydrophobic drug following a unique constant-then-burst mechanism which can be tuned by the amount of initial precursor.

Conclusions

We demonstrated that self-immolation can be designed in chemically fueled materials. The combined concepts result in a new type of transient materials: autonomous self-immolative materials, *i.e.*, materials that are transient and switch themselves off autonomously through a rapid, self-amplifying trigger. We showcase our finding with a transient emulsion that is regulated through a reaction cycle. We designed it such that the cycle releases a trigger for the self-immolation *in situ*. Unlike other transient emulsions, the self-immolative mechanism results in a very rapid off-response that we can accurately control. We preliminarily demonstrated the use of our finding as a self-expiring ticket and a drug delivery platform. In future work, we will implement self-immolation mechanisms to rapidly degrade other types of assemblies such as fibers or coacervate-based droplets. We envision that precise control over the degradation of the material could be used to create complex material behavior such as oscillations and patterns.

Materials and methods

Materials

2-Decen-1-ylsuccinic anhydride (anhydride) was purchased from TCI chemicals. 1-Ethyl-3-(3-dimethylamino-propyl) carbodiimide (EDC), 2-(*N*-morpholino)ethane-sulfonic acid (MES buffer), trifluoroacetic acid (TFA), Nimesulide, ammonium persulfate (APS) and Nile Red were purchased from Sigma-Aldrich. We purchased agar-agar, *N,N'*-methylene-bis-acrylamide, tetramethylethylenediamine (TEMED) and acrylamide from Carl Roth. All chemicals were used without any further purification unless otherwise indicated. High

Open Access Article. Published on 21 June 2021. Downloaded on 12/13/2021 9:00:06 AM.
 This article is licensed under a Creative Commons Attribution 3.0 Unported Licence.

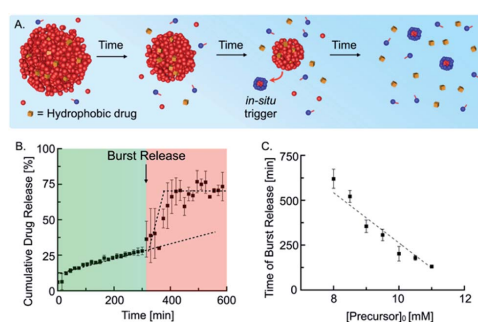


Fig. 4 Self-immolative emulsion as drug delivery platform. (A) Schematic representation of the temporal course of a self-immolative drug delivery platform. (B) Cumulative drug release of 15 mM anhydride droplets and 9 mM precursor embedded in an agar-agar gel. (C) Time of burst release in dependence on initial precursor concentration in the agar-agar gel. Measurements were performed in triplicates and lines were added to guide the eye.

performance liquid chromatography (HPLC) grade acetonitrile (ACN) was purchased from VWR.

Synthesis of the succinate precursors

5 mL of 2-decen-1-ylsuccinic anhydride (anhydride) was suspended in 30 mL MQ water and stirred for 3 days. Subsequently, the reaction mixture was freeze-dried and the corresponding 2-decen-1-ylsuccinic acid (precursor) was stored at $-20\text{ }^{\circ}\text{C}$ until further use.

Sample preparation

We prepared highly concentrated stock solutions of the acid precursor in 0.2 M MES buffer and adjusted the pH to pH 6.0. We used 35 mM, 20 mM and 7.5 mM stock solutions of the precursor. Stock solutions of 1.0 M and 3.0 M EDC were prepared freshly before each experiment by dissolving the powder in MQ water. We prepared 5 mM stock solutions of Nimesulide by dissolving the drug in acetonitrile. All stock solutions were stored at $8\text{ }^{\circ}\text{C}$ until further use. The reaction cycles were started by the addition of the appropriate amount of EDC stock solution to the precursor stock solution. All experiments were performed at $25\text{ }^{\circ}\text{C}$.

Webcam set-up and quantification of turbidity

We used a webcam-setup with Timelapse software to take images of the substrates in a 5 min interval. We analyzed the turbidity of the substrates using the grey value analysis tool of ImageJ. The raw data of the grey values was normalized to 1 to account for differences in the background and lighting. The kinetics in cuvettes (see Fig. 1C, F and 2B) were performed in an incubator at $25\text{ }^{\circ}\text{C}$ to account for the temperature dependency of the hydrolysis rate. The constant temperature allowed us to precisely determine the lifetimes of turbidity (see Fig. 2F). The imaging of the gels was performed at room temperature (see Fig. 3B).

Polyacrylamide (PAA) gel preparation

We prepared a 7.5 mM and 35 mM precursor solution containing 30% (29 : 1) acrylamide by dissolving 5.80 g acrylamide, 0.20 g *N,N'*-methylene-bis-acrylamide and the precursor (38,43 mg and 179,32 mg, respectively) in 20 mL of 200 mM MES buffer at pH 6. We diluted the stock solution with the appropriate precursor solution without acrylamide to a 15% acrylamide solution. The gels were prepared in Petri dishes (60 mm \times 15 mm) which were plasma oxidized prior to hydrogel formation. We prepared 4 mL of the 15% acrylamide solution in the Petri dish and started the hydrogel formation by the addition of 60 μL of a 10% ammonium persulfate (APS) solution in MQ water and 8 μL tetramethylethylenediamine (TEMED). The solution was mixed and heated for 10 minutes at $50\text{ }^{\circ}\text{C}$. The PAA hydrogel was cooled to room temperature for 30 min. We cut out hydrogel pieces with a scalpel, placed them in a Petri dish (35 mm \times 10 mm) and sealed with Parafilm®. The gels were prepared freshly before each experiment.

Spray deposition

Pulsed spray deposition of 200 μL of 3 M stock solutions of EDC in MQ water was performed using the air atomizing nozzle JAUCO D555000 (Spraying Systems Co.) The respective solutions were sprayed on 15% PAA hydrogels containing different concentrations of the precursor, which were placed in a Petri dish (35 mm \times 10 mm) at ambient temperature. Oil-free nitrogen was used as a carrier gas with a constant pressure set to 0.5 bar. The air atomizing nozzle was mounted on a custom-built spray coater at a distance of roughly 13.5 cm to the PAA gels. A magnetic valve of the type MEBH-5/2-1/8-B (Festo SE & Co. KG) was connected to a microcontroller and controlled the pulsed spray deposition with a periodicity of 50 ms spraying time followed by 450 ms of waiting time. The spray cone provided by the nozzle covered a circular area with a diameter of roughly 2.5 cm. In order to obtain an improved homogeneous coverage of the PAA hydrogels, the air atomizing nozzle was moved periodically within 1 cm by the spray coater, which was controlled by a second microcontroller. The obtained samples were sealed in closed Petri dishes (35 mm \times 10 mm) with Parafilm® and analyzed by a webcam set-up and subsequent grey value analysis.

Preparation of drug delivery platform

The drug-delivery emulsion was prepared by emulsifying the anhydride (60 mM) in MES-buffer (pH 6, 200 mM) with 40 μL of the drug stock solution and sonication for 2 min with a Branson Ultrasonics™ Sonifier™ SFX250 at 25% in an ice bath. These anhydride/drug emulsions were prepared freshly for each experiment. 250 μL of the emulsion was then mixed with 250 μL of a precursor stock (32–44 mM) and 500 μL of a 2% agar-agar stock in MES-buffer (pH 6, 200 mM) heated to $90\text{ }^{\circ}\text{C}$, was added subsequently. Then, 60 μL of this mixture was prepared on the bottom of a 96-well plate. The emulgel was cooled down to room temperature and 120 μL of an 8.0–11.0 mM precursor stock was added as supernatant. The cumulative drug release was measured in the supernatant by HPLC. All experiments were performed at $25\text{ }^{\circ}\text{C}$ in triplicate.

HPLC

We used analytical HPLC (ThermoFisher, Vanquish Duo UHPLC, HPLC1) with a Hypersil Gold 100 \times 2.1 mm C18 column (3 μm pore size) to monitor the concentration profiles of each reactant of the chemical reaction network. 1.0 mL samples were prepared into a screw cap HPLC vial following the sample preparation protocol described above. Samples were injected directly without any further dilution from the HPLC vial. We injected 2.5 μL for the detection of the precursor and anhydride. For the detection of EDC, we injected 0.1 μL . We used a UV/vis detector at 220 nm for detection. A linear gradient of MQ water: ACN with 0.1% TFA was used to separate the compounds. The separation method was based on a linear gradient from 60 : 40 to 2 : 98 for the anhydride and 95 : 5 to 2 : 98 for EDC in 5 min followed by 1 min at 2 : 98. Afterwards, the gradient changed from 2 : 98 back to 60 : 40 or 95 : 5 in 0.2 min and the column was equilibrated for 3.8 min. The drug



and acid releases from the emulgel were determined by analytical HPLC (ThermoFisher, Dionex Ultimate 3000, HPLC2) with a Hypersil Gold 250 × 4.8 mm C18 column (5 μm pore size) using a linear gradient of MQ water and ACN, each with 0.1% TFA. All compounds were detected with an UV/vis detector at 220 nm (precursor) and 330 nm (Nimesulide). We used a gradient of MQ water : ACN from 98 : 2 to 2 : 98 in 13 min for the separation. We performed calibration curves of all the compounds in triplicates. Calibration values and retention times are given in ESI, Table S1.†

Nuclear resonance spectroscopy (NMR)

We recorded NMR spectra on a Bruker AVIII-400 at 25 °C and a frequency of 400 MHz. Chemical shifts δ are reported in ppm and are referred to the residual solvent peak of the used deuterated solvent (chloroform- d_1 7.26 ppm for $^1\text{H-NMR}$). We abbreviated the signal multiplets as followed: s-singulet, d-doublet, t-triplet, m-multiplet. The coupling constant J is stated as average value in Hz and refers to coupling between two protons.

$^1\text{H NMR}$ (anhydride) 400 MHz, CDCl_3 : δ (ppm) = 5.61 (dt, $^3J_{\text{H-H}} = 13.8$, 6.6 Hz, 1H; CH=C), 5.29 (dt, $^3J_{\text{H-H}} = 15.3$, 7.6 Hz, 1H; CH=C), 3.20 (m, 1H; CH), 3.01 (dd, $^2,^3J_{\text{H-H}} = 18.9$, 9.7 Hz, 1H; CH_2), 2.73 (dd, $^2,^3J_{\text{H-H}} = 18.7$, 5.9 Hz, 1H; CH_2), 2.49 (m, 2H; CH_2), 2.01 (dt, $^3J_{\text{H-H}} = 7.2$, 6.9 Hz, 2H; CH_2), 1.27 (m, 10H; $(\text{CH}_2)_4$), 0.88 (t, $^3J_{\text{H-H}} = 6.6$ Hz, 3H; CH_3) (see ESI, Fig. 13†).

$^1\text{H NMR}$ (precursor) 400 MHz, CDCl_3 : δ (ppm) = 5.51 (dt, $^3J_{\text{H-H}} = 13.7$, 6.8 Hz, 1H; CH=C), 5.31 (dt, $^3J_{\text{H-H}} = 14.9$, 7.0 Hz, 1H; CH=C), 2.89 (m, 1H; CH), 2.67 (dd, $^2,^3J_{\text{H-H}} = 17.5$, 10.7 Hz, 1H; CH_2), 2.53 (dd, $^2,^3J_{\text{H-H}} = 17.3$, 3.9 Hz, 1H; CH_2), 2.44 (m, 1H; CH_2), 2.22 (m, 1H; CH_2), 1.99 (dt, $^3J_{\text{H-H}} = 7.0$ Hz, 2H; CH_2), 1.27 (m, 10H; $(\text{CH}_2)_4$), 0.88 (t, $^3J_{\text{H-H}} = 6.6$ Hz, 3H; CH_3) (see ESI, Fig. 14†).

UV/vis-spectroscopy

A Multiskan FC microplate reader (ThermoFisher) was used for UV/vis measurements. For the sample preparation a 96-well-plate (tissue culture plate non-treated) was used. Measurements were performed in triplicates at a wavelength of 600 nm and 25 °C.

Data availability

The authors confirm that the data supporting the findings of this study are available within the article and its ESI.

Author contributions

P. S. S., J. B. and P. M.-B. designed the experiments. P. S. S., L. T. and J. E. H. performed the experiments. P. S. S. and J. B. wrote the manuscript. All authors have given approval to the final version of the manuscript.

Conflicts of interest

There are no conflicts to declare.

Acknowledgements

This research was conducted within the Max Planck School Matter to Life supported by the German Federal Ministry of Education and Research (BMBF) in collaboration with the Max Planck Society. J. B. and P. S. S. are grateful for the funding by the European Research Council (ERC starting grant 852187). L. T. is grateful for funding from the Deutsche Forschungsgemeinschaft *via* the International Research Training Group ATUMS (IRTG 2022). J. E. H. and P. M.-B. are grateful for the funding from the Deutsche Forschungsgemeinschaft (DFG, German Research Foundation) under Germany's Excellence Strategy – EXC 2089/1 – 390776260 (e-conversion).

References

- (a) S.-W. Hwang, H. Tao, D.-H. Kim, H. Cheng, J.-K. Song, E. Rill, M. A. Brenckle, B. Panilaitis, S. M. Won, Y.-S. Kim, Y. M. Song, K. J. Yu, A. Ameen, R. Li, Y. Su, M. Yang, D. L. Kaplan, M. R. Zakin, M. J. Slepian, Y. Huang, F. G. Omenetto and J. A. Rogers, *Science*, 2012, **337**, 1640; (b) K. K. Fu, Z. Wang, J. Dai, M. Carter and L. Hu, *Chem. Mater.*, 2016, **28**, 3527.
- (a) J. B. Matson and S. I. Stupp, *Chem. Commun.*, 2012, **48**, 26; (b) P. Y. W. Dankers, T. M. Hermans, T. W. Baughman, Y. Kamikawa, R. E. Kieleyka, M. M. C. Bastings, H. M. Janssen, N. A. J. M. Sommerdijk, A. Larsen, M. J. A. van Luyn, A. W. Bosman, E. R. Popa, G. Fytas and E. W. Meijer, *Adv. Mater.*, 2012, **24**, 2703.
- (a) R. Li, L. Wang, D. Kong and L. Yin, *Bioact. Mater.*, 2018, **3**, 322; (b) C. W. Park, S.-K. Kang, H. L. Hernandez, J. A. Kaitz, D. S. Wie, J. Shin, O. P. Lee, N. R. Sottos, J. S. Moore, J. A. Rogers and S. R. White, *Adv. Mater.*, 2015, **27**, 3783.
- (a) U. Pagga, *Chemosphere*, 1997, **35**, 2953; (b) R. S. Boethling, E. Sommer and D. DiFiore, *Chem. Rev.*, 2007, **107**, 2207.
- (a) L. S. Kariyawasam, M. M. Hossain and C. S. Hartley, *Angew. Chem., Int. Ed.*, 2021, **60**, 12648; (b) G. Wang and S. Liu, *ChemSystemsChem*, 2020, **2**, e1900046; (c) R. Merindol and A. Walther, *Chem. Soc. Rev.*, 2017, **46**, 5588; (d) G. Ragazzon and L. J. Prins, *Nat. Nanotechnol.*, 2018, **13**, 882; (e) S. De and R. Klajn, *Adv. Mater.*, 2018, **30**, 1706750; (f) N. Singh, G. J. M. Formon, S. De Piccoli and T. M. Hermans, *Adv. Mater.*, 2020, **32**, 1906834; (g) B. Rief, R. K. Grötsch and J. Boekhoven, *Chem*, 2020, **6**, 552.
- (a) S. P. Afrose, S. Bal, A. Chatterjee, K. Das and D. Das, *Angew. Chem., Int. Ed.*, 2019, **58**, 15783; (b) S. Panja, B. Dietrich and D. J. Adams, *ChemSystemsChem*, 2020, **2**, e1900038; (c) M. Tena-Solsona, B. Rief, R. K. Grötsch, F. C. Löhner, C. Wanzke, B. Käs Dorf, A. R. Bausch, P. Müller-Buschbaum, O. Lieleg and J. Boekhoven, *Nat. Commun.*, 2017, **8**, 15895; (d) J. Boekhoven, A. M. Brizard, K. N. K. Kowligi, G. J. M. Koper, R. Eelkema and J. H. van Esch, *Angew. Chem., Int. Ed.*, 2010, **49**, 4825; (e) J. Boekhoven, W. E. Hendriksen, G. J. M. Koper, R. Eelkema and J. H. van Esch, *Science*, 2015, **349**, 1075; (f) K. Dai, J. R. Fores, C. Wanzke, B. Winkeljann, A. M. Bergmann, O. Lieleg and J. Boekhoven, *J. Am. Chem.*



- Soc.*, 2020, **142**, 14142; (g) S. Debnath, S. Roy and R. V. Ulijn, *J. Am. Chem. Soc.*, 2013, **135**, 16789; (h) B. A. Kriebisch, A. Jussupow, A. M. Bergmann, F. Kohler, H. Dietz, V. R. Kaila and J. Boekhoven, *J. Am. Chem. Soc.*, 2020, **142**, 20837; (i) E. Te Brinke, J. Groen, A. Herrmann, H. A. Heus, G. Rivas, E. Spruijt and W. T. Huck, *Nat. Nanotechnol.*, 2018, **13**, 849.
- 7 (a) E. A. Post and S. P. Fletcher, *Chem. Sci.*, 2020, **11**, 9434; (b) C. Wanzke, A. Jussupow, F. Kohler, H. Dietz, V. R. Kaila and J. Boekhoven, *ChemSystemsChem*, 2020, **2**, e1900044; (c) S. Maiti, I. Fortunati, C. Ferrante, P. Scrimin and L. J. Prins, *Nat. Commun.*, 2016, **8**, 725.
- 8 (a) M. A. Würbser, P. S. Schwarz, J. Heckel, A. M. Bergmann, A. Walther and J. Boekhoven, *ChemSystemsChem*, 2021, DOI: 10.1002/syst.202100015; (b) S. M. Morrow, I. Colomer and S. P. Fletcher, *Nat. Commun.*, 2019, **10**, 1.
- 9 B. Rieß, C. Wanzke, M. Tena-Solsona, R. K. Grötsch, C. Maity and J. Boekhoven, *Soft Matter*, 2018, **14**, 4852.
- 10 (a) P. S. Schwarz, S. Laha, J. Janssen, T. Huss, J. Boekhoven and C. A. Weber, *Chem. Sci.*, 2021, **12**, 7554; (b) M. Tena-Solsona, J. Janssen, C. Wanzke, F. Schnitter, H. Park, B. Rieß, J. M. Gibbs, C. A. Weber and J. Boekhoven, *ChemSystemsChem*, 2021, **3**, e2000034; (c) M. Tena-Solsona, C. Wanzke, B. Riess, A. R. Bausch and J. Boekhoven, *Nat. Commun.*, 2018, **9**, 2044; (d) C. Wanzke, M. Tena-Solsona, B. Rieß, L. Tebcharani and J. Boekhoven, *Mater. Horiz.*, 2020, **7**, 1397; (e) C. Donau, F. Späth, M. Sosson, B. A. Kriebisch, F. Schnitter, M. Tena-Solsona, H.-S. Kang, E. Salibi, M. Sattler and H. Mutschler, *Nat. Commun.*, 2020, **11**, 1; (f) F. Späth, C. Donau, A. M. Bergmann, M. Kränzlein, C. V. Synatschke, B. Rieger and J. Boekhoven, *J. Am. Chem. Soc.*, 2021, **143**, 4782.
- 11 (a) R. K. Grötsch, A. Angi, Y. G. Mideksa, C. Wanzke, M. Tena-Solsona, M. J. Feige, B. Rieger and J. Boekhoven, *Angew. Chem., Int. Ed.*, 2018, **57**, 14608; (b) R. K. Grötsch, C. Wanzke, M. Speckbacher, A. Angi, B. Rieger and J. Boekhoven, *J. Am. Chem. Soc.*, 2019, **141**, 9872; (c) B. G. P. van Ravensteijn, W. E. Hendriksen, R. Eelkema, J. H. van Esch and W. K. Kegel, *J. Am. Chem. Soc.*, 2017, **139**, 9763.
- 12 (a) L. Heinen, T. Heuser, A. Steinschulte and A. Walther, *Nano Lett.*, 2017, **17**, 4989; (b) L. Heinen and A. Walther, *Sci. Adv.*, 2019, **5**, eaaw0590.
- 13 R. Klajn, P. J. Wesson, K. J. Bishop and B. A. Grzybowski, *Angew. Chem., Int. Ed.*, 2009, **48**, 7035.
- 14 (a) M. M. Hossain, J. L. Atkinson and C. S. Hartley, *Angew. Chem., Int. Ed.*, 2020, **59**, 13807; (b) L. S. Kariyawasam and C. S. Hartley, *J. Am. Chem. Soc.*, 2017, **139**, 11949.
- 15 (a) S. Ahmed, A. Chatterjee, K. Das and D. Das, *Chem. Sci.*, 2019, **10**, 7574; (b) J. Heckel, S. Loescher, R. T. Mathers and A. Walther, *Angew. Chem., Int. Ed.*, 2021, **60**, 7117; (c) T. Heuser, E. Weyandt and A. Walther, *Angew. Chem., Int. Ed.*, 2015, **54**, 13258; (d) S. Panja, C. Patterson and D. J. Adams, *Macromol. Rapid Commun.*, 2019, **40**, 1900251; (e) N. Singh, B. Lainer, G. J. M. Formon, S. De Piccoli and T. M. Hermans, *J. Am. Chem. Soc.*, 2020, **142**, 4083.
- 16 (a) S. Dhiman, R. Ghosh and S. J. George, *ChemSystemsChem*, 2020, **2**, e1900042; (b) J. Leira-Iglesias, A. Tassoni, T. Adachi, M. Stich and T. M. Hermans, *Nat. Nanotechnol.*, 2018, **13**, 1021.
- 17 T. Heuser, R. Merindol, S. Loescher, A. Klaus and A. Walther, *Adv. Mater.*, 2017, **29**, 1606842.
- 18 (a) S. Chandrabhas, S. Maiti, I. Fortunati, C. Ferrante, L. Gabrielli and L. J. Prins, *Angew. Chem.*, 2020, **132**, 22407; (b) H. Che, S. Cao and J. C. M. van Hest, *J. Am. Chem. Soc.*, 2018, **140**, 5356.
- 19 (a) D. Zheng, Z. Gao, T. Xu, C. Liang, Y. Shi, L. Wang and Z. Yang, *Nanoscale*, 2018, **10**, 21459; (b) Y. Xu, S. Sen, Q. Wu, X. Zhong, R. H. Ewoldt and S. C. Zimmerman, *Chem. Sci.*, 2020, **11**, 3326.
- 20 (a) M. Gisbert-Garzarán, D. Lozano, M. Vallet-Regí and M. Manzano, *RSC Adv.*, 2017, **7**, 132; (b) M. Shamis, H. N. Lode and D. Shabat, *J. Am. Chem. Soc.*, 2004, **126**, 1726.
- 21 C. Ergene and E. F. Palermo, *J. Mater. Chem.*, 2018, **6**, 7217.
- 22 N. Velusamy, N. Thirumalaivasan, K. N. Bobba, S.-P. Wu and S. Bhuniya, *New J. Chem.*, 2018, **42**, 1590.
- 23 C. F. Riber, A. A. A. Smith and A. N. Zelikin, *Adv. Healthcare Mater.*, 2015, **4**, 1887.
- 24 (a) D. Han, X. Yu, Q. Chai, N. Ayres and A. J. Steckl, *ACS Appl. Mater. Interfaces*, 2017, **9**, 11858; (b) A. P. Esser-Kahn, N. R. Sottos, S. R. White and J. S. Moore, *J. Am. Chem. Soc.*, 2010, **132**, 10266.
- 25 A. M. DiLauro, G. G. Lewis and S. T. Phillips, *Angew. Chem.*, 2015, **127**, 6298.
- 26 J. M. Van Raden, B. M. White, L. N. Zakharov and R. Jasti, *Angew. Chem., Int. Ed.*, 2019, **58**, 7341.
- 27 (a) L. Peles-Strahl, R. Sasson, G. Slor, N. Edelstein-Pardo, A. Dahan and R. J. Amir, *Macromolecules*, 2019, **52**, 3268; (b) A. Sagi, R. Weinstein, N. Karton and D. Shabat, *J. Am. Chem. Soc.*, 2008, **130**, 5434.
- 28 (a) J. Weiss, J. N. Coupland and D. J. McClements, *J. Phys. Chem.*, 1996, **100**, 1066; (b) M. P. Aronson, *Langmuir*, 1989, **5**, 494.
- 29 (a) P. A. Bachmann, P. L. Luisi and J. Lang, *Nature*, 1992, **357**, 57; (b) P. A. Bachmann, P. Walde, P. L. Luisi and J. Lang, *J. Am. Chem. Soc.*, 1991, **113**, 8204; (c) P. A. Bachmann, P. Walde, P. L. Luisi and J. Lang, *J. Am. Chem. Soc.*, 1990, **112**, 8200; (d) P. A. Bachmann, P. L. Luisi and J. Lang, *Chimia*, 1991, **45**, 266; (e) A. J. Bissette, B. Odell and S. P. Fletcher, *Nat. Commun.*, 2014, **5**, 4607; (f) M. A. Lebedeva, E. Palmieri, P. Kukura and S. P. Fletcher, *ACS Nano*, 2020, **14**, 11160; (g) J. Ortega-Arroyo, A. J. Bissette, P. Kukura and S. P. Fletcher, *Proc. Natl. Acad. Sci. U. S. A.*, 2016, **113**, 11122.
- 30 H. Almoazen and A. P. Simonelli, *J. Dispersion Sci. Technol.*, 2008, **29**, 958.
- 31 T. Buhse, R. Nagarajan, D. Lavabre and J. C. Micheau, *J. Phys. Chem.*, 1997, **101**, 3910.
- 32 A. J. Bissette and S. P. Fletcher, *Angew. Chem., Int. Ed.*, 2013, **52**, 12800.
- 33 (a) J. Billingham and P. V. Coveney, *J. Chem. Soc., Faraday Trans.*, 1994, **90**, 1953; (b) Y. A. Chizmadzhev, M. Maestro and F. Mavelli, *Chem. Phys. Lett.*, 1994, **226**, 56.
- 34 T. Buhse, D. Lavabre, R. Nagarajan and J. C. Micheau, *J. Phys. Chem.*, 1998, **102**, 10552.



Electronic Supplementary Material (ESI) for Chemical Science.
This journal is © The Royal Society of Chemistry 2021

Supporting Information

Chemically Fueled Materials with a Self-Immolative Mechanism: Transient Materials with a Fast On/Off Response

*Patrick S. Schwarz, Laura Tebcharani, Julian E. Heger, Prof. Peter Müller-Buschbaum, Prof. Job Boekhoven**

P. S. Schwarz, L. Tebcharani, Prof. J. Boekhoven
Department of Chemistry, Technical University of Munich, Lichtenbergstraße 4, 85748 Garching, Germany.

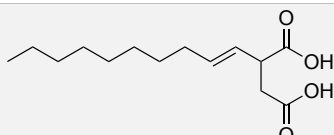
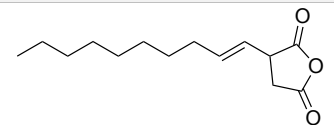
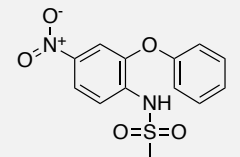
Prof. J. Boekhoven
Institute for Advanced Study, Technical University of Munich, Lichtenbergstraße 2a, 85748 Garching, Germany.
E-mail: job.boekhoven@tum.de

J. E. Heger, Prof. P. Müller-Buschbaum
Department of Physics, Technical University of Munich, James-Franck-Straße 1, 85748 Garching, Germany.

Prof. P. Müller-Buschbaum
Heinz Maier-Leibnitz Zentrum (MLZ), Technical University of Munich, Lichtenbergstraße 1, 85748 Garching, Germany

1. Supporting Tables

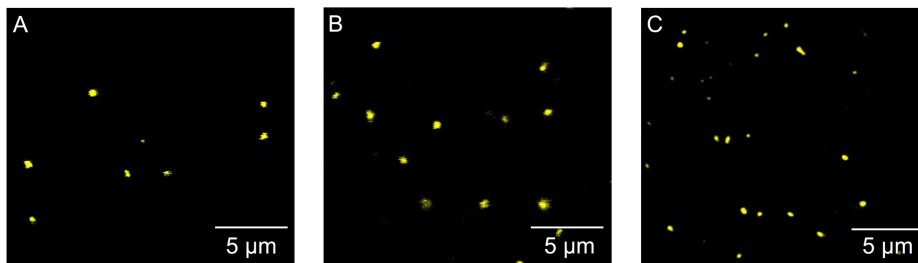
Supporting Table 1: Characterization of compounds.

Name	Structure	Mass calc. [g/mol]	Mass obs. [g/mol]	Retention time [min]	Calibration value [mAU mM ⁻¹]
Precursor		256.17 C ₁₄ H ₂₄ O ₄	257.1 [M+H] ⁺	5.22 (HPLC1) 11.79 (HPLC2)	0.76 (HPLC1) 3.25 (HPLC2)
Anhydride		238.16 C ₁₄ H ₂₂ O ₃	239.1 [M+H] ⁺	6.71 (HPLC1)	1.77 (HPLC1)
Nimesulide		308.05 C ₁₃ H ₁₂ N ₂ O ₅ S	309.1 [M+H] ⁺	10.99 (HPLC2)	0.15 (HPLC2)

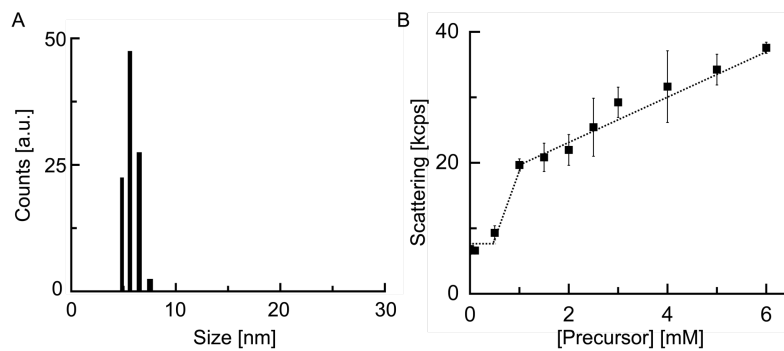
Supporting Table 2: Rate constants used in the kinetic model.

c ₀ (EDC) [mM]	c(Precursor) [mM]	k ₁ [M ⁻¹ s ⁻¹]	k ₂	k ₃	k ₄ [s ⁻¹]	CMC [mM]	S ₀ [mM]	SC
5	20	0.5	1*k ₁	0.3*k ₁	3.5E-3	16.5	1.10E-1	0.1
6	20	0.5	1*k ₁	0.3*k ₁	3.5E-3	16.5	0.90E-1	0.1
7	20	0.5	1*k ₁	0.3*k ₁	3.5E-3	16.5	0.65E-1	0.1
8	7.5	0.5	1*k ₁	0.3*k ₁	3.5E-3	16.5	0.25E-1	0.1
8	20	0.5	1*k ₁	0.3*k ₁	3.5E-3	16.5	0.55E-1	0.1
9	20	0.5	1*k ₁	0.3*k ₁	3.5E-3	16.5	0.53E-1	0.1

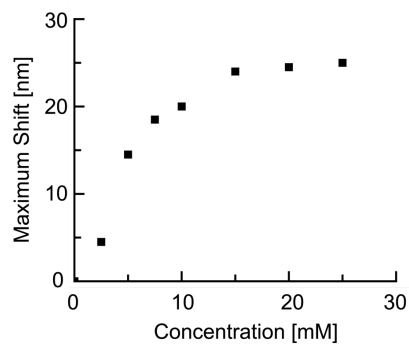
2. Supporting Figures



Supporting Figure 1: Confocal micrographs of A) 7.5 mM precursor and 2 mM EDC, B) 7.5 mM precursor and 8 mM EDC and C) 20 mM precursor and 8 mM EDC.

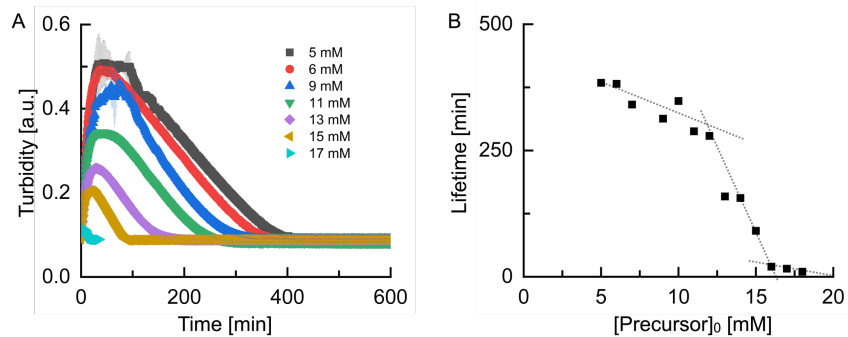


Supporting Figure 2: A) Size distribution of the hydrodynamic diameter of 20 mM precursor in 200 mM MES. B) Scattering for different amounts of precursor. Lines are added to guide the eye.

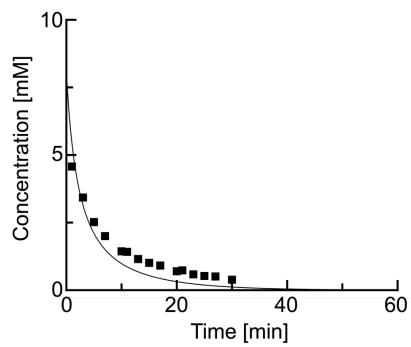


Supporting Figure 3: Nile Red fluorescence assay showing a fluorescence maximum shift for different precursor concentrations characteristic for incorporation into micelles.

Chemically Fueled Materials with a Self-Immolative Mechanism: Transient Materials with a Fast On/Off Response

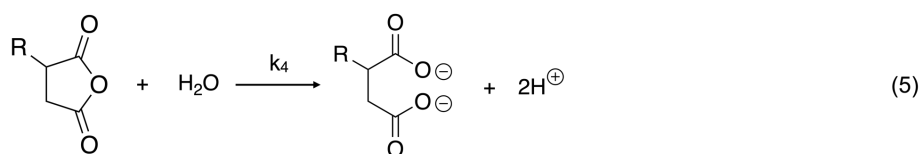
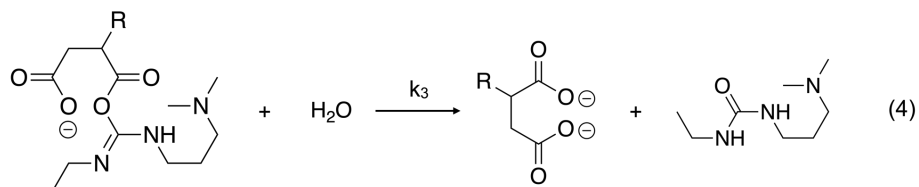
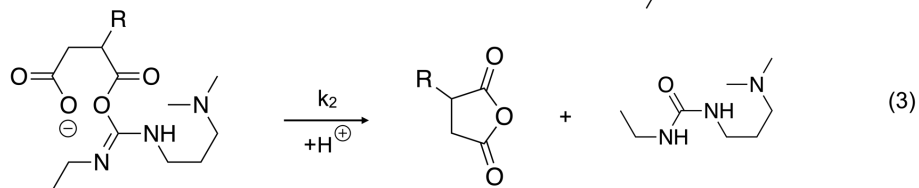
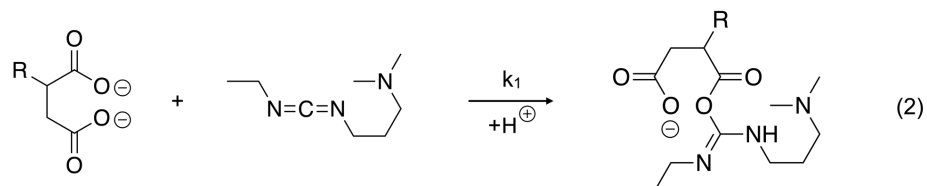
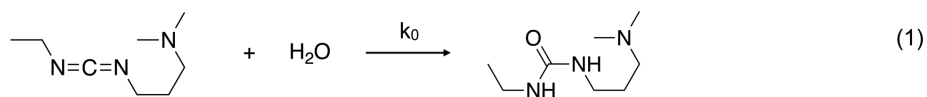


Supporting Figure 4: A) Turbidity at 600 nm for different precursor concentrations fueled with 2 mM EDC. B) Lifetime of the turbidity as a function of initial precursor concentration. Lines are added to guide the eye.

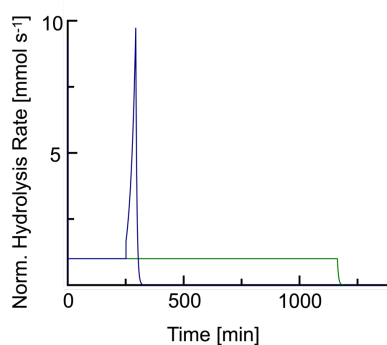


Supporting Figure 5: EDC consumption of 7.5 mM precursor fueled with 8 mM EDC. Markers represent HPLC data; solid lines represent data calculated by the kinetic model.

Chemically Fueled Materials with a Self-Immolative Mechanism: Transient Materials with a Fast On/Off Response

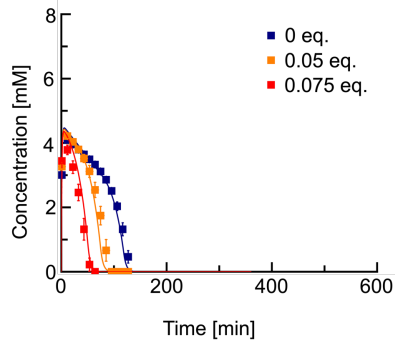


Supporting Figure 6: Chemical reactions considered in the kinetic model. Reaction (1) shows the direct hydrolysis of EDC. Reaction (2) shows the activation reaction of the succinate precursor with EDC. Reaction (3) shows the intramolecular anhydride formation reaction. Reaction (4) shows the direct hydrolysis of *O*-acylisourea. Reaction (5) shows the hydrolysis of the anhydride.

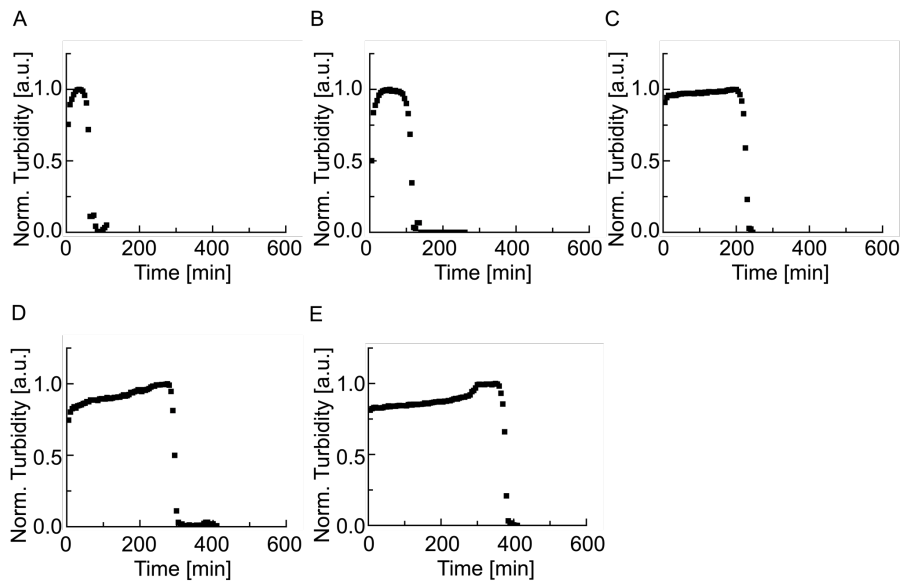


Supporting Figure 7: Normalized hydrolysis rate constant of 20 mM precursor (blue) and 7.5 mM precursor fueled with 8 mM EDC.

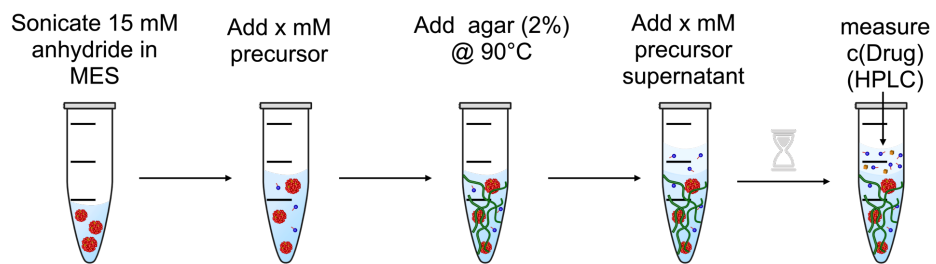
Chemically Fueled Materials with a Self-Immolative Mechanism: Transient Materials with a Fast On/Off Response



Supporting Figure 8: Anhydride concentration profiles of 20 mM precursor fueled with 6 mM EDC and seeded with different amounts of precursor. Markers represent HPLC data; solid lines represent data calculated by the kinetic model.

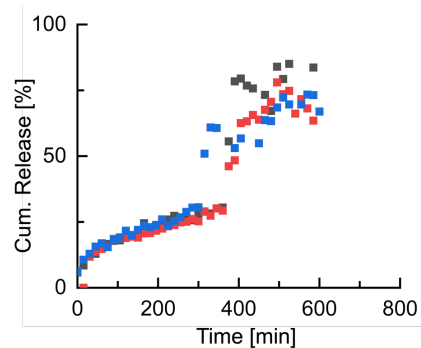


Supporting Figure 9: Normalized turbidity of 20 mM precursor fueled with A) 5 mM, B) 6 mM, C) 7 mM, D) 8 mM and E) 9 mM EDC.

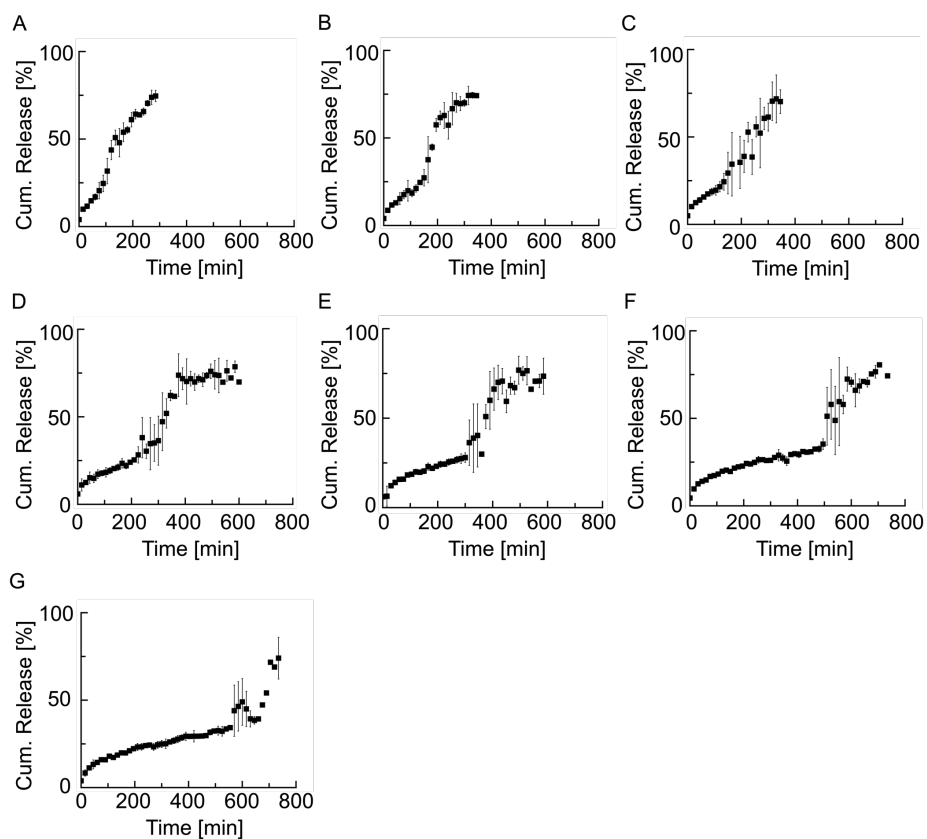


Supporting Figure 10: Schematic representation of the preparation of a self-immolative drug delivery platform.

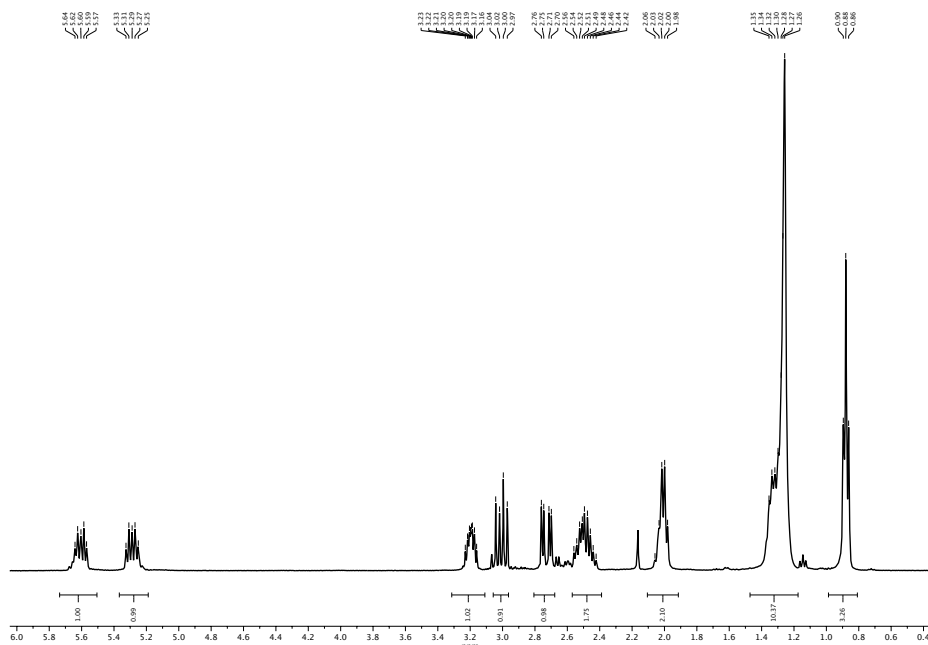
Chemically Fueled Materials with a Self-Immolative Mechanism: Transient Materials with a Fast On/Off Response



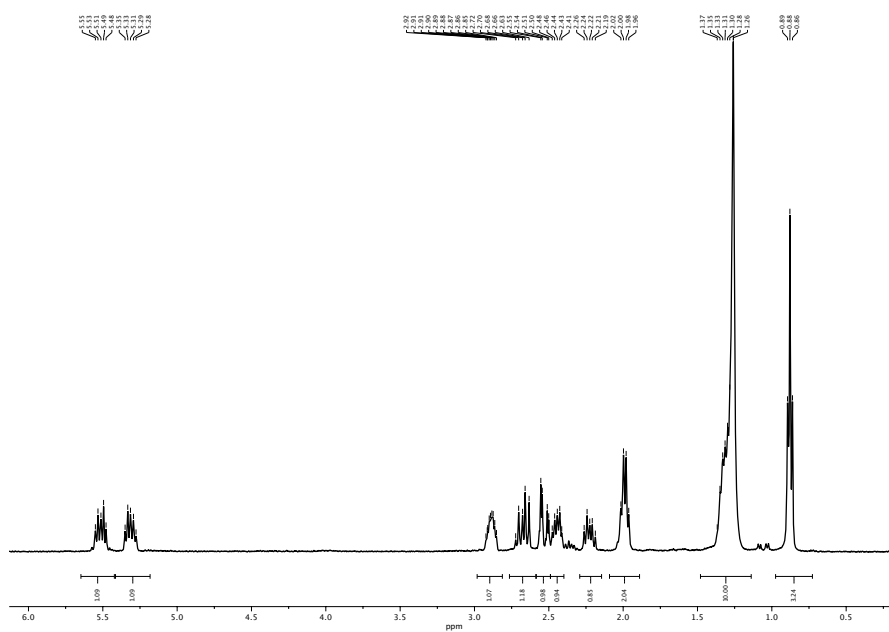
Supporting Figure 11: Triplicate measurements of the cumulative drug release of an agar agar hydrogel with 25 μM Nimesulide in an emulsion of 15 mM anhydride and 9 mM precursor



Supporting Figure 12: Cumulative drug release of an agar agar hydrogel with 25 μM Nimesulide in an emulsion of 15 mM anhydride and A) 11 mM precursor, B) 10.5 mM precursor, C) 10 mM precursor, D) 9.5 mM precursor, E) 9 mM precursor, F) 8.5 mM precursor and G) 8 mM precursor.



Supporting Figure 13: $^1\text{H-NMR}$ (CDCl_3 , 400 MHz) spectrum of the anhydride.



Supporting Figure 14: $^1\text{H-NMR}$ (CDCl_3 , 400 MHz) spectrum of the precursor.

Supporting Notes

Critical Micelle Concentration in an Emulsion. The critical micelle concentration (*CMC*) of a surfactant can be determined by various techniques, such as surface tension, conductivity, dynamic light scattering (DLS) and dye solubilization spectrophotometry. However, the accurate determination of the *CMC* of a surfactant in the presence of oil droplets remains challenging. Standard techniques like dynamic light scattering and photon correlation spectroscopy fail to analyze oil and micelles simultaneously. Moreover, oil droplets have an influence on the surface tension, conductivity and solubilize hydrophobic dyes which prevents other analytical techniques. We considered the lifetime of the emulsion as an indirect measurement of the formation of micelles when we fueled different amounts of precursor with 2 mM EDC (see Supporting Figure 4). We found that the lifetime decreased linearly when we increased the precursor concentration from 5 mM to 12 mM which we attributed to a salting-in effect of the additional precursor which slightly increases the solubility of the anhydride. However, at precursor concentrations higher than 12 mM, we observed a significant decrease of the lifetime of the turbidity by roughly 50 % which indicated the formation of micelles. In conclusion, when fueled with 2 mM EDC and subtracting an anhydride yield of roughly 1.5 mM, the *CMC* of the precursor is roughly 11 mM.

Kinetic Model. The concentration of each reactant (anhydride, precursor, *O*-acylisourea and EDC) was described for every second in the reaction cycle in a kinetic *Matlab* model. For the description of the chemical reaction network, a basis of five differential equations for the five underlying chemical reactions was used for the calculations of concentrations (see Supporting Figure 5): the direct hydrolysis of EDC r_0 (1), the activation of the precursor r_1 to form the intermediate product *O*-acylisourea (2), the anhydride formation r_2 (3), the direct hydrolysis of the intermediate product *O*-acylisourea r_3 (4), the hydrolysis of the anhydride r_4 (7,8). For the implementation of the self-amplifying decay, we defined the effective solubility of the anhydride $COOOC(i)$ as a variable $S_{eff}(i)$ which is constant below the *CMC* of the precursor $COOH(i)$ (5). Above the *CMC*, the solubility of the anhydride changes as a function of precursor concentration $COOH(i)$ (6). We defined a solubilization capacity (*SC*, see Supporting Table S3) which can be seen as the effectiveness of the surfactant precursor which increases the solubility of the anhydride in dependence on the number of precursor molecules above the *CMC*. In other words, the solubilization factor of 0.1 means that 10 molecules of precursor are necessary to dissolve 1 molecule of anhydride. We used two differential equations for the hydrolysis rate of the anhydride above and below its effective solubility $S_{eff}(i)$. Above the solubility, the hydrolysis rate is constant as long as $S_{eff}(i)$ is constant (see 5 and 6) (7). Below the solubility, the hydrolysis rate becomes a first order rate which is dependent on the anhydride concentration $COOOC(i)$ (8).

$$r_0(i) = k_0 \cdot EDC(i) \quad (1)$$

$$r_1(i) = k_1 \cdot EDC(i) \cdot COOH(i) \quad (2)$$

$$r_2(i) = k_2 \cdot COOEDC(i) \quad (3)$$

$$r_3(i) = k_3 \cdot COOEDC(i) \quad (4)$$

$$S_{eff}(i) = S_0, \quad \text{if } COOH(i) < CMC \quad (5)$$

$$S_{eff}(i) = S_0 + (SC * (COOH(i) - CMC)), \quad \text{if } COOH(i) > CMC \quad (6)$$

$$r_4(i) = k_4 \cdot S_{eff}(i), \quad \text{if } COOOC(i) > S_{eff}(i) \quad (7)$$

$$r_4(i) = k_4 \cdot COOOC(i), \quad \text{if } COOOC(i) < S_{eff}(i) \quad (8)$$

7. Conclusion and Outlook

This thesis aims to build a simple, synthetic system based on chemically fueled droplets in which the control and design of feedback mechanisms could result in life-like behavior. These systems could serve as model systems for the origin of life research or be a step towards developing smart, life-like materials.

In Chapter 1, I overview the origin of life research and different approaches for the synthesis of life. Moreover, I discuss biological systems' essential properties that a synthetic system must have to be considered alive, such as energy transduction, compartmentalization, information processing, growth and division, and adaptability.

As compartmentalization is an essential property of living systems, an ideal candidate to design such a system could be membraneless compartments which are droplets formed by LLPS. As discussed in Chapter 2, their liquid nature and the absence of a membrane facilitate the diffusion of reactants in- and outwards of the compartment. When phase separation of these compartments is controlled kinetically by chemical reactions, droplets can have significantly different properties from droplets in thermodynamic equilibrium, *e.g.*, suppression and acceleration of Ostwald ripening, self-division, or reduced concentration oscillations.

Due to these advantageous properties, I chose chemically regulated droplets as a starting point to design a system with life-like behavior because they already combine two essential properties of life: compartmentalization and energy transduction. Recently, many chemically fueled reaction cycles have been developed which can regulate the self-assembly of synthetic analogs of biological assemblies and compartments, *e.g.*, droplets, fibers, and vesicles. However, these systems are still far from being considered alive. Other essential properties of living systems could be observed when the assembly also regulates the reaction cycle's kinetics via feedback mechanisms discussed in Chapter 3.

Inspired by feedback regulation of networks in biology, the first aim of the thesis is to investigate how the negative feedback mechanism of oil droplets shown in Chapter 3 affects the kinetics of the products when multiple, simultaneously operating reaction cycles compete for fuel. In general, when two metabolic reaction cycles compete for a shared resource, both suffer. Counterintuitively, despite the fuel competition, we found in Chapter 5 that the success of a soluble precursor can increase when competing with a phase-separating competitor, *i.e.*, it survives longer or shows reduced concentration oscillations in the presence of periodic fueling. The success of the soluble product increases due to co-phase separation with droplets formed by the competitor, which decelerates the deactivation by hydrolysis. This behavior is

reminiscent of parasitic behavior in biology, where the parasite competes with the host for the shared resources and exploits the protective environment offered by the host.

In Chapter 6, we wanted to demonstrate that feedback mechanisms offer new ways to control transient materials. We used the surfactant nature of the precursor to design an opposing feedback mechanism to dissolve the oil droplets rapidly. The precursor forms micelles above its CMC, which act as a phase-transfer catalyst and accelerate the hydrolysis rate by solubilizing the anhydride product. More precursor is released upon hydrolysis of the anhydride product, which further amplifies the hydrolysis rate, *i.e.*, a self-immolative mechanism. Unlike common self-immolative materials, we designed the system such that the trigger for the self-immolation is released *in-situ* by the reaction cycle, which enables these materials to switch off themselves through a rapid self-amplifying decay without an external trigger. We applied this mechanism in a self-expiring ticket and a drug delivery platform with a unique linear-then-burst release profile.

In conclusion, this work shows that feedback mechanisms in simple networks of chemically fueled reaction cycles can result in complex, life-like behavior. We envision that the co-phase separation mechanism could be crucial to control concentrations of downstream chemical reactions. Moreover, the opposing feedback mechanism enables precise control over the material properties. We believe that self-immolation in chemically fueled reaction cycles could serve as a tool for more sophisticated, life-like materials. However, these results are all based on designing and tuning a negative feedback mechanism. Some essential properties of living systems are based on positive feedback mechanisms, *e.g.*, growth and division. In the future, finding how chemically fueled droplets can exert positive feedback on their reaction cycle could be a step towards the bottom-up synthesis of life.

8. Materials and Methods

Materials. We purchased (*E/Z*)-2-buten-1-ylsuccinic anhydride, (*E/Z*)-2-hexenyl-1-ylsuccinic anhydride and (*E/Z*)-2-decen-1-ylsuccinic anhydride from *TCI chemicals*. Succinic acid, succinic anhydride, Nile Red, 1-ethyl-3-(3-dimethylaminopropyl)carbodiimide hydrochloride (EDC), trifluoroacetic acid (TFA) and 2-(*N*-morpholino)ethane sulfonic acid (MES buffer), Nimesulide and ammonium persulfate (APS) were purchased from *Sigma-Aldrich*. We purchased agar agar, *N,N'*-methylene-bisacrylamide, tetramethylethylenediamine (TEMED), and acrylamide from *Carl Roth*. All chemicals were used without any further purification unless otherwise indicated. High-performance liquid chromatography (HPLC) grade acetonitrile (ACN) was purchased from VWR.

Synthesis of the Succinate Precursors. 5 mL (*E/Z*)-2-buten-1-ylsuccinic anhydride, (*E/Z*)-2-hexenyl-1-ylsuccinic anhydride or (*E/Z*)-2-decen-1-ylsuccinic anhydride was suspended in 30 mL MQ water and stirred for 3 days. Subsequently, the reaction mixture was freeze-dried and the corresponding succinate precursor was stored at -20 °C until further use.

Sample Preparation. We prepared highly concentrated stock solutions of the acid precursor in 0.2 M MES buffer and adjusted the pH to pH 6.0. Stock solutions of EDC were prepared freshly before each experiment by dissolving the powder in MQ water. We prepared 5 mM stock solutions of Nimesulide by dissolving the drug in acetonitrile. All stock solutions were stored at 8 °C until further use. The reaction cycles were started by the addition of the appropriate amount of EDC stock solution to the precursor stock solution. All experiments were performed at 25°C.

High-Performance Liquid Chromatography (HPLC). We used a *ThermoFisher* Vanquish Duo UHPLC (**HPLC1**) with a Hypersil Gold 100 x 2.1 mm C18 column (3 µm pore size) and a *ThermoFisher* Dionex Ultimate 3000 (**HPLC2**) with a Hypersil Gold 250x4.8 mm C18 column (5 µm pore size) to monitor the concentration profiles of each reactant of the chemical reaction network. 1.0 mL samples were prepared into a screw cap HPLC vial following the sample preparation protocol described above. Samples were injected directly without any further dilution from the HPLC vial. We injected 2.5 µL (**HPLC1**) and 25 µL (**HPLC2**) for the detection of the precursor and anhydride. For the detection of EDC, we injected 0.1 µL (**HPLC1**) and 1 µL (**HPLC2**). We used a UV/Vis detector at 220 nm (precursor, fuel, anhydrides) and 330 nm

(Nimesulide) for detection. Linear gradients of MQ water:ACN with 0.1 % TFA were used to separate the compounds. We performed calibration curves of all the compounds in triplicates

Nuclear Resonance Spectroscopy (NMR). We recorded NMR spectra on a *Bruker AVIII-400* at 25 °C and a frequency of 400 MHz. Chemical shifts δ are reported in ppm and are referred to the residual solvent peak of the used deuterated solvent (chloroform- d_1 7.26 ppm for ^1H -NMR). We abbreviated the signal multiplets as followed: s-singlet, d-doublet, t-triplet, m-multiplet. The coupling constant J is stated as the average value in Hz and refers to the coupling between two protons.

UV/VIS-spectroscopy. A *Multiskan FC* microplate reader (*ThermoFisher*) was used for UV/VIS measurements. For the sample preparation, a 96-well-plate (tissue culture plate non-treated) was used. Measurements were performed in triplicates at a wavelength of 600 nm and 25°C.

Fluorescence Spectroscopy. We performed the Nile Red assay on a *Jasco* (FP-8300) spectrofluorometer. We prepared the samples in disposable cuvettes (PS) by mixing different concentrations of (*E/Z*)-2-decen-1-ylsuccinic acid with 5 μM Nile Red. We measured fluorescence spectra from 600 nm to 700 nm with an excitation at 550 nm and calculated the blue shift by subtracting the wavelength of intensity maximum from the maximum of the blank at 648 nm.

Polyacrylamide (PAA) Gel Preparation. We prepared a 7.5 mM and 35 mM (*E/Z*)-2-decen-1-ylsuccinic acid solution containing 30 % (29:1) acrylamide by dissolving 5.80 g acrylamide, 0.20 g *N,N'*-methylene-bisacrylamide and the succinic acid derivative (38,43 mg and 179,32 mg, respectively) in 20 mL of 200 mM MES buffer at pH 6. We diluted the stock solution with the appropriate succinate solution without acrylamide to a 15 % acrylamide solution. The gels were prepared in Petri dishes (60 mm x 15 mm) which were plasma oxidized before hydrogel formation. We prepared 4 mL of the 15 % acrylamide solution in the petri dish and started the hydrogel formation by the addition of 60 μL of a 10 % ammonium persulfate (APS) solution in MQ water and 8 μL tetramethylethylenediamine (TEMED). The solution was mixed and heated for 10 minutes at 50 °C. The PAA hydrogel was cooled to room temperature for 30 min. We cut out hydrogel pieces with a scalpel, placed them in a petri dish (35 mm x 10 mm), and sealed them with Parafilm®. The gels were prepared freshly before each experiment.

Spray Deposition. Pulsed spray deposition of 200 μL of 3M stock solutions of EDC in MQ water was performed using the air atomizing nozzle JAUCO D555000 (*Spraying Systems Co.*) The respective solutions were sprayed on 15 % PAA hydrogels containing different concentrations of the precursor, which were placed in a petri dish (35 mm x 10 mm) at ambient temperature. Oil-free nitrogen was used as a carrier gas with a constant pressure set to 0.5 bar. The air atomizing nozzle was mounted on a custom-built spray coater at a distance of roughly 13.5 cm to the PAA gels. A magnetic valve of the type MEBH-5/2-1/8-B (*Festo SE & Co. KG*) was connected to a microcontroller and controlled the pulsed spray deposition with a periodicity of 50 ms spraying time followed by 450 ms of waiting time. The spray cone provided by the nozzle covered a circular area with a diameter of roughly 2.5 cm. To obtain an improved homogeneous coverage of the PAA hydrogels, the air atomizing nozzle was moved periodically within 1 cm by the spray coater, which was controlled by a second microcontroller. The obtained samples were sealed in closed Petri dishes (35 mm x 10 mm) with Parafilm® and analyzed by a webcam set-up and subsequent grey value analysis.

Webcam Set-Up and Quantification of Turbidity. We used a webcam set-up with *Timelapse* software to take images of the substrates in a 5 min interval. We analyzed the turbidity of the substrates using the grey value analysis tool of *ImageJ*. The raw data of the grey values were normalized to 1 to account for differences in the background and lighting. The kinetics in cuvettes were performed in an incubator at 25 °C to account for the temperature dependency of the hydrolysis rate.

Confocal Fluorescence Microscopy. We imaged the droplets using a *Leica SP8* confocal microscope with a 63x oil immersion objective. Samples were prepared as described above but with 0.1 μM Nile Red added before EDC addition. We added a 5 μL sample to a silicon grease reservoir on a PEG-coated glass slide covered with a 12 mm diameter coverslip. The samples were excited with a 543 nm laser and imaged at 580 – 700 nm.

Dynamic Light Scattering (DLS). The CMC and size of (*E/Z*)-2-decen-1-ylsuccinic acid micelles were determined on a Malvern Zetasizer Nano ZS using a laser wavelength of 633 nm in disposable cuvettes (PS). We performed triplicate measurements each with 3 acquisition times of 20 s.

Droplet Composition Experiments. We prepared 5 mL samples as described above to guarantee a sufficient droplet phase volume after centrifugation. After the depletion of the fuel, the reaction mixture was centrifuged at 4 °C for 3 minutes (rpm = 5000). We used an *Eppendorf*

pipette to take a 1 μL sample of the droplet pellet which we diluted in 200 μL ACN in an HPLC screw cap vial.

Supernatant Composition Experiments. We prepared 1 mL samples as described above in 1.5 mL *Eppendorf* reaction vessels. After 16 minutes, the samples were centrifuged at 25 $^{\circ}\text{C}$ for 1 minute (rpm = 13500). We directly analyzed the concentrations of the corresponding anhydrides in the supernatant of the sample with **HPLC2**.

Calculation of respective concentrations inside the droplets. We calculated the corresponding anhydride concentrations inside the droplets using the molecular volumes and the relation $n^{\text{I}} = n^{\text{total}} - n^{\text{II}}$, respectively. The superscripts I and II represent the droplet phase and dilute bulk phase, respectively.

Preparation of Drug Delivery Platform. The drug-delivery emulsion was prepared by emulsifying the (*E/Z*)-2-decen-1-ylsuccinic anhydride (60 mM) in MES-buffer (pH 6, 200 mM) with 40 μL of the drug stock solution and sonication for 2 min with a *Branson Ultrasonics*TM SonifierTM SFX250 at 25 % in an ice bath. These anhydride/drug emulsions were prepared freshly for each experiment. 250 μL of the emulsion was then mixed with 250 μL of a precursor stock (32 - 44 mM) and 500 μL of a 2 % agar-agar stock in MES-buffer (pH 6, 200 mM) heated to 90 $^{\circ}\text{C}$, was added subsequently. Then 60 μL of this mixture was prepared on the bottom of a 96-well plate. The emulgel was cooled down to room temperature and 120 μL of an 8.0-11.0 mM precursor stock was added as supernatant. The cumulative drug release was measured in the supernatant by **HPLC2**. All experiments were performed at 25 $^{\circ}\text{C}$ in triplicate.

9. Further Publications

I also contributed to other publications besides the two publications reprinted above. A list of all my publications is given in the following section.

Publications

- [1] P. S. Schwarz,* S. Laha,* J. Janssen, T. Huss, J. Boekhoven, C. A. Weber, *Chem. Sci.* **2021**, *12*, 7554.

- [2] P. S. Schwarz, L. Tebcharani, J. E. Heger, P. Müller-Buschbaum, J. Boekhoven, *Chem. Sci.* **2021**, *12*, 9969.

- [3] M. A. Würbser,* P. S. Schwarz,* J. Heckel, A. M. Bergmann, A. Walther, J. Boekhoven, *ChemSystemsChem*, *3*, e2100015.

- [4] P. S. Schwarz, M. Tena-Solsona, K. Dai, J. Boekhoven, *ChemComm*, **2021**, accepted.

- [5] B.-J. Niebuur, H. Hegels, M. Tena-Solsona, P. S. Schwarz, J. Boekhoven, C. M. Papadakis, *J. Phys. Chem. B* **2021**, *125*, 13542.

*These authors contributed equally.

10. Acknowledgments

I am thanking Prof. Job Boekhoven for the opportunity to work in his lab for a research internship, master thesis, and Ph.D. thesis. During my research internship and your lecture, I first got in contact with the field of supramolecular chemistry. Quickly, my interest got awakened and I became fascinated of the research field. I learned so many new techniques and skills and enjoyed working in the field of chemically fueled self-assembly. I appreciate that your door was always open and you were always available when I needed help or a problem appeared. Thank you!

Thanks to the senior Ph.D. students and postdocs Raphael, Benno, Caren, Schnitti, and Marta for the warm welcome and nice atmosphere in the lab. Despite working together with you guys, I enjoyed the nerf gun battles, paper parties, and lunch breaks. Special thanks to Marta for her supervision during my research internship and master thesis and Benno (aka Fetti 1) for being my go-to contact person for any kind of problems. You guys taught and helped me a lot and I am thankful for working with you. I also want to thank Jenni and Michi for proof-reading my thesis.

Thanks to my collaborators Dr. Christoph Weber, Sudarshana, Jacqueline, and Julian. It was a pleasure to work together with you on our collaborative projects and I am proud of what we achieved.

Also, I want to thank all the guys who joined the lab with and after me: Carsten, Kun, Michi, Laura, Ala, Jennifer, Xiaoyao, Brigitte, Christine, Judit, Spabi, Oleksii, and Michele. It was a pleasure working with you. I am a bit sad that the pandemic prevented most of the group activities for half of my Ph.D. but I am sure you guys will keep the great team spirit. Thanks also to the interns Sebi, Erika, Any, Michelle, Tabea, and Margot who enriched the daily life in the lab. Special thanks to Tabea who had a huge contribution to my first publication.

Thanks also to the best fellow students one could wish for: Makke, Carsten, Ala, Maxi, Steffen, Phil, Chris, Güllich, Aleks, Hertlein, Fuchsl, Eva, Simon, Sina, Jonas B. and Jonas F. I am glad that we met and became friends! We made it together through this university degree and many, many night-outs and esqualations.

Acknowledgments

In the end, I want to thank my family Daniela and Georg for their endless support during my studies. This wouldn't have been possible without you. Thanks for always being there for me. I also want to thank my brother Julian for his support and pleasant distraction from work in our home gym, el arenal, and in the warzone.

In the end, I want to thank Michi who always supported me. I am glad that we met and went this way together. I love you!

11. References

- [1] J. Loeb, *The mechanistic conception of life: biological essays*, University of Chicago Press Chicago, **1912**.
- [2] G. Wald, *Sci. Am.* **1954**, *191*, 44.
- [3] J. E. Greaves, *Sci. Mon.* **1926**, *23*, 496.
- [4] P. Mazzarello, *Nat. Cell Biol.* **1999**, *1*, E13.
- [5] F. Raulin-Cerceau, Springer Netherlands, Dordrecht, **2001**, pp. 39.
- [6] a) R. E. Dickerson, *Sci. Am.* **1978**, *239*, 70; b) C. Darwin, *On the Origin of Species: Or; The Preservation of the Favoured Races in the Struggle for Life*, Read Books Ltd, **2018**.
- [7] A. I. Oparin, *The origin of life on the earth.* **1957**.
- [8] S. L. Miller, *Science* **1953**, *117*, 528.
- [9] S. W. Fox, K. HARADA, *Science* **1958**, *128*, 1214.
- [10] a) L. E. Orgel, *J. Mol. Biol.* **1968**, *38*, 381; b) H. J. Morowitz, B. Heinz, D. W. Deamer, *Orig. Life Evol. Biosph.* **1988**, *18*, 281; c) P. Walde, R. Wick, M. Fresta, A. Mangone, P. L. Luisi, *J. Am. Chem. Soc.* **1994**, *116*, 11649.
- [11] K. Adamala, J. W. Szostak, *Science* **2013**, *342*, 1098.
- [12] T. Oberholzer, P. L. Luisi, *J. Biol. Phys.* **2002**, *28*, 733.
- [13] a) P. L. Luisi, *Orig. Life Evol. Biosph.* **1998**, *28*, 613; b) J. W. Szostak, D. P. Bartel, P. L. Luisi, *Nature* **2001**, *409*, 387.
- [14] J. W. Szostak, *J. Biomol. Struct. Dyn.* **2012**, *29*, 599.
- [15] J. Gayon, *Orig. Life Evol. Biosph.* **2010**, *40*, 231.
- [16] N. A. Yewdall, A. F. Mason, J. C. M. van Hest, *Interface Focus* **2018**, *8*, 20180023.
- [17] a) S. F. Banani, H. O. Lee, A. A. Hyman, M. K. Rosen, *Nat. Rev. Mol. Cell Biol.* **2017**, *18*, 285; b) S. Alberti, *Curr. Biol.* **2017**, *27*, R1097.
- [18] a) S. Hurlley, *Science* **2009**, *326*, 1205; b) A. H. Chen, P. A. Silver, *Trends Cell Biol.* **2012**, *22*, 662.
- [19] A. J. Dzieciol, S. Mann, *Chem. Soc. Rev.* **2012**, *41*, 79.
- [20] a) E. Mattia, S. Otto, *Nat. Nanotechnol.* **2015**, *10*, 111; b) K. Das, L. Gabrielli, L. J. Prins, *Angew. Chem. Int. Ed.* **2021**, *60*, 20120.
- [21] E. Schrödinger, *What is Life?: With Mind and Matter and Autobiographical Sketches*, Cambridge University Press, Cambridge, **1992**.
- [22] C. P. Brangwynne, G. H. Koenderink, F. C. MacKintosh, D. A. Weitz, *Phys. Rev. Lett.* **2008**, *100*, 118104.
- [23] E. Hernández-Lemus, *J. Thermodyn.* **2012**, *2012*, 432143.
- [24] C. P. Brangwynne, G. H. Koenderink, F. C. MacKintosh, D. A. Weitz, *J. Cell Biol.* **2008**, *183*, 583.
- [25] T. Ahsendorf, F. Wong, R. Eils, J. Gunawardena, *BMC Biology* **2014**, *12*, 102.
- [26] a) N. Singh, G. J. M. Formon, S. De Piccoli, T. M. Hermans, *Adv. Mater.* **2020**, *32*, 1906834; b) R. Merindol, A. Walther, *Chem. Soc. Rev.* **2017**, *46*, 5588.
- [27] a) P. Schwille, *Angew. Chem. Int. Ed.* **2017**, *56*, 10998; b) P. Adamski, M. Eleveld, A. Sood, Á. Kun, A. Szilágyi, T. Czárán, E. Szathmáry, S. Otto, *Nat. Rev. Chem.* **2020**, *4*, 386.
- [28] A. Pressman, C. Blanco, Irene A. Chen, *Curr. Biol.* **2015**, *25*, R953.
- [29] R. Pascal, A. Pross, J. D. Sutherland, *Open Biol.* **2013**, *3*, 130156.
- [30] D. Branton, D. W. Deamer, in *Membrane Structure*, Springer Vienna, Vienna, **1972**, pp. 1.
- [31] R. Heald, O. Cohen-Fix, *Curr. Opin. Cell Biol.* **2014**, *26*, 79.
- [32] H. Watson, *Essays Biochem.* **2015**, *59*, 43.
- [33] A. A. Hyman, C. A. Weber, F. Jülicher, *Annu. Rev. Cell Dev. Biol.* **2014**, *30*, 39.

- [34] C. P. Brangwynne, C. R. Eckmann, D. S. Courson, A. Rybarska, C. Hoege, J. Gharakhani, F. Jülicher, A. A. Hyman, *Science* **2009**, *324*, 1729.
- [35] S. Boeynaems, S. Alberti, N. L. Fawzi, T. Mittag, M. Polymenidou, F. Rousseau, J. Schymkowitz, J. Shorter, B. Wolozin, L. Van Den Bosch, P. Tompa, M. Fuxreiter, *Trends Cell Biol.* **2018**, *28*, 420.
- [36] E. Gomes, J. Shorter, *J. Biol. Chem.* **2019**, *294*, 7115.
- [37] C. A. Weber, C. Zechner, *Phys. Today* **2021**, *74*, 38.
- [38] C. A. Weber, D. Zwicker, F. Jülicher, C. F. Lee, *Rep. Prog. Phys.* **2019**, *82*, 064601.
- [39] a) Clifford P. Brangwynne, P. Tompa, Rohit V. Pappu, *Nat. Phys.* **2015**, *11*, 899; b) P. J. Flory, *J. Chem. Phys.* **1942**, *10*, 51.
- [40] C. T. Walsh, B. P. Tu, Y. Tang, *Chem. Rev.* **2018**, *118*, 1460.
- [41] B. Rieß, R. K. Grötsch, J. Boekhoven, *Chem* **2020**, *6*, 552.
- [42] A. D. and, T. J. Mitchison*, *Annu. Rev. Cell Dev. Biol.* **1997**, *13*, 83.
- [43] a) J. Deng, A. Walther, *Chem* **2020**, *6*, 3329; b) C. Donau, F. Späth, M. Sosson, B. A. K. Kriebisch, F. Schnitter, M. Tena-Solsona, H.-S. Kang, E. Salibi, M. Sattler, H. Mutschler, J. Boekhoven, *Nat. Commun.* **2020**, *11*, 5167; c) K. K. Nakashima, J. F. Baaij, E. Spruijt, *Soft Matter* **2018**, *14*, 361; d) K. K. Nakashima, M. H. I. van Haren, A. A. M. André, I. Robu, E. Spruijt, *Nat. Commun.* **2021**, *12*, 3819; e) F. Späth, C. Donau, A. M. Bergmann, M. Kränzlein, C. V. Synatschke, B. Rieger, J. Boekhoven, *J. Am. Chem. Soc.* **2021**, *143*, 4782.
- [44] a) M. Tena-Solsona, J. Janssen, C. Wanzke, F. Schnitter, H. Park, B. Rieß, J. M. Gibbs, C. A. Weber, J. Boekhoven, *ChemSystemsChem* **2021**, *3*, e2000034; b) M. Tena-Solsona, C. Wanzke, B. Riess, A. R. Bausch, J. Boekhoven, *Nat. Commun.* **2018**, *9*, 2044.
- [45] A. Klosin, F. Oltsch, T. Harmon, A. Honigmann, F. Jülicher, A. A. Hyman, C. Zechner, *Science* **2020**, *367*, 464.
- [46] D. Zwicker, R. Seyboldt, C. A. Weber, A. A. Hyman, F. Jülicher, *Nat. Phys.* **2017**, *13*, 408.
- [47] M. M. Fryd, T. G. Mason, *Annu. Rev. Phys. Chem.* **2012**, *63*, 493.
- [48] D. Zwicker, A. A. Hyman, F. Jülicher, *Phys. Rev. E* **2015**, *92*, 012317.
- [49] S. Waldherr, T. Eissing, F. Allgöwer, *IFAC Proceedings Volumes* **2008**, *41*, 15861.
- [50] R. Thomas, R. d'Ari, *Biological feedback*, CRC press, **1990**.
- [51] A. Y. Mitrophanov, E. A. Groisman, *Bioessays* **2008**, *30*, 542.
- [52] C. S. Barry, J. J. Giovannoni, *J. Plant Growth Regul.* **2007**, *26*, 143.
- [53] Y. Dublanche, K. Michalodimitrakis, N. Kümmerer, M. Foglierini, L. Serrano, *Mol. Syst. Biol.* **2006**, *2*, 41.
- [54] A. Khan, J. Pessin, *Diabetologia* **2002**, *45*, 1475.
- [55] a) V. Varga, C. Leduc, V. Bormuth, S. Diez, J. Howard, *Cell* **2009**, *138*, 1174; b) V. Varga, J. Helenius, K. Tanaka, A. A. Hyman, T. U. Tanaka, J. Howard, *Nat. Cell Biol.* **2006**, *8*, 957.
- [56] W.-K. Leung, N. Humphries, N. Afshar, B. Argunhan, Y. Terentyev, T. Tsubouchi, H. Tsubouchi, *J. Cell Biol.* **2015**, *211*, 785.
- [57] S. Bal, K. Das, S. Ahmed, D. Das, *Angew. Chem. Int. Ed.* **2019**, *58*, 244.
- [58] S. Bal, C. Ghosh, T. Ghosh, R. K. Vijayaraghavan, D. Das, *Angew. Chem. Int. Ed.* **2020**, *59*, 13506.
- [59] B. A. K. Kriebisch, A. Jussupow, A. M. Bergmann, F. Kohler, H. Dietz, V. R. I. Kaila, J. Boekhoven, *J. Am. Chem. Soc.* **2020**, *142*, 20837.
- [60] S. Borsley, D. A. Leigh, B. M. W. Roberts, *J. Am. Chem. Soc.* **2021**, *143*, 4414.
- [61] a) D. Sievers, G. von Kiedrowski, *Nature* **1994**, *369*, 221; b) J. A. Doudna, S. Couture, J. W. Szostak, *Science* **1991**, *251*, 1605.
- [62] S. Yang, G. Schaeffer, E. Mattia, O. Markovitch, K. Liu, A. S. Hussain, J. Ottel , A. Sood, S. Otto, *Angew. Chem.* **2021**, *133*, 11445.
- [63] J. Leira-Iglesias, A. Tassoni, T. Adachi, M. Stich, T. M. Hermans, *Nat. Nanotechnol.* **2018**, *13*, 1021.

References

- [64] S. M. Morrow, I. Colomer, S. P. Fletcher, *Nat. Commun.* **2019**, *10*, 1011.
- [65] C. Wanzke, M. Tena-Solsona, B. Rieß, L. Tebcharani, J. Boekhoven, *Mater. Horiz.* **2020**, *7*, 1397.